AD-A266 676

WL-TR-92-4051

STRUCTURE/PROPERTY RELATIONSHIPS OF SILOXANE-
BASED LIQUID CRYSTALLINE MATERIALS

Timothy J. Bunning
Herbert E. Klei
Jeffery T. Koberstein
Dept. of Chemical Engineering
University of Connecticut
Storrs, CT 06268

Edward T. Samulski
Dept. of Chemistry
University of North Carolina
Chapel Hill, NC 27599

W.W. Adams
R.L. Crane
Laser Hardened Materials Tech Group
Hardened Materials Branch

DTIC
ELECTE
JUL 14 1993
S E D
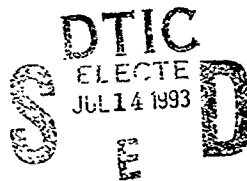
May 1992

Final Report for the Period January 1990 - May 1992

Approved for public release; distribution is unlimited.

93-15823

NOTICE

When Government drawings, specifications, or other data are used for any purpose other than in connection with a definitely Government-related procurement, the United States Government incurs no responsibility or any obligation whatsoever. The fact that the Government may have formulated or in any way supplied the said drawings, specifications, or other data, is not to be regarded by implication, or otherwise in any manner construed, as licensing the holder, or any other person or corporation; or as conveying any rights or permission to manufacture, use, or sell any patented invention that may in any way be related thereto.

This report is releasable to the National Technical Information Service (NTIS). At NTIS, it will be available to the general public, including foreign nations.

This technical report has been reviewed and is approved for publication.

ROBERT L. CRANE, WUD 26 Leader
Hardened Materials Branch
Electromagnetic Mat'ls & Surv Div

GARY K. WAGGONER, Chief
Hardened Materials Branch
Electromagnetic Mat'ls &
Surv Div

FOR THE COMMANDER

WILLIAM R. WOODY, Chief
Electromagnetic Mat'ls & Surv Div

REPORT DOCUMENTATION PAGE

Public report burden for this collection of information is estimated to average 1 hour per response including the time for reviewing instructions, searching existing data sources, gathering and maintaining the data needed and completing and reviewing the collection of information. Send comments regarding this burden estimate or any other aspect of this collection of information, including suggestions for reducing this burden to Washington Headquarters Services, Directorate for information Operations and Reports, 1215 Jefferson Davis Highway, Suite 1204, Arlington, VA 22202-4302 and to the Office of Management and Budget, Paperwork Reduction Project (0704-0188) Washington, DC 20503

1. AGENCY USE ONLY (Leave blank)	2. REPORT DATE	3. REPORT TYPE AND DATES COVERED
	May 1992	Final: Jan 90 to May 92

4. TITLE AND SUBTITLE
STRUCTURE/PROPERTY RELATIONSHIPS OF SILOXANE-BASED
LIQUID CRYSTALLINE MATERIALS

6. AUTHOR(S)
Bunning, T.J.; Klei, H.E.; Koberstein, J.T.;
Samulski, E.T.; Adams, W.W.; Crane, R.L.

5. FUNDING NUMBERS
PE: 62102F
PR: 2422
TA: 04
WU: 01

7. PERFORMING ORGANIZATION NAME(S) AND ADDRESS(ES)

W. W. Adams (513) 255-53808, Ext 3171
Hardened Materials Branch
Electromagnetic Materials & Surv Division

8. PERFORMING ORGANIZATION REPORT NUMBER

WL-TR-92-4051

9. SPONSORING/MONITORING AGENCY NAME(S) AND ADDRESS(ES)

Materials Directorate
Wright Laboratory
Air Force Systems Command
Wright-Patterson Air Force Base, OH 45433-6533

10. SPONSORING/MONITORING AGENCY REPORT NUMBER

WL-TR-92-4051

11. SUPPLEMENTARY NOTES

12a. DISTRIBUTION/AVAILABILITY STATEMENT

Approved for public release; distribution is unlimited

12b. DISTRIBUTION CODE

13. ABSTRACT (Maximum 200 words)

The structure/property relationships of a class of cyclic-siloxane based molecules were investigated. X-ray diffraction and electron microscopy techniques were used to initially investigate commercially available pentamethylcyclopentasiloxane rings with various molar ratios of biphenyl-4-allyloxybenzoate and cholesteryl-4-allyloxybenzoate mesogens attached. Results indicated a strong dependence of the X-ray diffraction patterns on the composition of the mesogens. Three dozen new siloxanes with mesogens were synthesized to investigate the packing behavior in more detail. Variables investigated included siloxane ring size, siloxane shape, leader group length, and mole fraction cholesterol. The phase behavior of these compounds was characterized using polarizing optical microscopy, differential scanning calorimetry, and X-ray diffraction including real-time synchrotron experiments. The amount of cholesterol and the leader group length both substantially affected the liquid crystalline packing behavior. Cholesterol served to disrupt the homogeneity of the interdigitated smectic structure while increasing the tendency of the mesophase to layer pack. Lengthening the leader group increased the packing efficiency among mesogens. Certain compounds could be drawn into long, birefringent fibers with the orientation of the mesogens parallel to the fiber axis. The advantage of using cyclic siloxane rings was shown to lie in their processability. Optically clear thin films and fibers were readily obtainable. The molecular and macromolecular packing structures could be controlled by both chemical synthesis and alignment techniques. Materials containing nonlinear optical and photochromic chromophores were synthesized. Preliminary experiments have shown second-order nonlinear optical response from these compounds a novel class of compounds containing spiropyran-based mesogens exhibiting photochromism and thermochromism was also initially investigated.

14. SUBJECT TERMS			15. NUMBER OF PAGES
Liquid crystal	Smectic	Spectroscopy	298
Cholesteric	X-ray diffraction		**16. PRICE CODE**
Siloxane	Electron Microscopy		

17. SECURITY CLASSIFICATION OF REPORT	18. SECURITY CLASSIFICATION OF THIS PAGE	19. SECURITY CLASSIFICATION OF ABSTRACT	20. LIMITATION OF ABSTRACT
UNCL	UNCL	UNCL	UL

FOREWORD

The following report was prepared under the AFOSR Laboratory Graduate Fellowship Program (LGFP) under Contract F49620-89-C-0083. The work was initiated under Project No. 2422, "Laser Hardened Materials," Task No. 0401, Work Unit Directive (WUD) 26. It was administered under the direction of the Materials Directorate, Wright Laboratory, Air Force Systems Command, Wright-Patterson Air Force Base, Ohio, with Dr. R.L. Crane as the Materials Directorate Project Scientist (WUD Leader). Coauthors were Timothy J. Bunning, Dept. of Chemical Engineering, University of Connecticut, on leave as a Ph.D. Doctoral Candidate under the LGFP program, Dr. H.E. Klei and Dr. J.T. Koberstein, Dept. of Chemical Engineering, University of Connecticut and Dr. E.T. Samulski, Dept. of Chemistry, University of North Carolina, who served as academic advisers to TJB, and Dr. R.L Crane and Dr. W.W. Adams, Materials Dii·· ·te (WL/MLPJ). This report covers the doctoral research performed at both the University of Connecticut and the Materials Directorate.

Because the research was conducted at Wright-Patterson AFB, there are many people who deserve thanks for ideas and support. Special thanks go to the Laser Hardened Materials Branch for the opportunity to conduct my research in-house at the base. The access to people and state-of-the-art equipment enhanced this work. I also thank the Air Force Office of Scientific Research Laboratory Graduate Fellowship Program for allowing it to happen.

TABLE OF CONTENTS

LIST OF FIGURES

LIST OF FIGURES (con't)

LIST OF FIGURES (con't)

LIST OF FIGURES (con't)

LIST OF FIGURES (con't)

LIST OF TABLES

LIST OF TABLES (con't)

Section I

INTRODUCTION

This introduction is divided into five major parts. The first part discusses in general low molecular weight liquid crystalline materials and their different structural classifications. The second part examines polymer liquid crystalline materials with an emphasis on linear and cyclic siloxane liquid crystalline compounds. The third part discusses the characterization techniques used in the study of liquid crystals. The X-ray diffraction literature on liquid crystals is briefly reviewed as this is a major tool used in the dissertation. The fourth part discusses the linear and nonlinear optical properties and applications of liquid crystalline materials. The last part discusses the proposed dissertation research. Pertinent background information is given and the general goals of the research are formulated.

1.1 Liquid Crystals

Liquid crystalline materials may be defined as a thermo-dynamically stable bulk state of matter with a degree of internal order between that of isotropic fluids and crystalline solids. This yields materials which combine the viscosity, elastic properties, dielectric properties, and response times of a liquid with the long-term order and birefringence characteristic of crystalline materials. These materials exhibit anisotropy in their mechanical, electrical, magnetic, and optical properties.

Liquid crystalline materials fall into two categories, namely, lyotropic and thermotropic, each based on a different set of physical parameters. Lyotropic systems are dependent on changes in concentration and although they possess unique physical properties and thus applications, much work has revolved around the other major class of liquid crystals, thermotropic materials, in recent years. This type of phase was first observed over 100 years ago by Reinitzer[1] with an ester of cholesterol. He observed that the material went through a repeatable process of forming a turbid, liquid-like phase upon heating. Further heating resulted in a transparent isotropic liquid which when cooled, reformed this turbid phase. Since this observation, much work has been done on elucidating the unique properties of these materials. Within the last 20 years, a number of very good review articles and books have been published[2-5].

The three-dimensional order present within a crystalline solid usually breaks down when heated to its melting point, yielding an isotropic liquid where the molecules translate and rotate freely. Thermotropic materials instead undergo an incremental melting whereupon heating there is a systematic breakdown in the molecular order (Figure 1.1). This controlled melting is driven by the anisotropy and chemical structure of the molecules. These phases are thermodynamically stable and thus have to be considered as a separate phase of matter intermediate between a liquid and a solid.

2

Crystalline - Orientational Order
3° Spatial Order

Smectic B - Orientational Order
2° Spatial Order

Smectic A - Orientational Order
1° Spatial Order

Increasing
Temperature

Nematic - Orientational Order
No Spatial Order

Isotropic - No Orientational Order
No Spatial Order
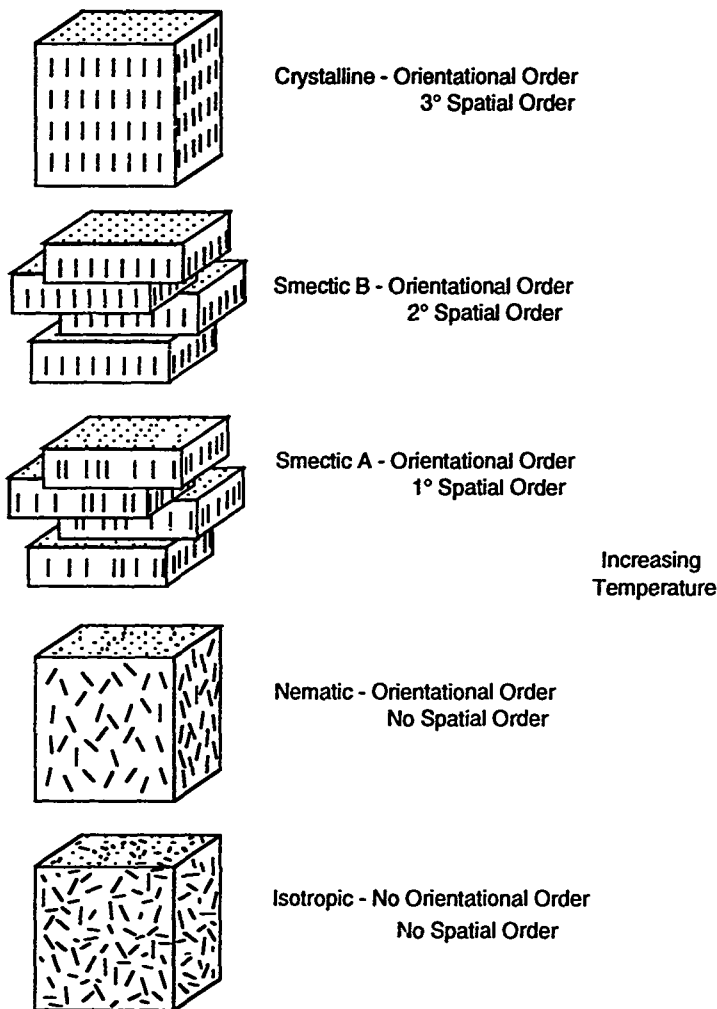
Figure 1.1: Schematic of the incremental melting process leading to the formation of liquid crystals

The breakdown in order has historically been used to classify thermotropic iiquid crystals. Rod- or lathe-shaped molecules can be divided into two main classifications: nematic and smectic. Nematic liquid crystals have no positional order and only maintain orientational order due to the physical anisotropy of the molecules (Figure 1.2(a)). The average directions of the molecular long axes are represented by a unit vector. The centers of mass of these molecules are free to translate in any direction thus forming an anisotropic liquid. The incorporation of a chiral center into a nematic-forming molecule will result in the formation of a cholesteric mesophase. Although this mesophase only has orientational order, the unit director is rotated in space yielding a material which has an optic axis perpendicular to the plane of the molecules (Figure 1.2(b)). The mesophase can be modeled as sheets of nematic liquid crystals where each layer is slightly rotated with respect to each other. This rotation has been the study of many theoretical examinations and was attributed to quadrapole-quadrapole, dipole-dipole interactions induced by the chiral center[6].

(a)

PITCH
(P)
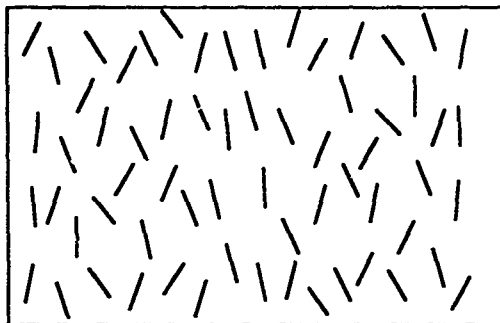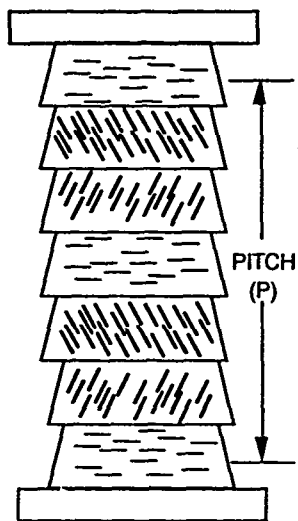
(b)

Figure 1.2:   Nematic (a) and cholesteric (b) liquid crystals

The second major classification for lathe-shaped molecules is the smectic mesophases. This class of materials has at least one degree of positional order as well as the orientational order present for nematic systems. Although there are at least nine different smectic classifications, the most common mesophases are shown in Figure 1.3. Smectic-A materials pack in a layered form although the layers freely slide over one another and the molecules are free to rotate and traverse within the layers. Smectic-B layers are similar except they have hexagonal order within the layers. Again, the molecules are free to rotate and the layers are free to slide over one another. The smectic-C mesophase is the tilted analog of the smectic-A mesophase and these can exhibit unique optical properties when the molecules are chiral. A very good theoretical and practical guide to all smectic liquid crystalline phases known to date has been published by Gray and Goodby[7].
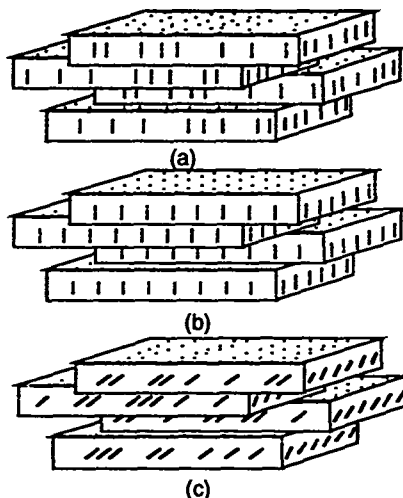
Figure 1.3: Smectic-A (a), smectic-B (b), and smectic-C (c)
architectures

1.2   Liquid Crystalline Polymers

1.2.1   General Liquid Crystalline Polymers

The field of thermotropic macromolecular (polymeric) liquid
crystalline materials is in its infancy compared to that of the low
molecular weight liquid crystals.   Where the latter has been known
and studied for over 100 years, liquid crystalline polymers have
only been examined since the early 1970's.   The combination of
mesogenic behavior with the macroscopic behavior of polymeric
systems yields high molecular weight materials which exhibit
anisotropic behavior.   Because of the ease in processing polymeric
materials, this allows the fabrication of films, fibers, and coatings
which combine both of these properties.   Recently, several very

7

good literature reviews on the field of liquid crystalline polymeric materials have been published[8-12].

The classifications for liquid crystalline phases are the same used for low molecular weight systems. In addition, there are two major types of polymeric liquid crystalline systems. Polymers with mesogenic groups incorporated within the backbone are called main-chain liquid crystalline polymers. These are formed by attaching one or more mesogenic units in a head-to-tail fashion using either flexible or rigid linkages (Figure 1.4(a,b)). The length and the chemical structure of the groups used to attach two units ultimately determine whether a liquid crystalline phase is formed. Rigid rod materials and semiflexible materials are possible. Physical properties such as tensile strength and flexural strength along the direction of orientation are enhanced due to the macroscopic orientation. Other possibilities include disc-like mesogenic units (Figure 1.4(d,e)) in various geometries and laterally attached rod-like mesogens (Figure 1.4(c)).
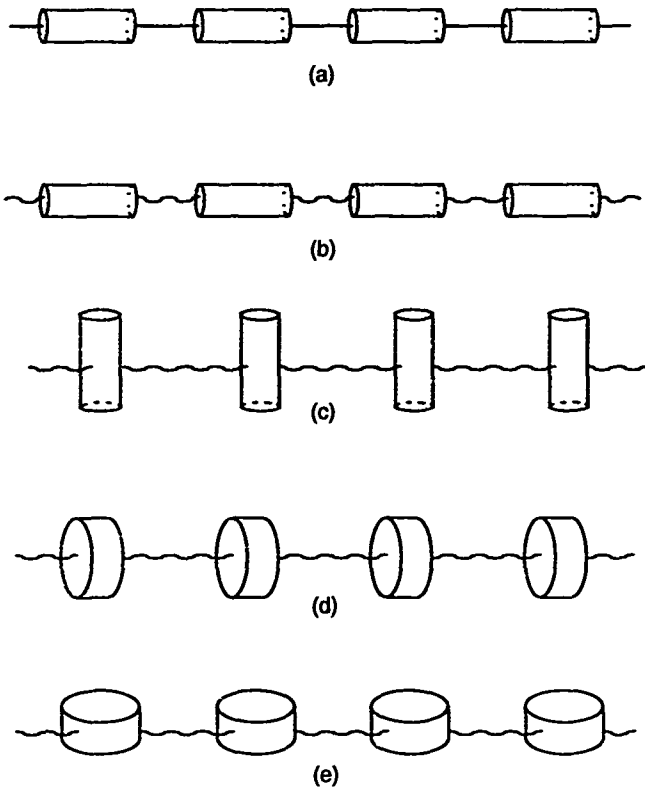
Figure 1.4: Main-chain liqud crystalline polymers based on rod-like (a-c) and disk-like mesogens (d,e)

9

The second type, side-chain liquid crystalline polymers, is formed by the attachment of mesogenic units on a polymeric backbone or by polymerization of suitable mesogenic units. These compounds exhibit all the characteristics of low molecular weight mesophases and have milder processing conditions than main-chain systems. They may be visualized as rigid blocks attached to a flexible polymer chain through an appropriate leader group (Figure 1.5(a-d)).

In contrast to main-chain liquid crystalline polymers, the liquid crystalline behavior of these materials is governed by two factors. These are the rigidity of the polymer main-chain and the tendency of the rigid mesogenic groups towards orientational order. The attachment of a mesogenic unit to a polymer backbone does not by itself guarantee a polymeric liquid crystalline phase and in most cases amorphous polymers are observed. This is due in part to the increased rotational and translational restrictions induced by steric interactions with the main chain. The liquid crystalline phases can be induced, however, by attachment of the mesogenic unit to the main chain with a flexible leader group. The liquid crystalline phase observed in a polymeric material is usually not the same as that exhibited by the low molecular weight compound. Polymeric materials usually exhibit higher order phases compared to the neat liquid crystalline mesogen and higher phase transition temperatures.
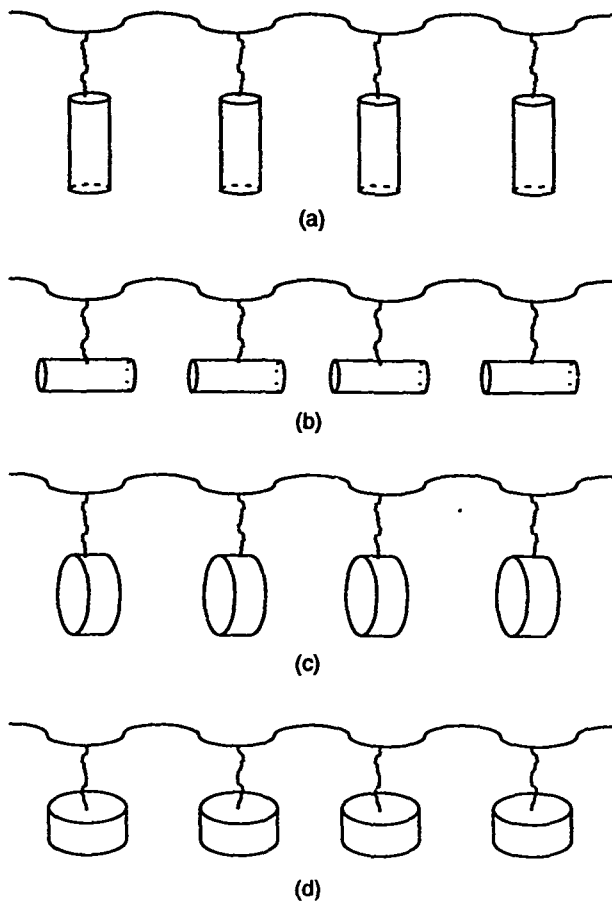
Figure 1.5: Side-chain liquid crystalline polymers based on rod-like (a, b) and disk-like mesogens (c, d)

11

The rigidity of the polymer main chain also greatly affects the mesogenic behavior of these materials. Very rigid backbone structures have very high glass transition and melting temperatures, sometimes exceeding their thermal stabilities. Changing the chemical constitution of the polymer main chain will alter the glass transition temperature for noncrystallizable polymers. Many applications of polymer liquid crystals make use of the ability of the mesogens to align in the anisotropic phase followed by a quench cooling below the glass transition. As the polymer vitrifies, the liquid crystalline structure is frozen into the glassy matrix, resulting in a material that maintains its anisotropy in the optical, mechanical, and electrical properties. Methods of lowering the glass transition temperature have therefore been sought to facilitate preparation of materials that may be processed more easily. One method that has received a considerable amount of interest over the last 15 years is the incorporation of siloxane units into the polymer backbone and linking units.

1.2.2 Linear Siloxane-Based Liquid Crystalline Polymers

General investigations into linear polysiloxane liquid crystalline materials grew out of the original work of Finkelmann and Ringsdorf[13]. They pioneered the idea that a sufficient length leader group would decouple the motions of the mesogenic group from the polymer chain. To enhance this behavior, they incorporated the highly flexible siloxane linkage into the polymer chain to allow for almost independent behavior of the polymer backbone and the mesogenic units. Rather than polymerize a

12

monomer using step- or chain-growth reactions, these materials are formed by the attachment of a mesogen to a polysiloxane backbone as shown in Figure 1.6. These reactions, hydrosilations, are discussed in more detail in Section IV.
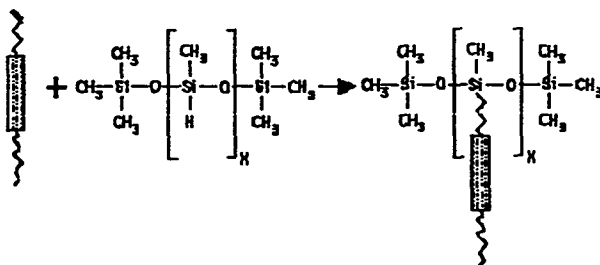
Figure 1.6: Hydrosilation reactions

In a series of five papers in the early 1980's[14-18], Finkelmann first discussed various aspects of structural behavior as a function of chemical composition with respect to polysiloxanes. He observed various phases including crystalline, nematic, and smectic depending on the type of mesogenic unit. Glass transition temperatures in the vicinity of room temperature were observed. Others[19-21] succeeded in the synthesis of low glass transition materials by copolymerizing dimethylsiloxane segments along the polymer backbone. Because of the unique flexibility of this material, glass transition temperatures that approached that of polydimethylsiloxane (-127ºC) were achieved and found to be a strong function of the amount of dilution. The nonmesogenic dilutent acted to weaken the interactions between the mesogenic

13

side groups and the main-chain. Ringsdorf has also examined polysiloxanes with disc-shaped mesogenic units attached[22].

First attempts to synthesize a cholesteric homopolymer failed as higher ordered smectic phases were formed instead. This was overcome by copolymerizing a nematic group onto the main chain to act as a dilutent[13,16-18]. Within certain concentration regimes, the cholesteric mesophase was formed. Other successful attempts have used nonsteroidal chiral derivatives of phenyl benzoate molecules to form cholesteric liquid crystalline phases. A recent review describes the history of cholesteric polymeric liquid crystals[23].

Since this pioneering work, many research groups have synthesized and characterized a wide variety of side-chain liquid crystalline polysiloxanes including those containing cyano-substituted mesogens[24-26], laterally attached mesogens[27-30], steroidal-based mesogens[31], and phthalocyanines-based compounds[32,33]. Several groups have tried to produce chiral smectic-C siloxanes[34-43] as the low glass transition temperatures are useful in exploiting their inherent ferroelectric behavior which is promising for display applications[44-46]. A new class of materials also first investigated by Finkelmann is liquid crystalline polysiloxane elastomers[16,18,47-50]. These are polysiloxane liquid crystalline systems that have been crosslinked using a low molecular weight vinyl-terminated dimethylsiloxane. These materials are observed to exhibit both rubber elasticity and liquid crystalline properties which result in applications such as mechanical-optical switches and waveguides[51]. Zentel[51-54] has

14

synthesized elastomers containing chiral mesogens which have reportedly exhibited piezo-electric behavior.

1.2.3   Cyclic-Siloxane Compounds

A new type of siloxane-based system which has received little attention is the combination of cyclic-siloxane units and liquid crystalline mesogens as shown schematically in Figure 1.7.   The exact nature of the siloxane ring is still unknown, as many isomers of the crown-shaped structure exist.   Computer simulations[55,56] have predicted phases ranging from discotic to the conventional nematic depending on the size of the siloxane ring and the flexibility and length of the leader group used to attach the mesogenic groups.   Discotic phases were predicted when there was strong coupling of the mesogens attached to the ring while conventional nematics were predicted for a weak coupling.
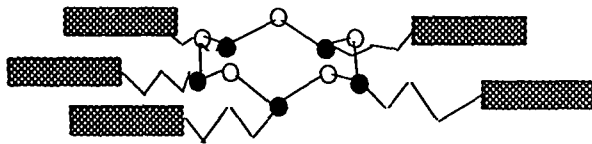
Figure 1.7:   Schematic of cyclic-siloxane based liquid crystals

Percec[57,58] has synthesized such a compound using a tetramethylcyclotetrasiloxane ring with four mesogens attached. He observed thermal behavior very similar to that of linear polysiloxanes with the same mesogens attached.   This is quite

15

unexpected as the degree of polymerization was much different for the two cases. Polarized optical microscopy seemed to indicate a discotic type of mesophase although a detailed examination was not performed. This is contrary to the behavior of cyano-based cyclic and linear systems as much different thermal behavior was observed[59]. Maxima and minima obtained for the thermal transitions of a 11-membered cyclic siloxane were attributed to an adaptation of a low energy, all trans conformation. No such behavior was observed for the linear analogs which exhibited linear dependences of thermal transitions versus size.

A cholesteric, cyclic-siloxane liquid crystalline material prepared commercially by Wacker Chemie Co. is the only other reported cyclic siloxane system. This material has a pentamethylcyclopentasiloxane ring onto which is attached cholesteryl 4'-allyloxybenzoate and biphenyl 4'-allyloxybenzoate[60,61]. This material forms a cholesteric mesophase with a wavelength of reflection that can be varied from the UV to the NIR by manipulating the ratio of the two mesogens[62].
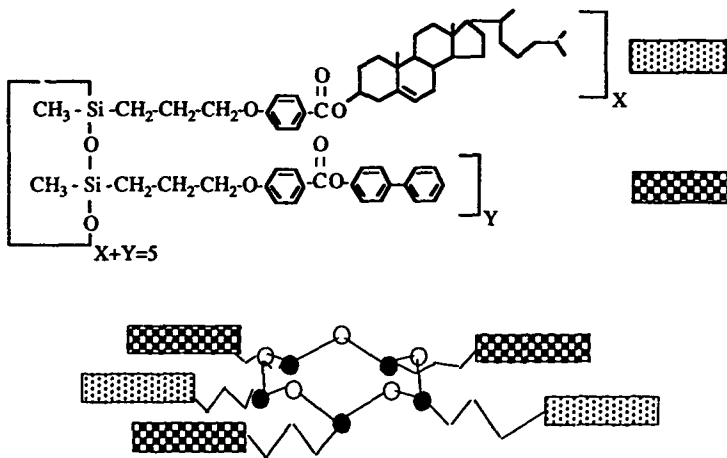
Figure 1.8: Schematic of cyclic-siloxane ring with cholesterol- and biphenyl-based mesogenic groups attached

Several optical devices have been fabricated based on this material including an optical notch filter[63] which exhibited an optical density of 2 within the rejection band while maintaining good transmission outside this region. This device was based on a reflecting composite made from these cyclic siloxanes and poly(benzyl-L-glutamate) compounds. These cholesteric materials have also been used in the preparation of reversible holographic-optical data storage devices[64]. Along with the two mesogens shown above, two photochromic compounds based on azobenzene moieties were attached to the ring. These multifunctional materials can store holographic information by variations in their structure

17

induced by light-sensitive photochromic and/or thermochromic processes. If the glass transition temperatures of the liquid crystalline siloxanes are above room temperature, the hologram is frozen into the glassy state of the polymer and can be read easily. The information may be erased by heating the material above the glass transition temperature.

1.3   Characterization

Liquid crystalline materials are primarily examined with the three analytical techniques of polarized optical microscopy (POM), differential scanning calorimetry (DSC), and X-ray diffraction. Due to the anisotropic nature of the molecules, polarized light can be used to probe the molecular architecture present. By examining thin films of liquid crystalline material under crossed polarized transmitted light, distinct textures due to defect structures appear. An understanding of these textures allows for a determination of the type of liquid crystal phase present. Several reviews have illustrated characteristic textures for a number of different liquid crystalline phases[7,65].

Liquid crystalline polymers due not generally exhibit easily identifiable textures. This can be due to a number of reasons including multiphase behavior, polydispersity, and high viscosities[66]. Their microstructures are also typically an order of magnitude finer in scale than low molecular weight liquid crystal phases[67]. Samples typically have to be annealed for a considerable length of time before distinct textures are obtained.

Due to the glassy nature typical of most polymer compounds, characteristic textures can be frozen into room temperature glasses.

Differential scanning calorimetry (DSC) provides a thermal map of the phase behavior. Typical spectra exhibit a glass transition temperature followed by one or more first order transitions. Some crystallizable polymer compounds exhibit a first-order melting transition. Transition temperatures are very dependent on thermal history and molecular weight. Several authors have discussed the thermal behavior of liquid crystalline polymeric materials[66,68,69].

The third method of characterization, used extensively in this research, is X-ray diffraction. Orientation and phase types can be determined from examinations of unaligned and aligned samples in a simple Laue-type geometry. Collimated monochromatic X-rays are focused on a sample mounted perpendicular to the beam. The resulting diffraction pattern can be obtained by placing a detector, either flat film or electronic, behind the sample at a known distance as shown in Figure 1.9. Diffraction patterns from unaligned samples are similar to powder patterns with the number and sharpness of the rings dependent on the molecular architecture[10,70-74].
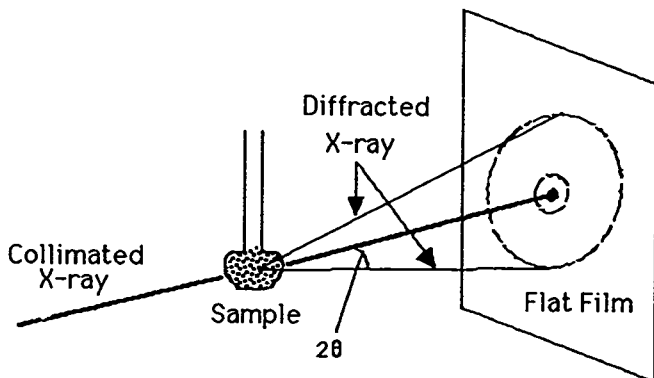
Figure 1.9: Schematic of Laue diffraction

The resulting X-ray patterns give all the reticular spacings but no information about the spatial orientation of these phases. They serve to distinguish between classes of liquid crystals including nematic, smectic-A, and smectic-B phases. The structural classifications of liquid crystals as a function of translational and positional order are well documented[75]. Because of the large amount of disorder present in liquid crystalline systems, less than 10 independent Bragg reflections are typically observed. Nematic materials usually exhibit a broad diffuse halo at large 2θ values and sometimes a diffuse ring at small 2θ values. This is indicative of the lack of positional order among the molecules. The smectic-A phase typically exhibits a sharp inner reflection and a diffuse outer reflection while the smectic-B phase exhibits sharp inner and outer reflections. X-ray patterns from unoriented polymeric liquid

crystals generally exhibit the same features as their low molecular weight analogs.

The spacings from the large 2θ reflections are related to the lateral interaction among mesogens. The spacings from the small 2θ reflections yield information on the positional interactions among mesogens. Nematic and smectic-A materials exhibit a primary d-spacing approximately 10-20% shorter than the extended molecular length, L. This is indicative of an interdigitated packing structure where the slight difference is due to a random tilting that statistically lowers the d-spacings. This packing is schematically shown in Figure 1.10(a). The primary layer reflection is typically much sharper for smectic compounds than for nematic compounds. This is due to a lack of translational order for the nematic compounds. Unoriented smectic-C phases exhibit similar patterns to smectic-A compounds except the d-spacings are smaller (Figure 1.10(d)) due to the inherent tilt. Diffraction patterns from unoriented smectic-C phases cannot be distinguished from smectic-A patterns. The transition from the tilted molecular scheme to an orthogonal packing scheme can be observed with X-ray diffraction as an increase in the d-spacing with temperature. Thus, elevated temperature diffraction serves as a particularly useful characterization technique for unaligned samples. When no interdigitation is allowed, the d-spacing corresponds to a head-to-tail noninterdigitated packing scheme as shown in Figure 1.10(b). Here the d-spacing is approximately twice the molecular length. This is only present for polymer systems where mesogens can reside on either side of the backbone. For highly polar low

21

molecular weight molecules, d-spacings equal to 1.4*L have been attributed[76-80] to molecular association of the mesogens as shown in Figure 1.10(c). This type of packing can also be driven by steric considerations as the flexibility of the polymer backbone and spacer group length and flexibility largely dictate intermolecular interactions. Large bulky cholesterol units show different degrees of interdigitation[81,82] depending on the flexibility of the leader group used to attach them to the backbone.

Further information can be obtained from oriented samples. Alignment may be induced by magnetic, electric, or shear fields[74,76,83-89]. The alignment of the molecules allows for the translational and orientational distribution functions to be examined for both low molecular weight and polymeric compounds[74,90-95]. Aligned nematic patterns usually exhibit two wide-angle crescents due to lateral interactions among mesogens. If these reflections are on a horizontal line as shown in Figure 2.1, they are defined as equatorial reflections. Sometimes, a small-angle reflection is observed which is indicative of a pseudo-layered structure. Smectic-A materials exhibit, in addition to the equatorial wide-angle reflections, sharp perpendicular reflections. These reflections are defined as meridional reflections. This is indicative of the orthogonol nature of the molecular packing structure.
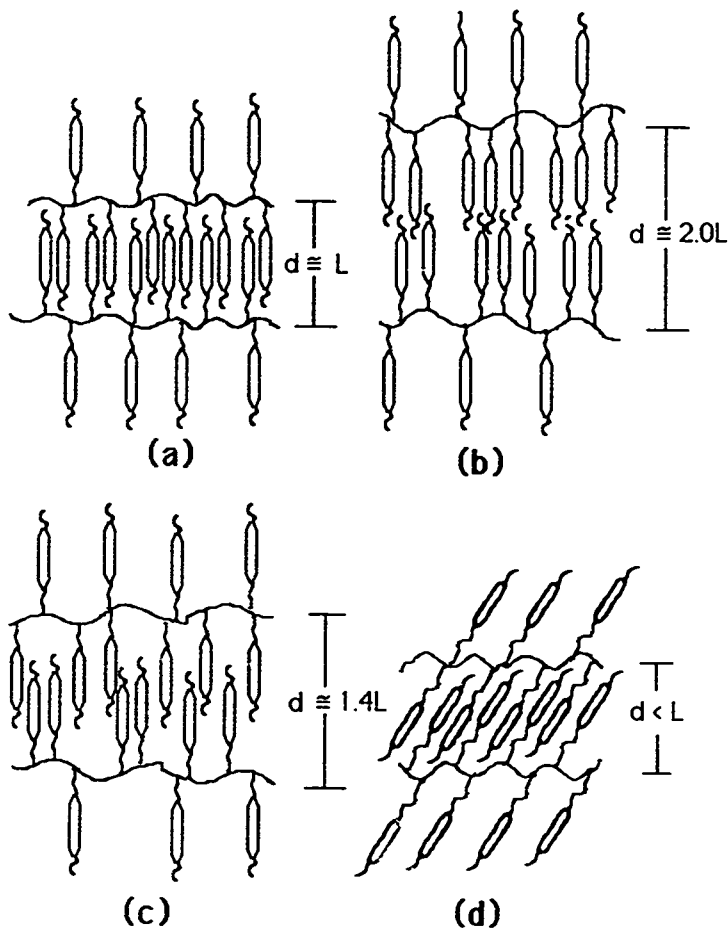
Figure 1.10: Packing schemes for liquid crystalline polymers fully interdigitated (a), not interdigitated (b), partially interdigitated (c) and tilted interdigitated (d)

Splitting of the small-angle reflections into four spots has been attributed to both cybotactic-nematic[86,96] and smectic-C packing structures[74,97,98]. A cybotactic-nematic is a weakly ordered nematic which, because of its tendency to layer pack, shows a strong first-order reflection. When the molecules are tilted within the layer planes, the first-order reflection is split into fourspots residing off-axis to the meridian. Determination of the tilt angle is straightforward and this can be used in deriving the molecular packing scheme. The cause of this local smectic-C-like packing scheme has been the subject of debate as DeVries[96] has pictured this as consisting of one smectic-C layer where the molecules are parallel to the nematic director but the layer boundaries are tilted at an angle, where Azaroff[90] instead suggested that they were due to finite stacks of parallel sheets. Highly aligned smectic-C compounds should not, however, exhibit a splitting of the small-angle reflection but instead the wide-angle reflection. Although the molecules are tilted within the layers causing four diffuse crescents at large angles, the layers themselves should be orthogonal and only two Bragg spots should be observed. However, a number of compounds exhibiting smectic-C phases (confirmed with POM) have exhibited split small-angle reflections. Alignment has also served an important role in the the examination of higher ordered smectic phases[94,95,99-103].

Due to the rigidity imparted by attachment to a backbone, liquid crystalline polymers generally exhibit more detail in their diffraction patterns. The second-order and in rare instances, third-order, reflections are more likely to be present for a polymer liquid

crystal than for its low molecular weight analog. This is attributed to a buffering effect of the random-coil backbones which, in general, are squeezed between the smectic layers. Due to these backbones, the structure is much more stratified and, therefore, more rigid. X-ray patterns for polymer LC's can also exhibit diffuse lines and spots which are related to local fluctuations from the mean structure[85,88,104-106]. Equally spaced diffuse lines have been attributed to uncorrelated periodic columns which are out of the mean position in the layer plane. The existence of this kind of disorder is evidence of the rigidity of the smectic layers in liquid crystalline polymers since such disorder is mainly observed in quasi-crystalline phases of small mesogenic molecules[88]. This behavior is typically only observed for smectic compounds.

Fiber diffraction patterns can also be used to probe the molecular architecture of liquid crystalline polymer systems[52,54,90,107,108]. Oriented fibers from liquid crystalline side-chain polymers are well suited for structural investigations by X-rays[10,109,110]. These patterns allow for a determination of phase type and the orientation of the mesogenic groups relative to the main-chain. Fibers are typically formed by drawing with tweezers strands of material from the anisotropic melt. Spin casting is also used to form fibers. Mechanical stretching of polymers typically yields fibers with the polymer backbones parallel to their axis. This results in small-angle reflections on the equator and crescents on the meridian. For tilted mesophases, these reflections are split into four spots. Some nematic materials exhibit diffraction patterns with the wide-angle crescents aligned

25

on the equator which indicates the polymer backbones are perpendicular to the fiber axis. Considering the internal stiffness of the macromolecules, this behavior is unusual for polymer systems[54].

Siloxane liquid crystalline polymers have exhibited, in addition to these general behaviors, several traits which are unusual. Recently, several groups have observed microphase separated[20,37,111] behavior which has been attributed to chemical differences between the hydrocarbon mesogens and siloxane backbones. Increasing the dimethylsiloxane concentration resulted in an increase in the layer spacing. This could be accounted for only by having a morphology consisting of distorted random-coil backbones squeezed between the hydrocarbon layers. Ordering of the backbones has also been observed although it is not fully understood[112,113]. Additional reflections have also been observed for siloxane systems and have been attributed to uncorrelated periodic columns[114-116], additional ordering[80], or contributions from the backbone.

Recently studied were smectic-A and smectic-B siloxane polymers which also exhibited unusual long-range ordering[117,118]. This behavior has also been attributed to a highly decoupled, phase-separated system. Electron density calculations indicated the observed d-spacings were due to a segregation into sublayers consisting of mesogenic cores, spacers, aliphatic tails, and squeezed backbones. The large number of layer reflections observed was related to the distribution of the polymer backbones. The large correlation length obtained using high-resolution X-ray diffraction

26

for another polysiloxane liquid crystal also supports the notion of long-range order for some systems[119].

1.4. Linear and Nonlinear Optical Applications

Linear optical applications of liquid crystals typically exploit the physical anisotropy of the dielectric tensor or index of refraction and the liquid-like properties of the material. The electro-optical effects of nematic liquid crystals have been exploited over the past 20 years in the fabrication of devices including alpha-numeric displays[120,121], multiplexing applications[122,123], matrix screens, image converters, radiation modulators, integrated optical devices[124,125], and light shutters[126]. The electro-optical and magneto-optical effects of nematic liquid crystals are investigated thoroughly in a book by Blinov[127]. Recently, a number of papers have investigated the use of nematic and chiral nematic liquid crystals as materials in laser optical systems[128-138].

Cholesteric materials have also received much attention due to their helical structure which exhibits optical activity. Optical properties such as birefringence, circular dichroism, and optical rotation are observed although the phenomena of selective reflection has been the most widely exploited. This occurs when the mesophase has been sheared, which transforms the packing behavior from a focal-conic texture (Figure 1.11(a)) to a Grandjean texture (b). The molecules in this latter texture all reside more or less parallel to the substrate surfaces (planar). Perpendicular to these surfaces, a macroscopic twist (discussed earlier) of the

molecules imparts unique optical properties. In this planar conformation, when circularly polarized light of the same helical sense as the material is incident parallel to the optic axis (Figure 1.11(c)), selective reflection occurs, as first described by deVries[139].

When the intrinsic pitch of the material is such that the wavelength given in Figure 1.11 resides in the visible region, highly colored materials are observed. Practically, these types of materials have been utilized mainly due to their highly iridescent appearance for a number of applications. These include notch filters[63,128,129,140,141], thermometry materials[142], decorative films[143,144], stereoscopic imaging materials[145], and wavelength modulating materials[146].

Smectic liquid crystals have also been utilized for optical display technologies. These materials possess different physical properties than nematics due to their layered structure. These mesophases typically exhibit better optical clarity than nematics due to a decrease in the optical scattering[147]. Advantages to using a smectic-A material with an upper temperature nematic phase are the smaller size and higher density of scattering centers and possible erasure of written areas[148].

(a)

(b)

Unpolarized $\rightarrow \lambda = \lambda_0$
Radiation

Reflected RH

Reflected RH

Optic
Axis

Right-handed
helices
$\lambda_0 = nP$

(c)

LH Radiation
Transmitted
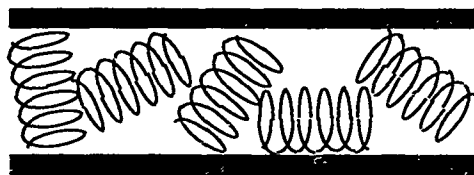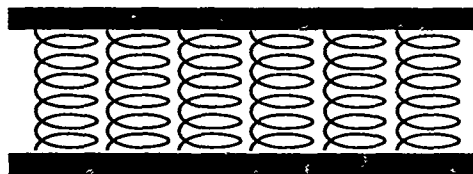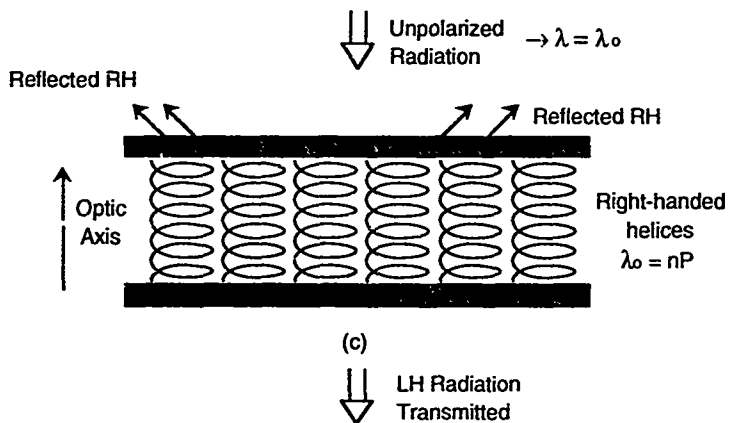
Figure 1.11: Focal-conic (a) and Grandjean (b) packing structures.
Selective reflection (c) from a Grandjean thin film. LH-left-
handedness, RH-right-handedness

Applications of these mesophases are again in display devices. Laser addressed smectic-A displays[149], thermal addressed smectic-A displays[150,151], and electrically addressed smectic-A displays[152] have been examined. The other major application of smectic materials is display devices based on the chiral smectic-C* phase which can exhibit ferroelectricity[153]. Ferroelectric liquid crystals exhibit spontaneous polarization[45,154,155] which results in fast electro-optic effects and memory capabilities in the case of surface stabilized structures[156]. These materials can exhibit a large permanent birefringence, low switching energy, low threshold switching voltages, and subsequently their optical properties are the center of attention[41,153,156-159].

Recently, a considerable amount of research has been performed in examining the nonlinear optical properties of organic materials[160,161]. The advent of the laser has allowed for large enough fields to induce second- and third-order optical effects in materials. These effects, the result of interactions between an electromagnetic field and the electron density of molecules, result in changes in phase, frequency, or amplitude. Mathematically, the total dielectric polarization of electrons in an electromagnetic field can be expressed as the following power series:

$$P_i = \chi^{(1)}{}_{ij}E_j + \chi^{(2)}{}_{ijk}E_jE_k + \chi^{(3)}{}_{ijkl}E_jE_kE_l + ... \qquad \text{Eq. 1.1}$$

The subscripts i, j, k, and l represent the Cartesian coordinate system, E's the cartesian components of the electric field, and $\chi^{(n)}$ represents the nth order susceptibility[161,162].

Currently, there is a tremendous amount of research being performed to optimize both $\chi^{(2)}$ and $\chi^{(3)}$. The former describes the quadratic susceptibility while the latter describes the cubic susceptibility. The former term is nonzero only if a noncentrosymmetric electron distribution is present. This stems from the fact that contributions from even- and odd-order terms to the polarization equation depend heavily on the symmetry of the medium. This is graphically demonstrated in Table 1.1 which indicates that orientational order of the molecules leads to higher responses for both second- and third-order processes.

Table 1.1[163]

Packing and relative responses for polar molecules

Packing[a]	Symmetry[b]	Order	Magnitude
	Centro	Second	None
	Noncentro	Second	Moderate
	Noncentro	Second	Strong
	Centro	Third	Weak
	Centro	Third	Strong

[a]- ↑- Refers to a polar molecule possessing a dipole moment
[b]- centrosymmetric or noncentrosymetric

31

The majority of work reported on organic materials has focussed on the second-order properties because of larger inherent NLO responses than third-order effects[160,161,164-166]. In general, one needs noncentrosymmetry, planarity, and delocalized electron systems[160,161,163] for good second-order response. Optically nonlinear side chain materials are very attractive for $\chi^{(2)}$ applications as they are easily processed, exhibit fast response times, and they are easily tailored on a molecular level[167]. Inorganic materials have several inherent limitations including poor responses at optical frequencies, difficult crystal growing, and poor processability.

A tremendous volume of research has been done on different matrices for second-order materials including guest-host, glassy polymer, and liquid crystal systems[160,161,167]. To eliminate the centrosymmetric behavior of the polar molecules, electric field poling has been extensively used[168-170]. Problems present are the temporal stability of the NLO response, solubility, and optical clarity. A large amount of work is currently being done to increase the temporal stability of alignment by a number of techniques including increasing the glass transition temperature and chemically crosslinking the system[169,171-175].

One of the most active areas of organic materials development involves liquid crystalline materials[175-183]. $\chi^{(2)}$ values on the order of 10^{-9} esu have been reported with response times on the order of microseconds[163]. Further work is needed in controlling the molecular orientation of the NLO molecules, understanding the temporal stability, and controlling the optical

properties (transparency). The possibility of designing high NLO response mesogens, their ease of dipolar orientation, and vitrification of the aligned state into a glass are promising. Extension to liquid crystalline elastomeric systems shows promise as shear can be used to generate optically clear, optically responsive thin films of siloxanes[184]. Liquid crystalline elastomers have also been shown to increase temporal stability of $\chi^{(2)}$ materials.

$\chi^{(3)}$ processes depend on intensity dependent refractive index changes. Much work has been done with highly conjugated materials including polyacetylene, organometallics, and fused polymer systems[166,185-191]. Their enhanced planar conjugation leads to enhanced third-order effects. These materials do not need to be noncentrosymmetric although alignment does lead to enhanced response values as shown in Table 1.1. This suggests the anisotropic nature of liquid crystalline polymers (both main- and side-chain) may be beneficial for these applications. Incorporation of third-order materials into main-chain liquid crystalline systems is currently being examined extensively. Their poor processing ability has led several groups to investigate side-chain liquid crystalline polymers[183,192,193] as possible $\chi^{(3)}$ materials.

Possible applications of nonlinear materials are shown in Table 1.2. Second-order materials have major applications in frequency doubling, phase modulation, and optical communication. Third-order materials have applications in frequency tripling, optical bistability, optical limiting and switching, and phase conjugation. The former materials are being examined primarily in

33

thin film geometries processed using Langmuir-Blodgett, spin coating and dipping techniques. Third-order materials can be used in both thin film form and in solution.

Table 1.2[194]

Applications of linear and nonlinear materials

Term	Effect	Applications
$\chi^{(1)}$	Refraction	Lenses Optical Fibers
$\chi^{(2)}$	Frequency doubling	2nd harmonic generation
	Frequency mixing	Frequency converters Parametric oscillators Spectroscopy
	Pockels effect	Q-switching Phase/amplitude modulators Beam deflectors
$\chi^{(3)}$	Frequency Tripling	3rd harmonic generation Spectroscopy
	DC Kerr effect	Variable phase retarder
	AC Kerr effet Raman scattering Brillouin Scattering	Fast switching Gratings-time resolved Agile wavelength generation
	Intensity-dependent refractive index Self-focusing Degenerate four-wave mixing	Optical bistability Optical limiters and switches Phase conjugation Real time holography

1.5 Proposed Research

Preliminary investigations with X-ray diffraction techniques performed on the cholesteric cyclic-siloxane system discussed earlier revealed an unusual packing behavior[195]. A model of the molecular packing which accounts for the measured d-spacings indicates a layered structure in which the siloxane units and the mesogens have phase separated. The observation of multiple X-ray reflections suggests structural complexity in these compounds. The appearance of periodic diffuse reflections at higher order multiples of the primary layer spacing was observed. Previous observations of these lines suggest a stratified mesophase as only smectic compounds have been observed to exhibit them. This may indicate that although the phase of the cyclic compounds was cholesteric, there is a psuedo-layered molecular structure present. A strong dependence of the diffraction behavior on composition was observed as compounds within a narrow range of compositions exhibited vastly different X-ray diffraction patterns. This was attributed to two competing types of molecular packing as will be discussed in Section III.

These compounds have also been observed by us to draw fibers which is unique for a low molecular weight material. The orientation of the lamellae, normal to the fiber axis, is much different than the transverse orientation generally exhibited by polymer liquid crystals. The formation of a psuedo-main chain polymer where the mesogens align with the fiber axis would account for the observed diffraction patterns.

35

The objective of this dissertation research is to examine in more detail the packing behavior exhibited by these cyclic siloxane-based liquid crystalline materials. No systematic structural investigation of any cyclic-based liquid crystalline structures has been performed. With linear polymers, the flexible backbone in conjunction with decoupled mesogenic side-chains enables the rotational and translational motions of the mesogens to be dictated primarily by excluded volume interactions between nearest neighbor mesogens. These interactions are the dominant intermolecular interactions responsible for mesomorphism in low molar mass liquid crystals[196,197]. For a ring system with mesogens attached by short spacer groups, intramolecular constraints might not allow certain kinds of intermesogen interactions. In addition, these ring systems contain three elements which have separately been shown to induce layer packing in liquid crystalline structures. These include a core that is chemically dissimilar to the attached mesogens[37,117,118,198,199], a high degree of lateral interaction among mesogens caused by the cyclic nature of this core[20,111,198,200], and the incorporation of large steroidal molecules[23,81,82,201]. The structure/property relationships for a number of synthesized materials will be examined in an attempt to further understand these controlling factors and determine their individual influences on the observed packing behavior and fiber drawing capabilities. Molecular packing will be examined with X-ray diffraction techniques. Trends with respect to the optical and thermal properties will be explored as a function of composition. The full compositional range of the cholesteric system initially

examined will be explored. Compatibility with the proposed packing model[195] will be examined. Linear analogs of these cyclic compounds will be synthesized and their structural similarities examined. Different ring sizes in addition to low molecular weight model compounds will also be examined. The leader group length and flexibility will be explored. Tendencies to form discotic phases with short leader groups as suggested in the literature will be invstigated. Chemical manipulation of these materials will allow a better understanding of how the chemical structure affects the optical properties and the macroscopic and microscopic packing behavior.

This research is funded by a 3-year doctoral fellowship awarded by the Air Force Office of Scientific Research. These investigations of this unique packing behavior will benefit the in-house research effort in the Wright Laboratory Laser Hardened Materials Branch (WL/MLPJ), Wright-Patterson AFB OH, which currently is investigating highly ordered molecular structures in organic materials for nonlinear optical purposes. Multifunctional materials will be synthesized using the structure/property relationships learned. The feasibility of using these compounds as nonlinear systems will also be addressed by attaching NLO chromphores to yield desired structural and thermal properties. Molecular modeling calculations will be performed to examine the global molecular conformation of the siloxane ring with respect to the pendant mesogens. Simulated X-ray meridional sections will be compared to the experimental data and trends with respect to conformation, interdigitation, and composition will be examined.

37

The following sections describe the research performed to examine these cyclic compounds in more detail. Section II describes the experimental procedures used in the investigation. Section III describes, in detail, the preliminary research on the commercial materials which served as the driving force behind the bulk of the research. Within this chapter, a molecular packing structure is proposed and the fiber drawing characteristics are detailed. Section IV describes the methodology employed in the synthesis of various analogs of these compounds. All characterization results for the precursors are presented here. Section V describes the structure/property relationships of the synthesized siloxane compounds. These include the effect of composition, ring size, leader group length, and siloxane functionality. Emphasis is placed on the WAXS and SAXS patterns obtained for sheared films and fibers. Real-time X-ray diffraction experimental results obtained at the Cornell High Energy Synchrotron Source (CHESS) are also presented here. Section VI describes several multifunctional compounds synthesized using the structure/property relationships obtained from the bulk of the research. These include novel photochromic and NLO siloxane compounds. Section VII briefly summarizes the molecular modeling results. Section VIII discusses the major conclusions obtained and recommendations for future work.

1.6 References

(1)   Reinitzer, F., *Monatsh. Chem.*, **9**, 421(1888).

(2)   *Thermotropic Liquid Crystals*, Gray, G.W., Ed., John Wiley and Sons; NY, **22**, pp 178, (1987).

(3)   Vertogen, G. and deJeu, W.H., *Thermotropic Liquid Crystals: Fundamentals*; Springer-Verlag; NY, pp 324, (1988).

(4)   *Liquid Crystals and Plastic Crystals*, Gray, G.W. and Winsor, P.A., Ed., Ellis Horwood; Chichester, **I and II**, (1978).

(5)   DeGennes, P.G., *The Physics of Liquid Crystals*; Clarendon Press; Oxford, (1974).

(6)   Goossens, N.J.A., *Mol. Cryst. Liq. Cryst.*, **12**, 237-244(1971).

(7)   Gray, G.W. and Goodby, J.W.G., *Smectic Liquid Crystals-Textures and Structures*; Leonard Hill; Glasgow, pp 224, (1984).

(8)   Finkelmann, H. and Rehage, G. in *Liquid Crystals and Polymers*, Springer; Berlin, Heidelberg, NewYork, Tokyo, **II/III,** pp 99-172, (1989).

(9)   Finkelmann, H. and Rehage, G., *Adv. in Polym. Sci.*, **60/61**, 101-171(1984).

(10)   Shibaev, V.P. and Plate, N.A., *Adv. in Polym. Sci.*, **60/61**, 184-252(1984).

(11)   *Liquid Crystalline Order in Polymers*, Blumstein, A., Ed., Academic Press; NY, (1980).

(12)   *Side Chain Liquid Crystal Polymers*, McArdle, C.B., Ed., Blackie; Glasgow, pp 448, (1989).

(13)   Finkelmann, H., Ringsdorf, H., Siol, W., and Wendorff, J. H., *Makromol. Chem.*, **179**, 829-832(1978).

(14)   Finkelmann, H. and Rehage, G., *Makromol. Chem., Rapid Commun.*, **1**, 31-34(1980).

(15)   Finkelmann, H. and Rehage, G., *Makromol. Chem., Rapid Commun.*, **1**, 733-740(1980).

(16)   Finkelmann, H., Kock, Hans-J., and Rehage, G., *Makromol. Chem., Rapid Commun.*, **2**, 317-322(1981).

(17)   Finkelmann, H. and Rehage, G., *Makromol. Chem., Rapid Commun.*, **3**, 859-864(1982).

(18)   Finkelmann, H., Kock, Hans-J., Gleim, W., and Rehage, G., *Makromol. Chem., Rapid Commun.*, **5**, 287-293(1984).

(19)   Ringsdorf, H. and Schneller, A., *Makromol. Chem., Rapid Commun.*, **3**, 557-562(1982).

(20)   Diele, S., Oelsner, S., Kuschel, F., Hisgen, B., and Ringsdorf, H., *Mol. Cryst. Liq. Cryst.*, **155**, 399-408(1988).

(21)   Nestor, G., Gray, G.W., Lacey, D., and Toyne, K.J., *Liq. Cryst.*, **6(2)**, 137-150(1989).

(22)   Kreuder, W. and Ringsdorf, H., *Makromol. Chem., Rapid Commun.*, **4**, 807(1983).

(23)   Shibaev, V.P. and Freidzon, Ya. S. in *Side Chain Liquid Crystal Polymers*, C. B. McArdle, Ed., Blackie; Glasgow, pp 260-286, (1989).

(24)   Gemmell, P.A., Gray, G.W., and Lacey, D., *Mol. Cryst. Liq. Cryst.*, **122**, 205-218(1985).

(25)   Gray, G.W., Lacey, D., Nestor, G., and White, M.S., *Makromol. Chem., Rapid Commun.*, **7**, 71-76(1986).

(26)   Becker, R.S., Chakravorti, S., and Das, S., *J. Chem. Phys.*, **90(5)**, 2802-2806(1989).

(27)   Gray, G.W., Hill, J.S., and Lacey, D., *Mol. Cryst. Liq. Cryst. Letters*, **7(2)**, 47-52(1990).

(28)   Gray, G W., Hill, J.S., and Lacey, D., *Mol. Cryst. Liq. Cryst.*, **197**, 43-55(1991).

40

(29) Hessel, F. and Finkelmann, H., *Polym. Bull.*, **15**, 349-352(1986).

(30) Rotz, U., Lindau, J., Weissflog, W., Reinhold, G., Unseld, W., and Kushel, F., *Mol. Cryst. Liq. Cryst.*, **170**, 185-193(1989).

(31) Adams, N.W., Bradshaw, J.S., Bayong, J.M., Markides, K.E., and Lee, M.L., *Mol. Cryst. Liq. Cryst.*, **147**, 43-60(1987).

(32) Sirlin, C., *Mol. Cryst. Liq. Cryst.*, **155**, 231-238(1988).

(33) Sauer, T. and Wegner, G., *Makromol. Chem., Macromol. Symp.*, **24**, 3303-309(1989).

(34) Percec, V. and Rodenhouse, R., *Macromolecules*, **22**, 4408-4412(1989).

(35) Percec, V. and Rodenhouse, R., *Macromolecules*, **22**, 2043-2047(1989).

(36) Percec, V. and Hahn, B., *Macromolecules*, **22**, 1588-1599(1989).

(37) Percec, V., Hahn, B., Ebert, M., and Wendorff, J.H., *Macromolecules*, **23**, 2092-2095(1990).

(38) Percec, V. and Tomazos, D., *Polymer*, , 1658-1662(1990).

(39) Ungar, G., Percec, V., and Rodenhouse, R., *Macromolecules*, **24**, 1996-2002(1991).

(40) Suzuki, T., Okawa, T., Ohnuma, T., and Sakon, Y., *Makromol. Chem., Rapid Commun.*, **9**, 755-760(1988).

(41) Dumon, M., Nguyen, H.T., Mauzac, M., Destrade, C., Achard, M.F., and Gasparoux, H., *Macromolecules*, **23**, 355-357(1990).

(42) Keller, P., *Mol. Cryst. Liq. Cryst.*, **157**, 193-202(1988).

(43) Rettig, W., Naciri, J., Shashidhar, R., and Duran, R.S., *Macromolecules*, **24**, 6539-6541(1991).

(44) Clark, N. and Lagerwall, S., US Patent #4,367,924, (1980).

(45) Clark, N.A. and Lagerwall, S.T., *Appl. Phys. Lett.*, **36**, 899(1980).

(46) Lagerwall, S. and Dahl, I., *Mol. Cryst. Liq. Cryst.*, **114**, 151(1984).

(47) Finkelmann, H., *Angew. Chem., Int. Ed. Engl.*, **26**, 816-82÷(1987).

(48) Schatzle, J. and Finkelmann, H., *Mol. Cryst. Liq. Cryst.*, **142**, 85(1987).

(49) Keller, P., *Chem. Mater.*, **2**, 3-4(1990).

(50) Gleim, W. and Finkelmann, H. in *Side Chain Liquid Crystal Polymers*, C. B. McArdle, Ed., Blackie; Glasgow, pp 287-308, (1989).

(51) Zentel, R., *Angew. Chem., Int. Ed. Engl. Adv. Mater.*, **28(10)**, 1407-1415(1989).

(52) Zentel, R., Schmidt, G.F., Meyer, J., and Benalia, M., *Liq. Cryst.*, **2**, 651-657(1987).

(53) Zentel, R. and Benalia, M., *Makromol. Chem.*, **188**, 665-674(1987).

(54) Zentel, R. and Strobl, G.R., *Makromol. Chem.*, **185**, 2669-2676(1984).

(55) Everitt, D.R.R., Care, C.M., and Wood, R.M., *Mol. Cryst. Liq. Cryst.*, **201**, 41-49(1991).

(56) Everitt, D.R.R., Care, C.M., and Wood, R.M., *Mol. Cryst. Liq. Cryst.*, **153**, 55-62(1987).

(57) Hahn, B. and Percec, V., *Mol. Cryst. Liq. Cryst. Inc. Nonlin. Opt.*, **157**, 125-150(1988).

(58) Percec, V. and Pugh, C. in *Side Chain Liquid Crystal Polymers*, C. B. McArdle, Ed., Blackie; Glasgow, pp 30-105, (1989).

(59) Richards, R.D.C., Hawthorne, W.D., Hill, J.S., White, M.S., Lacey, D., Semlyen, J.A., Gray, G.W., and Kendrick, T.C., *J. Chem. Soc., Chem. Commun.*, , 95-97(1990).

(60) Kreuzer, F.H. and Gawhary, G.W., U.S. Patent # 4,410,570, (1983).

(61) Kreuzer, F.H., Andrejewski, D., Haas, W., Haberle, N., Riepl, G., and Spes, R., *Mol. Cryst. Liq. Cryst.*, **199**, 345-378(1991).

(62) Chemie, Wacker, Provisional data sheet provided with the Wacker LC-Silicones, (March 1988).

(63) Tsai, M.L., Chen, S.H., and Jacobs, S.D., *Appl. Phys. Lett.*, **54(24)**, 2395-2397(1989).

(64) Ortler, R., Brauchle, C., Miller, A., and Riepl, G., *Makromol. Chem., Rapid Commun.*, **10**, 5-8(1989).

(65) Demus, D. and Richter, L., *Textures of Liquid Crystals*; Verlag Chemie; Weinheim, (1978).

(66) Noel, C. in *Side Chain Liquid Crystal Polymers*, C. B. McArdle, Ed., Blackie; Glasgow, pp 159-195, (1989).

(67) Viney, C. in *Liquid Crystalline Polymers*, R. A. Weiss and C. K. Ober, Ed., American Chemical Society; Washington, **ACS Symp. Series 435,** pp 241-255, (1990).

(68) Wunderlich, B. and Grebowicz, J., *Adv. Polym. Sci.*, **60/61**, 1(1984).

(69) Keller, A., Ungar, G., and Percec, V. in *Liquid Crystalline Polymers*, R. A. Weiss and C. K. Ober, Ed., American Chemical Society; Washington, **ACS Symp. Series 435,** pp 308-334, (1990).

(70) Azaroff, L.V., *Mol. Cryst. Liq. Cryst.*, **145**, 31-58(1987).

(71) Basu, S., Rawas, A., and Sutherland, H.H., *Mol. Cryst. Liq. Cryst.*, **132**, 23-28(1986).

(72) Diele, S., Brand, P., and Sackmann, H., *Mol. Cryst. Liq. Cryst.*, **16**, 105-116(1972).

(73) Plate, N.A., Freidzon, Ya.S., and Shibaev, V.P., *Pure Appl. Chem.*, **57(11)**, 1715-1726(1985).

(74) Kostromin, S.G., Sinitzyn, V.V., Talroze, R.V., Shibaev, V.P., and Plate, N.A., *Makromol. Chem., Rapid Commun.*, **3**, 809-814(1982).

(75) Lea·'>etter, A.J. in *Thermotropic Liquid Crystals*, G. W. Gray, Ed., John Wiley & Sons; Chichester, **22**, pp 1-27, (1987).

(76) Leadbetter, A.J., Frost, J.C., Gaughan, J.P., Gray, G.W., and Mosley, A., *J. Phys.*, **40**, 375-380(1979).

(77) Richardson, R.M. and Herring, N.J., *Mol. Cryst. Liq. Cryst.*, **123**, 143-158(1985).

(78) Allman, J.M., Richardson, R.M., Chan, L.K.M., Gray, G.W., and Lacey, D., *Liq. Cryst.*, **6(1)**, 31-38(1989).

(79) Brownsey, G.J. and Leadbetter, A.J., *Phys. Rev. Lett.*, **44(24)**, 1608-1611(1980).

(80) Sutherland, H.H. and Rawas, A., *Mol. Cryst. Liq. Cryst.*, **138**, 179-186(1986).

(81) Freidzon, Ya.S., Kharitonov, A.V., Shibaev, V.P, and Plate, N.A., *Eur. Polym. J.*, **21(3)**, 211-216(1985).

(82) Freidzon, Ya.S., Tropsha, Ye.G., Tsukruk, V.V., Shilov, V.V., Shibaev, V.P., and Lipatov, Yu.S., *Polym. Sci. USSR*, **29(7)**, 1505-1511(1987).

(83) Diele, S., Manke, S., Weibflog, W., and Demus, D., *Liq. Cryst.*, **4(3)**, 301-307(1989).

(84) Diele, S., Naumann, M., Kuschel, F., Reck, B., and Ringsdorf, H., *Liq. Cryst.*, **7(5)**, 721-729(1990).

(85) Davidson, P. and Levelut, A.M., *J. Phys.*, **49**, 689-695(1988).

(86) Chistyakov, I.G. and Charkowsky, W.M., *Mol. Cryst. Liq. Cryst.*, **7**, 269-277(1969).

(87) Chistyakov, I.G., Schabischev, L.S., Jarenov, R.I., and Gusakova, L.A., *Mol. Cryst. Liq. Cryst.*, **7**, 279-284(1969).

(88) Davidson, P., Keller, P., and Levelut, A.M., *J. Phys.*, **46**, 939-946(1985).

(89) Leadbetter, A.J. and Norris, E.K., *Mol. Phys.*, **38(3)**, 669-686(1979).

(90) Azaroff, L.V., *Mol. Cryst. Liq. Cryst.*, **60**, 73-98(1980).

(91) Haase, W., Fan, Z.X., and Muller, H.J., *J. Chem. Phys.*, **89(5)**, 3317-3322(1988).

(92) Fain, Z.X., Buchner, S., Haase, W., and Zachmann, H.G., *J. Chem. Phys.*, **92(8)**, 5099-5106(1990).

(93) Mandeal, P., Mitra, M., Paul, S., and Paul, R., *Liq. Cryst.*, **2(2)**, 183-193(1987).

(94) Leadbetter, A.J. and Wrighton, P.G., *J. Phys.*, **3**, 234-242(1979).

(95) Leadbetter, A.J., Tucker, P.A., Gray, G.W., and Tajbaksh, A.R., *Liq. Cryst.*, **8(1)**, 1-12(1990).

(96) deVries, A., *Mol. Cryst. Liq. Cryst.*, **10**, 219-236(1970).

(97) Tsukrok, V.V., Shilov, V.V., Konstantinov, I.I., Lipatov, Yu.S., and Amerik, Yu.B., *Eur. Polym. J.*, **18**, 1015-1020(1982).

(98) Ouchi, Y., Lee, J., Takezoe, H., Fukuda, A., Kondo, K., Kitamura, T., and Mukoh, A., *Jap. J. Appl. Phys.*, **27(5)**, L725-L728(1988).

(99) Klamke, W., Fan, X.J., Hasse, W., Muller, H.J., and Gallardo, H., *Ber. Buns. Phys. Chem.*, **93**, 478-482(1989).

(100) Gierlotka, S., Przedmojski, J., and Pura, B., *Liq. Cryst.*, , 1989).

(101) Leadbetter, A.J., Gaughan, J.P., Kelly, B., Gray, G.W., and Goodby, J., *J. Phys.*, **40(4)**, 178-184(1979).

(102) Levelut, A.M., Germain, C., Keller, P., Liebert, L., and Billard, J., *J. Phys.*, **44(5)**, 623-629(1983).

(103) Diele, S., Brand, P., and Sackmann, H., *Mol. Cryst. Liq. Cryst.*, **17**, 163-169(1972).

(104) Decobert, G., Soyer, F., Dubois, J.C., and Davidson, P., *Polym. Bull.*, **14**, 549-556(1985).

(105) Doucet, J. in *The Molecular Physics of Liquid Crystals*, G. R. Luckhurst and G. W. Gray, Ed., Academic Press; NY, Ch. 14, (1979).

(106) Esselin, S., Bosio, L., Noel, C., Decobert, G., and Dubois, J.C., *Liq. Cryst.*, **2**, 505(1987).

(107) Freidzon, Ya. S., Talroze, R.V., Boiko, N.I., Kostromin, S.G., Shibaev, V.P., and Plate, N.A., *Liq. Cryst.*, **3(1)**, 127-132(1988).

(108) Decobert, G., Dubois, J.C., Esselin, S., and Noel, C., *Liq. Cryst.*, **1(4)**, 307-317(1986).

(109) Alexander, L.E., *X-ray Diffraction Methods in Polymer Science*; Wiley-Interscience; NY, (1969).

(110) Gray, G. W. and Winsor, P. A., *Liquid Crystals and Plastic Crystals: Physico-Chemical Properties and Methods of Investigation*; Ellis; Horwood, **2**, pp 62ff, (1974).

(111) Diele, S., Oelsner, S., Kuschel, F., Hisgen, B., Ringsdorf, H., and Zentel, R., *Makromol. Chem.*, **188**, 1993-2000(1987).

(112) Zugenmaier, P. and Mugge, J., *Makromol. Chem., Rapid Commun.*, **5**, 11-19(1984).

(113) Mugge, J. and Zugermaier, P., *Mol. Cryst. Liq. Cryst.*, **113**, 193(1988).

(114) Sutherland, H.H. and Gasgous, B., *Liq. Cryst.*, **7(2)**, 181-183(1990).

(115) Adib, Z. A., Ph.D. Thesis, University of Hull, (1987).

(116) Sutherland, H.H., Adib, Z.A., Gasgous, B., and Nestor, G., *Mol. Cryst. Liq. Cryst.*, **155**, 327-336(1988).

(117) Davidson, P., Levelut, A.M., Achard, M.F., and Hardouin, F., *Liq. Cryst.*, **4(5)**, 561-571(1989).

(118) Davidson, P. and Levelut, A.M., *J. Phys.*, **50**, 2415-2430(1989).

(119) Keller, E.N., Halfon, R., Nachaliel, E., Davidov, D., and Zimmermann, H., *Phys. Rev. Lett.*, **61(10)**, 1206-1209(1988).

(120) Elliot, G., *Microele.*, **7**, 19(1976).

(121) Goodman, L.A., *RCA Rev.*, **35**, 447(1974).

(122) Raynes, E.P., *IEEE Trans. Elec. Dev.*, **ED-26**, 1116(1979).

(123) Toriyama, K., Suzuki, K., Nagagoni, T., Ishibashi, T., and Odawara, K., *J. Phys.*, **40**, 317(1979).

(124) Sheridan, J.P., Schnur, J.M., and Giallorenzi, T.G., *Appl. Phys. Lett.*, **22**, 560(1973).

(125) Channin, D.J., *Appl Phys. Lett.*, **22**, 365(1973).

(126) Drzaic, P.S., *J. Appl. Phys.*, **60**, 6(1986).

(127) Blinov, L.M., *Electro-optical and Magneto-optical Properties of Liquid Crystals*; John Wiley and Sons; NY, pp 341, (1983).

(128) Jacobs, S.D., Cerqua, K.A., Marshall, K.L., Schmid, A., Guardalben, M.J., and Skerrett, K.J., *J. Opt. Soc. Am., B*, **9**, 1962-1978(1988).

(129) Jacobs, S.D., *J. Fus. Ener.*, **5(1)**, 65-75(1986).

(130) Bleha Jr., W. P., U.S. Patent #4,343,535, (1982).

(131) Lee, J. C., Jacobs, S. D., and Schmid, A., *Mol. Cryst. Liq. Cryst.*, **150b**, 617-629(1987).

(132) Song, J-W., Shin, S-Y., and Kwon, Y-S., *Appl. Opt.*, **23(10)**, 1521-1524(1989).

(133) Bly, V. T., U.S. Patent # 4,423,927, (1984).

(134) Santamato, E., Daino, B., Romagnoli, M., Settembre, M., and Shen, Y.R., *Mol. Cryst. Liq. Cryst.*, **143**, 89-100(1987).

(135) Lee, J.C., Kelly, J.H., Smith, D.L., and Jacobs, S.D., *IEEE J. Quant. Elect.*, **24(11)**, 2238-2242(1988).

(136) Ichimura, K., Suzuki, Y., Seki, T., and Kawanishi, Y., *Makromol. Chem., Rapid Commun.*, **10**, 5-8(1989).

(137) Lee, J-C., Schmid, A., and Jacobs, S.D., *Mol. Cryst. Liq. Cryst.*, **166**, 253-265(1989).

(138) Hacker, H., Lefkowitz, I., and Lontz, R., *Appl. Opt.*, **19(19)**, 3257-3259(1980).

(139) DeVries, H.L., *Acta. Cryst.*, **4**, 219-226(1951).

(140) Adams, J., *J. Appl. Phys.*, **42(10)**, 4096(1971).

(141) Tsutsui, T. and Tanaka, R., *Polym. Commun.*, **21**, 1351-1352(1980).

(142) Parker, R., US Pat.# 3822594, (1974).

(143) Makow, D., *Mol. Cryst. Liq. Cryst.*, **123**, 347-353(1985).

(144) Makow, D., *Color Research and Application*, **11(3)**, 205-208(1986).

(145) Makow, D., *Mol. Cryst. Liq. Cryst.*, **99**, 117-122(1983)

(146) Umeton, C., Bartolino, R., Cipparrone, G., Xu, F., Ye, F., and Simoni, F., *Mol. Cryst. Liq. Cryst.*, **144**, 323-336(1987).

48

(147) Casagrande, C., Fabre, P., Veyssie, M., Weill, M., and Finkelmann, H , *Mol. Cryst. Liq. Cryst.*, **113**, 193(1984).

(148) Coates, D. in *Thermotropic Liquid Crystals*, G. W. Gray, Ed., John Wiley & Sons; Chichester, **22,** pp 99-119, (1987).

(149) Kahn, F.J., *Appl. Phys. Lett.*. **22**, 111(1973).

(150) LeBerre, S., Hareng, M., Hehlen, R., and Perbet, J.N., *Displays*, 349(1981).

(151) Dubois, J.C., *Ann. Phys.*, **3**, 131(1978).

(152) Coates, D., Crossland, W.A., Morrissy, J.H., and Needham, B., *J. Phys. D, Appl. Phys.*, **11**, 2025(1978).

(153) LeBarny, P. and Dubois, J. C. in *Side Chain Liquid Crystal Polymers*, C. B. McArdle, Ed., Blackie; Glasgow, pp 130-158, (1989).

(154) Clark, N.A. and Lagerwall, S.T., *Ferroelec.*, **58**, 389(1984).

(155) Goodby, J.W., *Science*, **231**, 350-355(1986).

(156) LePesant, J.P., Perbet, J.N., Mourey, B., Hareng, M., Decobert, G., and Dubois, J.C., *Mol. Cryst. Liq. Cryst.*, **129**, 61-74(1985).

(157) Hori, K., *Mol. Cryst. Liq. Cryst. Letters*, **82**, 13-17(1982).

(158) Hori, K.., *Mol. Cryst. Liq. Cryst.*, **100**, 75-83(1983).

(159) Aronishidze, S.N , Chilaya, G.S., Kushnirenko, M.N., and Osadchii, S.M., *Mol. Cryst. Liq. Cryst.*, **102**, 187-192(1984).

(160) *Nonlinear Optical Properties of Organic and Polymeric Materials*, Williams, D.J., Ed., American Chemical Society; Washington, **ACS Symp. Ser. 233**, pp 212, (1985).

(161) *Nonlinear Optical Properties of Organic Molecules and Crystals*, Chemla, D.S. and Zyss, J., Ed., Academic Press; NY, **I & II**, (1987).

(162) Mills, D.L., *Nonlinear Optics*; Springer-Verlag; Berlin, pp 184, (1991).

(163) Boyle, M.E. and Cozzens, R.F., *Eye/Sensor Protection Against Laser Irradiation: Organic Nonlinear Optical Materials*, Naval Research Lab, Report 6482, (1989).

(164) *Advances in Materials for Active Optics*, Musikant, S., Ed., SPIE; Washington, 567, (1985).

(165) *Molecular and Polymeric Optoelectronic Materials: Fundamentals and Applications*, Khanarian, G., Ed., SPIE; Washington, 682, (1986).

(166) *Nonlinear Optical and Electroactive Polymers*, Prasad, P. and Ulrich, D., Ed., Plenum Press; NY, (1988).

(167) Mohlmann, G.R. and van der Vorst, C.P.J.M. in *Side Chain Liquid Crystal Polymers*, C. B. McArdle, Ed., Blackie; Glasgow, pp 330-356, (1989).

(168) Watanbe, T., Yoshinaga, K., Fichou, D., and Miyata, S., *J. Chem. Soc., Chem. Commun.*, , 2501-251(1988).

(169) Ye, C., Marks, T.J., Yang, J., and Wong, G.K., *Macromolecules*, **20**, 2322-2324(1987).

(170) Singer, K D., Sohn, J.E., King, L.A.. Gordon, H.M., Katy, H.E., and Dirk, C.W., *J. Opt. Soc. Am., B.*, **6(7)**, 1339-1350(1989).

(171) Hampsch, H.L, Yang, J., Wong, G.K., and Torkelson, J.M, *Macromolecules*, **23(15)**, 3628-3654(1990).

(172) Hampsch, H.L, Torkelson, J.M., Bethke, S.J., and Grubb, S.G., *J. Appl. Phys.*, **67(2)**, 1037-1041(1990).

(173) Hampsch, H.L., Yang, J., Wong, G.K., and Torkelson, J.M., *Macromolecules*, **23(15)**, 3640-3647(1990).

(174) Mandal, B.K., Chen, Y.M., Jeng, R.J., Takasahi, T., Huang, J.C., Kamar, J.. and Tripathy, S., *Eur. Polym. J.*, **27(7)**, 735-741(1991).

(175) Meredith, G.R., VanDusen, J.G., and Williams, D.J., **15(5)**, 1385-1389(1982).

(176) LeBarny, P., Ravaux, G., Dubois, J.C., Parneix, J.P., Njeumo, R., Legarand, C., and Levelut, A.M., in *Molecular and Polymeric Optoelectronic Materials: Fundamentals and Applications*, SPIE, **682**, G. Khanarian Ed., pp. 56, (1986).

(177) Stamatoff, J.B., Buckley, A., Calundann, G., Choe, E.W., DeMartino, R., Khanarian, G., Leslie, T., Nelson, G., Stuetz, D., Teng, C.C., and Yoon, H.N., in *Molecular and Polymeric Optoelectronic Materials: Fundamentals and Applications*, SPIE, **682**, G. Khanarian Ed., pp. 85, (1986).

(178) Griffin, A.C., Bhatti, A.M., and Hung, R.S.C., in *Molecular and Polymeric Optoelectronic Materials: Fundamentals and Applications*, SPIE, **682**, G. Khanarian Ed., pp. 65, (1986).

(179) McCulloch, I.A. and Bailey, R.T., *Mol. Cryst. Liq. Cryst.*, **200**, 157-165(1991).

(180) Fouquey, C., Lehn, J. M., and Malthete, J., *J. Chem. Soc., Chem. Commun.*, 1424-1426(1987).

(181) Noel, C., Friedrich, C., Leonard, V., LeBarny, P., Ravaux, G., and Dubois, J.C., *Makromol. Chem., Macromol. Symp.*, **24**, 282-301(1989).

(182) Lo, S.K. and Galarneau, L.M., *Mol. Cryst. Liq. Cryst*, **201**, 137-145(1991).

(183) Ford, W.T., Bautista, M., Zhao, M., Reeves, R.J., and Powell, R C., *Mol. Cryst. Liq. Cryst.*, **198**, 351-356(1991).

(184) Hirschmann, H., Meier, W., and Finkelmann, H., in *Photopolymer Device Physics, Chemistry, and Applications II*, San Diego, CA, SPIE, **1559**, R. A. Lessard Ed., (1991).

(185) Prasad, P.N., *Roy. Soc. Acad., Spec. Publ.*, 264-274(1990).

(186) Prasad, P.N., *Polymer*, **32(10)**, 1746-1751(1991).

(187) Wolfe, J.F., in *Molecular and Polymeric Optoelectronic Materials; Fundamentals and Applications*, SPIE, **682**, G. Khanarian Ed., pp. 70, (1986).

(188) Prasad, P., *Thin Solid Films*, **152**, 275-294(1987).

(189) Ulrich, D.R., *Polymer*, **28(4)**, 533-542(1987).

(190) Ulrich, D. R., *Mol. Cryst. Liq. Cryst.*, **160**, 1(1988).

(191) Porter, P. L., Guha, S., Kang, K, and Frazier, C. C., *Polymer*, **32(10)**, 1756-1760(1991).

(192) McEwan, K.J., Harrison, K.J., and Madden, P.A., *Inst. Phys. Conf. Ser. 103*, 193-196(1989).

(193) Madden, P.A., Saunders, F.C., and Scott, A.M., *Opt. Acta.*, **33**, 405-417(1986).

(194) Kolinsky, P.V. and Jones, R.J., *GEC J. Res.*, **7(1)**, 46-58(1989).

(195) Bunning, T.J., Klei, H.E., Samulski, E.T., Crane, R.L., and Linville, R.J., *Liq. Cryst.*, **10(4)**, 445-456(1991).

(196) Cotter, M.A., *Mol. Cryst. Liq. Cryst.*, **97**, 29(1984).

(197) Gelbart, W.A., *J. Phys. Chem.*, **86**, 4298(1982).

(198) Westphal, G., Diele, S., Madicke, A., Kushel, F., Scheim, F., Rohlmann, K., Hisgen, B., and Ringsdorf, H., *Makromol Chem., Rapid Commun.*, **9**, 489-493(1988).

(199) Lipatov, Yu.S., Tsukruk, V.V., and Shilov, V.V., *Polym. Commun.*, **24(3)**, 75-77(1983).

(200) Eidenschink, R., Kreuzer, F.H., and Dejeu, W.H., *Liq. Cryst.*, **8(6)**, 879-884(1990).

(201) Freidzon, Y. S. in *Polymeric Liquid Crystals*, A. Blumstein, Ed., Plenum Press; New York, (1985).

Section II

EXPERIMENTAL METHODS

This section describes the general techniques and analytical equipment used during this dissertation research. The details of some techniques are described where most appropriate. All synthetic techniques and starting materials are described in Section IV.

2.1 X-ray Diffraction

X-ray diffraction experiments were performed on either a Rigaku RU-300 (operated at 12kW at 40kV, 300mA) or a Rigaku RU-200 (operated at 12kW at 60 kV, 200mA) rotating anode generator using $CuK\alpha$ radiation (graphite monochromator). Transmission photographs were recorded with an evacuated Statton camera (flat film) using various sample-to-film distances including 50 mm, 72.9 mm and 170 mm. Several samples were also examined with a Philips X-ray microcamera equipped with a 50 µm collimator. D-spacing calibrations were performed with a National Bureau of Standard's Reference Material 640 (Si powder). Some elevated temperature diffraction from within liquid crystalline mesphases was performed on capillaries packed with the powered material in a homemade heating block fitted to the inside of the Statton camera. The heater was powered with a variable voltage source and temperature was monitored with an Omega 650 Type J thermocouple. Optical densities were extracted from the X-ray films using a Joyce-Loebl Scandig 3 densitometer.

53

No conversion of this data to intensity was performed. When maximum values of the optical density are compared, films with values less than 1.0, if available, were compared to ensure linearity in the measurements. Therefore, intensities (optical densities) should be viewed qualitatively as they have not been corrected for Lorentz or polarization factors.

Film samples were run in two separate geometries designated edge and normal as shown in Figure 2.1. They were mounted directly on the collimator. Film thicknesses were 0.5-1.0 mm and the edge samples were 1-2 mm deep. Fiber samples were run in the geometry shown in Figure 2.2. Fiber diameters ranged from $300\mu m$ to a few millimeters. These were also mounted on the colllimator.
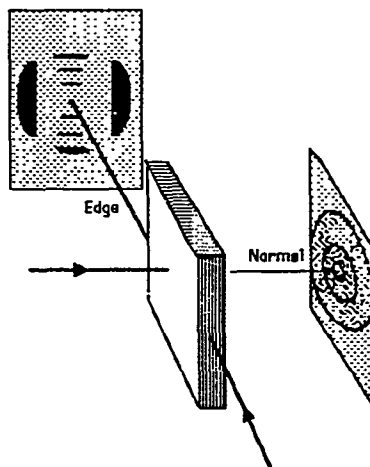
Figure 2.1: Film edge and normal X-ray orientations
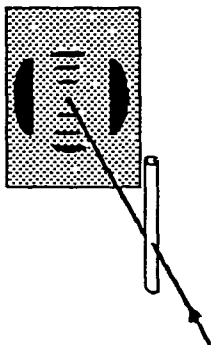
Figure 2.2: X-ray diffraction geometry used with fibers

The bulk of the elevated temperature diffraction (up to 250ºC) and electric field studies were performed at the Cornell High Energy Synchrotron Source (CHESS) on the Al-beam line with the assistance of Dr. C.K. Ober. Samples had been cleared once before data aquisition. Flat-film photographs (perpendicular to the beam) were taken at sample-to-film distances ranging from 40-150 mm. Real-time electric field alignment experiments were possible due to the very intense and highly focussed radiation source. Sample cells consisted of two 0.5 mm electrodes separated by a gap of 100-200 µm contained within a Mettler FP82HT hotstage as shown in Figure 2.3. Samples were melted between the electrodes by heating above the clearing temperatures. Electric fields up to 170V were applied at AC frequencies ranging from 1 to 10,000 Hz. The resulting diffraction patterns were recorded with an image intensifier and digital camera or with flat film when greater resolution was

55

required. A sample-to-film distance of 80 mm was used with exposure times of 15-45 seconds.
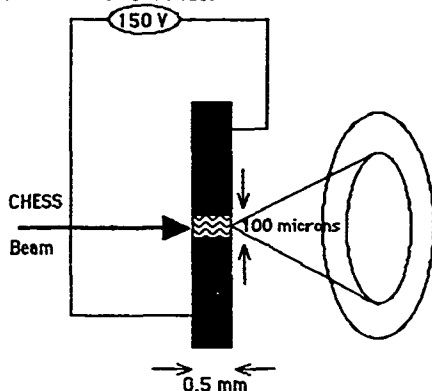
Figure 2.3: Schematic of electrodes for real-time X-ray diffraction experiments

Films of the siloxanes were obtained by shearing the material between two Teflon sheets sandwiched between two microscope slides. Film shearing was performed in the liquid crystalline phase at elevated temperatures of 130-150°C on a hot plate. Upon removal of the film from the heat source, ambient air cooling quenched the material into a glass thus freezing in the liquid crystalline order.

Fibers were drawn by pulling strands of various diameters with tweezers from the liquid crystalline melt (130-150°C). These fibers quickly cooled in air. Although brittle at room temperature due to their glassy texture, fibers of long length (tens of meters) could be drawn from the liquid crystal mesophase rather easily.

56

2.2 Thermal Analysis

Differential scanning calorimetry (DSC) measurements were carried out on either a Perkin-Elmer DSC-2C equipped with a Thermal Analysis Data Station or a Dupont 910 DSC equipped with an OMNITHERM ATVANTAGE II controller. All reported transition values were taken from the second of two heating scans.

Thermal Gravimetric Analysis (TGA) was performed on a Dupont TGA controlled with an OMNITHERM 35053 controller. Samples were run in air or helium. Mass spectroscopy was performed on the degradation products by Systems Research Laboratories through MLBP (Polymer Branch).

2.3 Optical Microscopy

Polarized optical microscopy (POM) was performed on a Nikon Optiphot-Pol microscope equipped with a Microflex UFX-II photomicrographic attachment. Photographs were taken with either a Nikon FX-35WA 35-mm camera or a Polaroid Model 545 4x5 film holder. Other color prints were obtained with a Javelin color video thermal printer. A Panasonic WV-6000 color video camera attached to the microscope was used to obtain images for the thermal printer.

Hot stage microscopy was performed with a Lietz Vario-Orthomat ORTHOLUX II POL-BK microscope and a Mettler FP82HT hot stage controlled with a FP80HT central processor. Powdered samples were placed between two cover glass slips and heated to the desired temperature. Samples were cleared before examining their liquid crystalline textures.

57

2.4 UV-VIS-NIR Spectroscopy

The visible optical properties (selective reflection and scattering) were examined with a Perkin-Elmer Lambda 4B UV/VIS spectrophotometer and a Lambda 9 UV-VIS spectrophotometer. The Lambda 4B was equipped with an integrating sphere which allowed th. specular reflection to be measured. The optical properties in the near infrared region were examined with a Perkin-Elmer Lambda 9 UV/VIS/NIR spectrophotometer.

Samples to be examined were sheared between microscope slides on a hot plate at 150°C. The microscope slides were cleaned with toluene before use. The siloxane material was sheared to align the cholesteric helices and then cooled in air. Spectra were taken with the light propagation direction normal to the glass slides. A blank substrate spectrum was subtracted from the sample spectrum. Films (foils) of the Wacker LC-Silicones sheared on black paper obtained from F.H. Kruezer were examined in the reflection mode. Sheared samples between glass slides were measured in the absorption mode. Since these siloxane materials do not absorb in the visible, the absorption spectra were almost identical to the reflection spectra. All slides were reexamined after annealing for 72 hours at 120-130°C.

2.5 Scanning and Transmission Electron Microscopy (SEM/TEM)

SEM was performed on either an HP550B Coates and Welter field emission SEM equipped with a cold cathode (at the University of Connecticut) or an Hitachi S-900 SEM equipped with a field

58

emission gun and an immersion lens system (at MLLM characterization facility). This latter instrument allowed for very low operating voltages to be employed enabling microstructures to be recorded without having to coat a conductive layer of metal on the surface to be examined. A freeze-fracture technique was employed with both film and fiber samples. This consisted of immersing the sample in liquid nitrogen followed by fracturing along the desired axis. Annealed fiber samples were prepared by floating them on water at 70-80°C until the desired shrinkage was obtained. These fibers were then cooled in ice water and fractured.

TEM was performed with a Philips 300 electron microscope. Samples investigated were embedded within an epoxy matrix and thin samples (<1000 Å) were microtomed with a diamond knife. The original epoxy system needed an elevated temperature (60-70°C) to cure. This heating was observed to shrink the sample thereby destroying the alignment of the cholesteric helices. A second room temperature curing epoxy system was subsequently employed in the preparation of the TEM samples.

2.6 Other Experimental Methods

FTIR spectra were recorded on a Perkin Elmer 1725X FT-IR spectrometer and analyzed with Perkin Elmer IRDM software. Proton NMR measurements were performed on a Bruker AM-360 machine located at the Wright State University Cox Heart Institute. Gas chromatography. was recorded with a Perkin Elmer 8600 Gas Chromatograph using a capillary column. Elemental analyses were performed by the microanalytical services branch, MLS.

Section III

COMMERCIAL CYCLIC SILOXANES

3.1 Introduction

As discussed in the Introduction, the initial materials examined were commercially available from Wacker Chemie and supplied by Dr. F.H. Kreuzer of the Consortium fur elektrochemische Industrie GmbH. Due to the chiral nature of these cholesterol-based molecules, they form cholesteric liquid crystalline materials which reflect 100% right-handed circularly polarized light at a given wavelength. This selective reflection wavelength can be varied from the ultraviolet to the near infrared by changing the relative proportions of the biphenyl- and cholesterol-based mesogens attached to the siloxane ring.

Preliminary investigations were performed on four separate materials with reflection wavelengths ranging from 440 nm to 1190 nm. As described in their US Patent[1], little effort was made to purify these materials. It has been shown[2,3] that these materials consist of a variety of ring sizes with 5 being the predominant ring size. The presence of unreacted alkene[4,5] in the final products has also been observed experimentally and has been removed with supercritical carbon dioxide extraction.

This section details the structural, thermal, and optical properties of these Wacker LC-Silicone materials. These results will be used as the basis of comparison for the physical properties of the synthesized siloxanes discussed later. Emphasis is placed on the preliminary X-ray diffraction results which served as the initial

driving force behind this research. These data were used to formulate a molecular packing model[6] which will be examined in detail in subsequent sections.

3.2 Phase Behavior

The glass transition (T_g) and clearing temperatures (T_{cl}) for the four Wacker LC-Silicone products examined are listed in Table 3.1. Values obtained, 40-50°C for the T_g and 180-210°C for the T_{cl}, are consistent with reported[7] data.

Table 3.1

Thermal transitions of Wacker LC-Silicones

Compound	X_{chol}	λ_{max} (nm)	T_g (°C)	T_{cl} (°C)
1	0.40	440	44.0	196.2
2	0.36	515	45.1	206.3
3	0.31	610	42.4	191.3
4	0.14	1190	47.3	182.9

TGA revealed a three-step degradation process in air. Mass spectroscopy of the degradation products revealed fragments were released primarily at two temperatures, 335°C and 440°C. Comparison between compounds 1 and 4 revealed that 11% of the initial sample weight for compound 4 and 55% of the initial sample weight for compound 1 were lost at 335°C. This difference was attributed to the increased mole fraction of cholesterol in

61

compound 1. Breakup of the cholesterol-containing pendant groups account for the lower temperature fragments. Also noted was the poor agreement between weight loss and volatile-product detection in compound 1 which is an indication of sublimation. This suggests cholesterol mesogens are less stable than the biphenyl mesogens when heated in air.

Optical microscopy was used to examine the phase behavior of these materials as well as the homogeneity of the isotropic liquids. Crossed polarizing microscopy clearly indicated one of two types of textures at elevated temperatures characteristic of cholesteric materials[8]. Figure 3.1 shows a typical focal-conic texture characteristic of the random orientation of the helical axes through the film. Upon movement of the top cover glass slip, the helices orient to a Grandjean (planar) state. Under crossed polarizers, this aligned packing orientation exhibited a characteristic "oily" texture[8] as shown in Figure 3.2.

The homogeneity of these materials was examined qualitatively by examining the texture of the liquid crystalline and isotropic phases. These examinations revealed the presence of foreign particles within the bulk of the material. These foreign particles can act as scattering and nucleation sites which disrupt the relative orientation of the helices and thus the optical performance of these materials.

Figure 3.1: Characteristic focal-conic texture of a cholesteric phase (200 X)
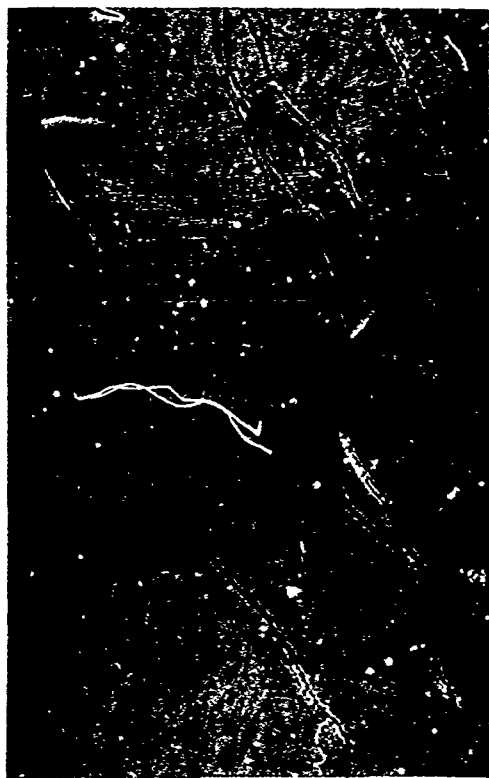
Figure 3.2: Characteristic planar texture of a cholesteric phase (200 X)

Microscopy was also used to examine the birefringence of fibers drawn from these materials. The ability of this low molecular weight compound to draw into fibers is surprising as typically this behavior is found only in polymeric systems. Fibers were drawn from the melt with a spatula or tweezers and long lengths (>10 ft) could easily be obtained. These were quenched by the ambient air and the resulting fibers were brittle. Under crossed polarizers, fibers of all four materials were birefringent. As Figure 3.3 shows, when the stage is rotated through 45°, the fibers originally extinct become light and those light become extinct. Also noted was a dependence of the relative magnitude of this birefringence on the composition. Compound 4 exhibited a much lower birefringence than the other compounds. The ability to draw fibers was also noted to be much poorer for this compound.
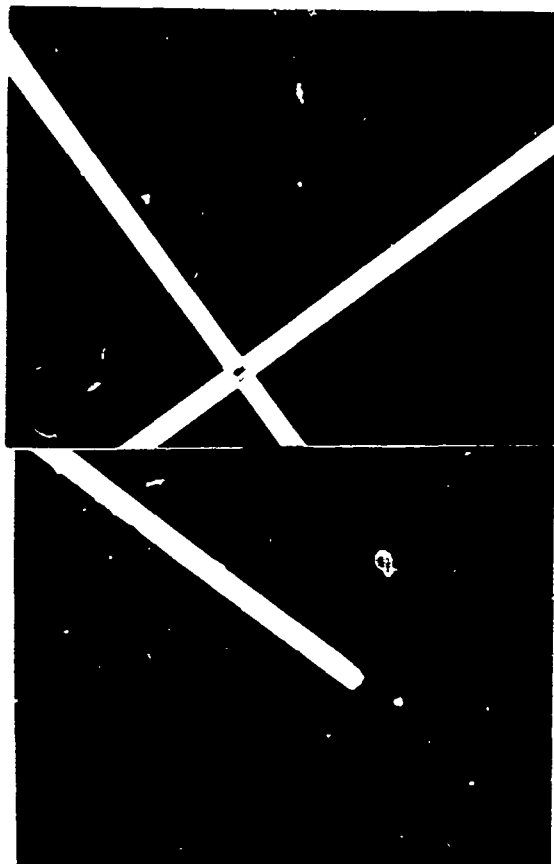
Figure 3.3: *Fibers observed with optical microscopy. Bottom fibers have been rotated 45° with respect to the top fibers (crossed polarizers) (compound 1-fiber diameters~100μm)*

3.3 UV-VIS-NIR Spectroscopy Results

The selective reflection wavelengths shown in Table 3.1 were measured using UV-VIS-NIR spectroscopy on sandwiched films using microscope slides as the substrates. The behavior of unpolarized radiation incident normal to an aligned cholesteric film, represented in Figure 3.4, was discussed in Section I. If the pitch of the material is such that the wavelength obtained from Equation 3.1 is the same wavelength as the unpolarized radiation, half the radiation will be reflected while the other half is transmitted. The handedness of the reflected radiation is the same as that of the material. Opposite handedness radiation is transmitted unaffected. The reflection bandwidth is governed by Equation 3.2.
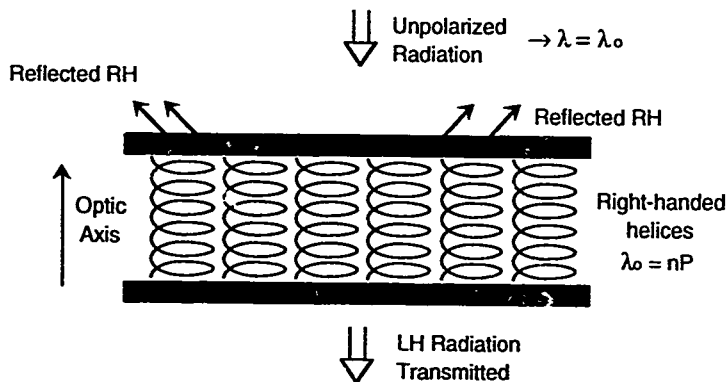
Figure 3.4: Schematic of selective reflection behavior from aligned cholesteric helices

$$\lambda = n * P \qquad \text{Eq. 3.1}$$

$$\Delta\lambda = \Delta n * P \qquad \text{Eq. 3.2}$$

In these equations, n is the average index of refraction, P is the pitch of the helix (distance it takes the director to traverse 360° (Figure 1.2)), Δn is the birefringence, λ is the selective reflection wavelength, and $\Delta\lambda$ is the bandwidth of the reflection band. These equations have been developed based on the pioneering work of DeVries[9]. When the pitch of the helices are on the order of the wavelength of visible light, these materials become highly iridescent. Figure 3.5 shows a typical reflection spectra obtained with an integrating sphere attached to a UV-VIS spectrophotometer.
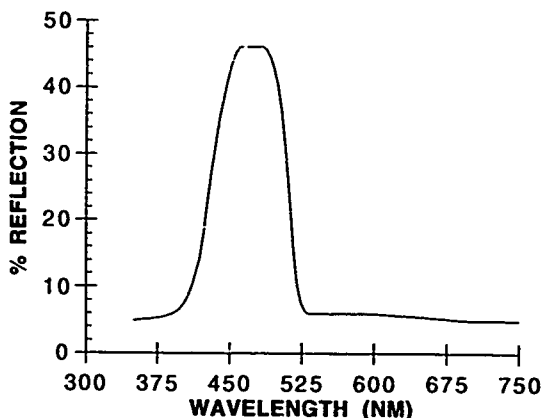
Figure 3.5: Typical reflection spectra of compound 1

The reflection wavelengths and bandwidths were observed to be partially controllable by thermal annealing. Table 3.2 shows both the reflection wavelengths and bandwidths for the visibly reflecting materials both before and after annealing on sandwiched films (glass substrates) at 120-130°C for 72 hours.

Table 3.2

Annealing results on wavelength and bandwidth

Sample	Before Annealing		After Annealing		Change	
	λ (nm)	$\Delta\lambda$ (nm)	λ (nm)	$\Delta\lambda$ (nm)	λ (nm)	$\Delta\lambda$ (nm)
1	475	77	440	68	-35	-9
2	553	112	515	93	-38	-19
3	674	133	610	117	-64	-16

As indicated, the reflection wavelengths were shortened and the reflection bandwidths shrank with annealing. This was attributed to an increase in the packing efficiency of the liquid crystalline mesogens thus allowing a better continuity from layer to layer which subsequently shortens the pitch. Examinations were also conducted at an annealing temperature of 90°C but very small changes in the reflection wavelength were observed. However, comparable changes in the reflection bandwidth were observed. Investigations with the top substrate removed resulted in similar changes to the reflection behavior. The resulting wavelengths and

bandwidths were stable at room temperature indefinitely. These results indicate the possibility of "tuning" both the reflection wavelength and bandwidth by controlled annealing for given periods of time.

Also measured were the reflection wavelengths obtained from these three materials coated on black paper as supplied by Dr. F.H. Kreuzer. Crosssections of these films were also investigated with SEM which allowed for direct visual measurement of the pitch distances. With these two figures, the average index of refraction as given in Eq. 3.1 was calculated and will be discussed in the next section.

3.4 SEM/TEM Results

The uniformity of the macroscopic packing needed for high optical quality components was examined with both scanning electron microscopy (SEM) and transmission electron microscopy (TEM). Various types of defects present in cholesteric materials, contaminants introduced in the synthesis and handling, and misalignment due to poor shear conditions can be observed with electron microscopy. Fracture surfaces of an edge geometry from cholesteric materials also reveal a regular lamellar stratification corresponding to the half-helical pitch $P/2$[10-12]. This topography is due to the continually changing orientations of the mesogens with respect to the fracture plane as they rotate through the thickness of the film.

Examinations of sheared films from these materials indicate a very good macroscopic alignment of the cholesteric axis with

70

respect to the glass substrates. Fracture surfaces tangent to the cholesteric axis (i.e., edge surfaces formed by fracturing a thin sample) vividly show the Grandjean texture. Figure 3.6, which shows the entire fracture surface of a film, indicates the spacing of the cholesteric planes was fairly uniform and parallel to the film surface. Higher magnification examinations reveal areas where the alignment was very good and allow for direct measurement of the cholesteric pitch distances (Figure 3.7). In both of these figures, the lamellar spacing corresponds to a distance of P/2. Even with this apparent uniformity, there is considerable room for improvement as evidenced by the surface layers of Figure 3.6 which exhibit much poorer alignment than those in the middle of the film. This misalignment and the large number of disclinations (liquid crystalline defects) present in the bulk greatly reduce the optical quality of these materials. The granularity present in Figure 3.7 was attributed to a conductive coating applied on nonconductive samples with standard SEM techniques. Examinations with the Hitachi low voltage SEM confirmed this behavior as samples viewed with this microscope showed no granularity.

Figure 3.6: SEM micrograph of cross-section of fractured area (25.4 mm=5 μm)
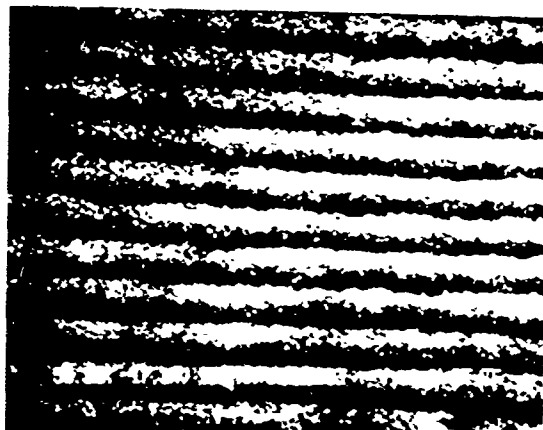
Figure 3.7: Magnified view of selected area in Figure 3.6
(6 mm=100 nm)

The actual pitch distances were measured using SEM on compounds 1-3. Great care was taken to ensure that photographs were taken with a viewing angle of 90°. Other work has shown the resulting fracture pattern observed with electron microscopy is greatly dependent on the viewing angle[13,14]. Data were obtained by measuring the distance over a number of repeats and then averaging them to obtain an average distance of the pitch. Table 3.3 shows the measured values of the pitch along with the measured reflective wavelengths obtained for the same samples. This allows the index of refraction of these materials to be calculated. The λ_{max} values were obtained from the thin films on black paper.

Table 3.3

Measured pitch lengths and reflection wavelengths with the calculated average index of refraction

Compound	Pitch (nm)	λ_{max} (nm)	n
1	288	457	1.6
2	335	531	1.6
3	400	652	1.6

Materials that were annealed above their clearing temperatures and then cooled to room temperature without applying shear were also investigated. As Figure 3.8 shows, the random disclination-containing packing of the cholesteric helices was clearly evident. The lines or layers have an average spacing of P/2 and reveal the periodic macroscopic layered structure expected of a helical material. This microstructure also shows the randomness of a focal-conic structure. This misalignment of the cholesteric axes results in random reflection (scatter) of light in all directions which results in an optically opaque material.

The presence of absorbing or scattering particulates within films of these materials ultimately decreases optical quality and lowers laser damage threshold. Figure 3.9 shows an inclusion of dust within a fracture cross-section of one of these films and the misaligned layers surrounding this inclusion. Optimization of shear stress during formation of thin films, elimination of inclusions, and achievement of uniform thicknesses would be needed to produce sufficient optical clarity for optical uses of these materials. Use of thinner coatings would lower the probability of inclusions but increase the effect of surface randomness.
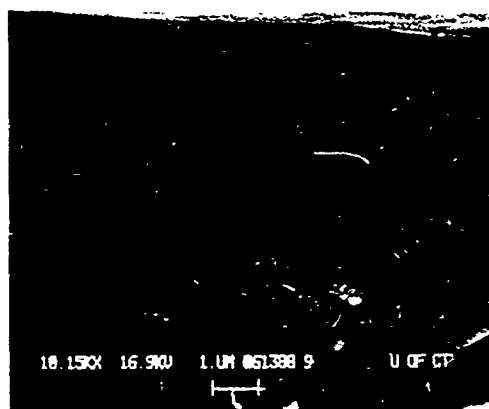
Figure 3.8: Typical focal-conic packing texture of helices as observed with SEM (10 mm=1 μm)
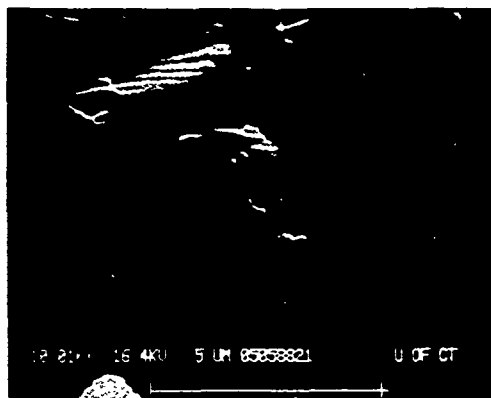
Figure 3.9: Inclusion present within film as observed with SEM (51 mm=5 µm)

Fibers of various diameters were also examined with electron microscopy (Figure 3.10). The holes in the surface plane are due to air bubbles being stretched when the fibers are drawn. No evidence of a mature cholesteric texture was observed for thin fractured fibers drawn and quenched from the melt. A featureless morphology, Figure 3.11, was observed for all cross-section fractures of thin fibers. Fibers which were annealed, however, did show the characteristic lamellar fracture surfaces in a random orientation. Upon annealing, however, fibers were observed to shrink quickly back into a random blob. The temperature where shrinkage started was slightly below the T_g. This behavior was attributed to an untwisting of the helical axis along the length of the fiber due to the high draw stress. This results in a uniaxial packing structure with no macroscopic helical twist. The elimination of this twist results in the supression of the characteristic lamellar fracture morphology. Upon annealing, however, the material relaxes back to its most thermodynamically stable state, a random packing structure, and the lamellar fracture surfaces reappear.
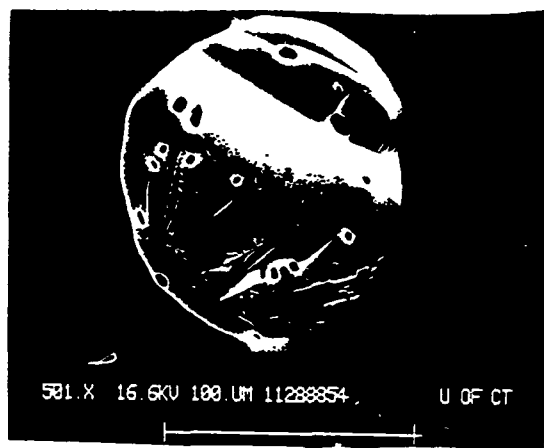
Figure 3.10: Cross-section of a typical fiber (51 mm=100 μm)
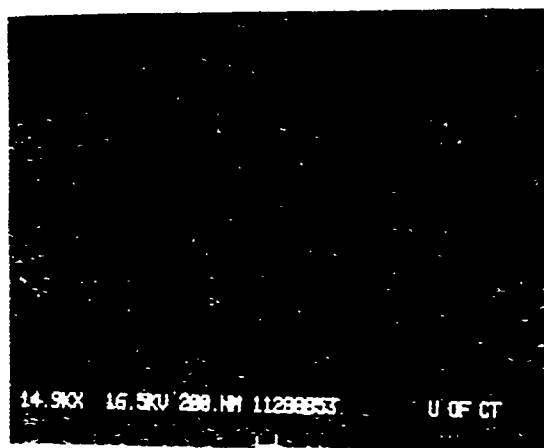
Figure 3.11: Fiber (unannealed) cross-section fracture exhibiting a featureless morphology

TEM results generally confirm the results of the SEM analysis. Due to different orientations of the molecules as it twists in its cholesteric state, a series of bright and dark lines were observed with TEM. A typical micrograph, shown in Figure 3.12, reveals the high degree of contrast among striations. These lines were attributed to the periodic structure of the cholesteric axes and minimum distances between parallel light or dark lines correspond well to the measured spacings obtained with SEM. Since the least transmission of an electron beam makes a dark region on the TEM print, the dark striations correspond to molecules normal to the beam direction and the white striations correspond to molecules parallel[15]. In analogy to the SEM results, Figure 3.12 shows regions where a relatively high degree of parallelism among striations indicates good macroscopic order.

Due to the high degree of contrast, this method is very powerful in examining not only the relative packing structure but also defects including disclinations and dislocations[16] as well as foreign particulate matter embedded within the material. Figure 3.13 shows a region containing a number of liquid crystalline defect structures.
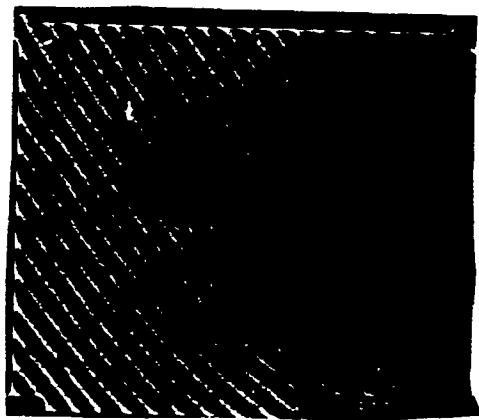
Figure 3.12: TEM micrograph showing good macroscopic order.
A single edge disclination is apparent (25.4 mm=1.2 μm)
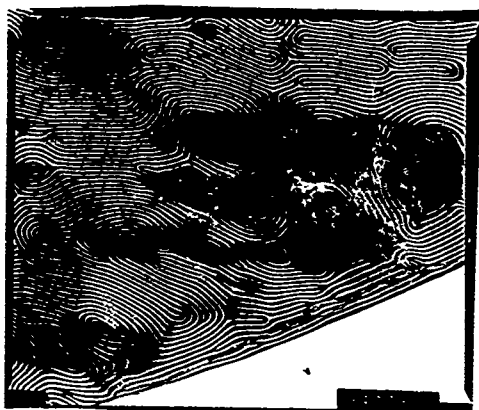
Figure 3.13: Characteristic TEM photograph showing high contrast resulting from the cholesteric phase behavior (25.4 mm=6.1 μm)

3.5 X-Ray Diffraction Results

3.5.1 Thin Film Scattering

Figure 3.14 shows a characteristic WAXS pattern for the compounds (compound 4) listed in Table 3.1. The most striking attributes of these diffraction patterns were the periodic reflections observed along the meridian[6]. The appearance of many periodic reflections for a nematic system was originally thought unique and attributed to the presence of a layered molecular packing structure. This section proposes models based on the intensity and spacing of pertinent reflections and discussions regarding the origins of the higher-order reflections will be left for Section V.

Table 3.4 lists the observed X-ray reflections from edge diffraction patterns for all four compounds. The low-angle reflections listed will be discussed in detail later. Three of these compounds showed four meridional reflections while compound 4 (x_{chol}=0.14) showed 6 layer lines. These correspond nicely to multiple order reflections from the primary layer line as shown. Structure was also evident in the intensity variation as the ~8.0Å reflection was much stronger than the 12.0 and 6.0Å reflections. There was a substantial change in the progression of reflection intensities and d-spacings with x_{chol}. Also present in these edge patterns were diffuse equatorial crescents with broad azimuthal intensity distributions which correspond to the lateral intermolecular distances (4.5-6.0 Å) within a single layer. This reflection moved towards lower angles (higher spacings) as x_{chol} was increased. The broad distribution of these reflections indicate the liquid-like motion of the mesogens.

Figure 3.14: WAXS pattern from compound 4

Table 3.4

X-ray edge diffraction data

$x_c = 0.40$ film (edge)   Compound 1

Meridional spacings, Å	Diffraction order	Calculated spacings **
49.0 (small angle)		
25.4	1	25.0
12.2 (weak)	2	12.5
8.2	3	8.3
6.4 (weak)	4	6.3
Equatorial crescent - 5.1 Å		

$x_c = 0.36$ film (edge)   Compound 2

Meridional spacings, Å	Diffraction order	Calculated spacings **
50.0 (small angle)		
25.0	1	24.6
12.1 (weak)	2	12.3
8.1	3	8.2
6.2 (weak)	4	6.2
Equatorial crescent - 5.0 Å		

Table 3.4 (con't)

x_c=0.31 film (edge) Compound 3

Meridional spacings, Å	Diffraction order	Calculated spacings **
50.0 (small angle)		
24.0	1	24.1
12.0 (weak)	2	12.1
8.0	3	8.0
6.1 (weak)	4	6.0
Equatorial crescent - 4.8 Å		

x_c=0.14 film (edge) Compound 4

Meridional spacings, Å	Diffraction order	Calculated spacings **
-- (no small angle maximum)		
22.3	1	23.2
11.6	2	11.6
7.8	3	7.7
5.8	4	5.8
4.7	5	4.6
3.9	6	3.9
Equatorial crescent - 4.5 Å		

** -- Calculated from average d-spacing obtained from observed layer spacings-This is assuming observed reflections are Bragg reflections.

X-ray patterns taken normal to a film surface exhibit uniform azimuthal intensity rings with the same d-spacings as observed for the edge samples. A WAXS normal pattern of compound 4 is shown in Figure 3.15. These rings are a consequence of the helicoidal arrangement of the cholesteric phase with the twist axis perpendicular to the film surface. The intensity variation of the reflections were the same as that exhibited by the edge samples.

Also listed in Table 3.4 are low-angle reflections (50 Å) observed on the meridian for both edge and normal geometries. A typical small-angle pattern, shown in Figure 3.16, shows the primary layer reflection and the 8.0Å reflection in addition to a low-angle reflection. The intensity of the 11-12Å reflection was too weak in some instances to be observed. A loss of the higher order intensities was coupled to the appearance of this low-angle reflection as x_{chol} was increased. As Figure 3.17 shows, the low-angle reflection becomes weaker compared to the normalized primary layer reflection as x_{chol} was decreased. Compound 1 exhibited a strong low-angle reflection while compound 4 exhibited no low-angle reflection. This dependence suggests the frequency of the packing domains causing this low-angle reflection increased with x_{chol}. The growth of the low-angle reflection was coupled with a weakening of the other meridional reflections as shown in Figure 3.18. Compound 4 clearly exhibited four reflections with a marked absence of the small-angle reflection. Contrary to this behavior, compound 1 clearly shows the presence of a strong low-angle reflection and very weak higher order meridional reflections.
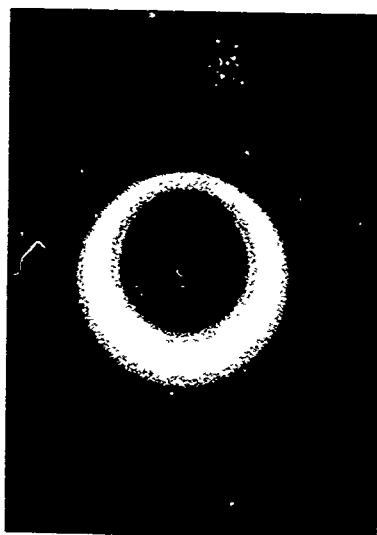
Figure 3.15: Normal WAXS diffraction pattern of compound 4

Figure 3.16: Typical small-angle diffraction pattern (compound 4)
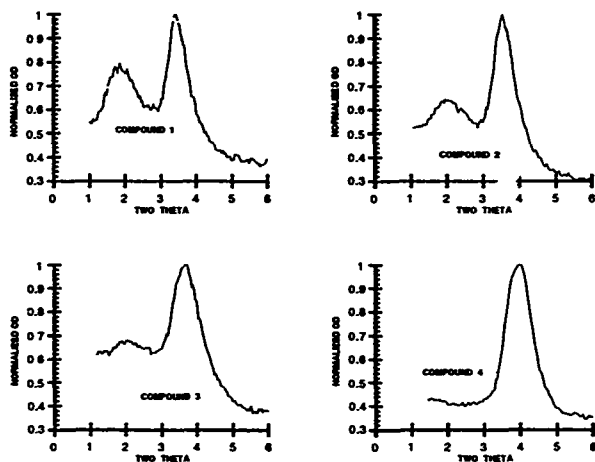
Figure 3.17: Intensity variations of small-angle reflections with respect to mole fraction cholesterol
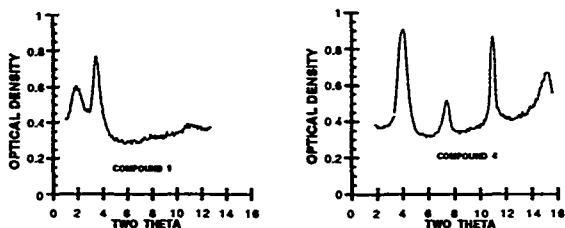
Figure 3.18: Disruption of long-range order based on SAXS

3.5.2 Proposed Packing Structure

The large numbers of periodic reflections were originally attributed to multiple-order reflections of the primary layer spacing. Calculated higher order spacings from the primary layer spacing were consistent with those observed experimentally on the meridian. These higher angle meridional reflections are now attributed to uncorrelated longitudinal disorder of columns of molecules as discussed by Levelut[17-20]. Their appearance plus the strength of the primary layer reflection are suggestive of a layered-like molecular packing. The large changes with respect to the low-angle and primary layer spacing support the evolution of two smectic-like packing structures which are dependent on x_{chol}[6]. The low x_{chol} data support a highly interdigitated structure where the biphenyl and cholesterol moieties interdigitate to form a single layer. Differences in the calculated molecular extended head-to-tail distances for a given composition and the observed lamellae spacing supports the existence of a thin interface of siloxane-rich material as shown in Figure 3.19. The extensive interdigitation of mesogens in the (B+C) layer resembles more of an S_{Ad} phase, a semi-bilayer with extensive mesogen association[21], rather than an S_{A1} phase, a monolayer with completely random head-to-tail disorder. Different classifications of smectic-A structures, S_{Ad} vs S_{A1} vs S_{A2}, have been thoroughly reviewed by Leadbetter[22].

92
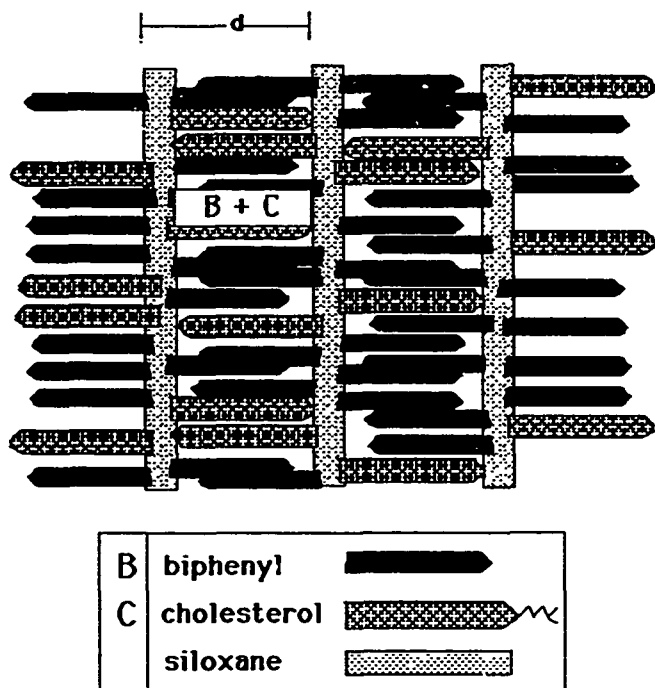
Figure 3.19 Packing structure for low x_{chol} compounds

At higher concentrations, a small-angle spacing (50Å) appears which coincides with the weakening of the periodic meridional reflections. This has been attributed to an additional S_{A2} bilayer consisting of partially overlapped cholesterol molecules (C+C) as shown in Figure 3.20.
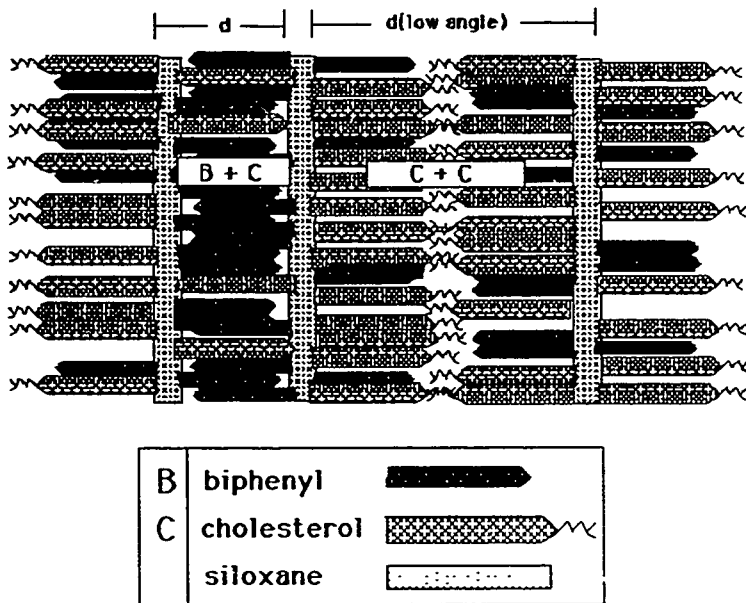
Figure 3.20: Packing structure for high x_{chol} compounds

The domination of cholesterol in the packing structure of liquid crystalline polymers has been observed before by Freidzon[23-25]. Specifically, when medium length leader groups were used to attach cholesterol to a polymer backbone, both a highly ordered interdigitated packing structure and a less ordered structure were observed. The highly interdigitated structure corresponded closely to the molecular length of the mesogen. The less ordered packing structure was attributed to the partial overlap of the cholesterol mesogens. Due to steric hinderances, the cholesterol mesogens were only allowed to superimpose their

94

aliphatic tails. The measured low-angle reflection corresponded closely to the calculated extended end-to-end molecular dimensions of this model. These cyclic siloxane compounds exhibit an analogous type behavior as the low x_{chol} material ($x_c=0.14$) behaves as a single component where the mesogens are forced apart into a pseudo-layered S_{Ad}-like separated by regions of siloxane material. As more cholesterol mesogens are added, they disrupt the highly interdigitated structure as sterically they are unable to "squeeze" into the layered structure. Instead, they form regions where they cannot interdigitate and thus a larger (low-angle) spacing is observed. This partially interdigitated structure disrupts the continuity of the long-range order which is evidenced by the weaker higher order layer lines in the diffraction patterns of the higher x_{chol} samples.

This model has been extrapolated to a macromolecular scale as shown in Figure 3.21. The individual lamellae slowly twist on a molecular scale giving rise to the helicoidal twist (normal to the film substrates) typical of cholesteric materials.

The exact details of the cyclic siloxane global molecular conformation and the possible intermolecular arrangements among pendant mesogens will be examined later with molecular modeling (Section VII). The arrangement of pendant mesogenic cores relative to one another around the siloxane ring may assume some rather different global shapes. Three extreme global conformations were envisioned and these will be discussed in Section VII.
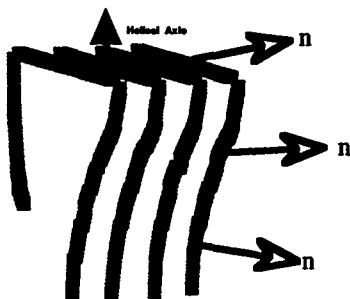
Figure 3.21: Macroscopic helical twist of lamellae induced
by chiral mesogens

3.5.3 Fiber Diffraction

As mentioned in the Introduction, the fiber drawing capability of these materials is unique due to their low molecular weights. Glassy fibers of various diameters were investigated with WAXS and SAXS geometries shown in Figure 2.2. X-ray patterns taken from fibers resemble those of the film edge as shown in Figure 3.22. The higher order layer lines residing on the meridian suggest the mesogens were aligned parallel to the fiber direction and subsequently the lamellar structure was perpendicular to the fiber axis. This behavior was partially confirmed with SEM as discussed earlier.
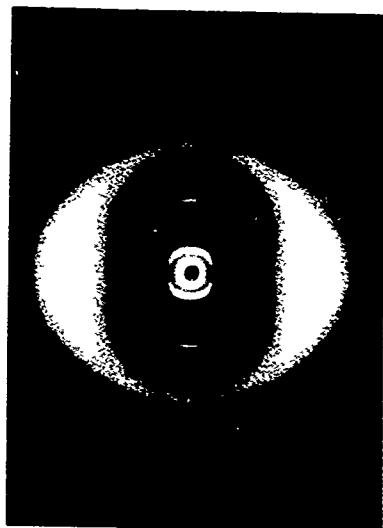
Figure 3.22: Typical WAXS pattern of fiber-compound 4

This arrangement is contrary to most fiber patterns of side-chain liquid crystalline polymers where the backbone is typically aligned parallel to the fiber direction with the side-chain mesogens aligned perpendicular to the fiber axis[26]. The typical pattern has small-angle reflections on the equator and wide-angle cresents on the meridian. Based on these patterns, these materials pack in a fashion similar to main-chain liquid crystalline material where long axes of the molecules are parallel to the fiber direction as shown in Figure 3.23. Although not drawn to scale, this figure suggests the mesogens themselves are parallel to the fiber direction for the cyclic siloxane compounds. It has been hypothesized that as the material was drawn, the cholesteric helix is untwisted to give a fiber with uniaxial order.

Polymer l.c. fiber   Cyclic siloxane l.c. fiber
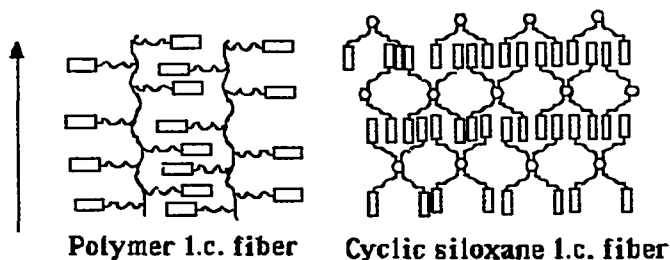
Figure 3.23: Schematic of orientational behavior of smectic-like layers for polymer and cyclic siloxane materials. The arrow indicates the direction of the fiber axis.

3.5.4   Microcamera   Examination   of   Thin   Fibers

Several attempts were made to examine individual thin fibers ($<30\mu$m) using a microcamera.   Fibers were formed when the Wacker LC-Silicones were spin-coated onto glass substrates using an in-house spin coater.   Fibers were observed to form, as individual filaments exited the glass substrates radially and subsequently became wrapped around the rotor.   This very fast rotation formed mats of thin fibers with a consistency similar to cotton candy as shown in Figure 3.24.   Groups of these fibers were first examined by pulling them roughly parallel and examining these with a Statton camera (50 mm).   These mats exhibit X-ray patterns (Figure 3.25) similar to individual hand-drawn fibers.

Individual filaments ($<30\mu$m) from these spun coat fibers were examined with a microcamera to investigate the relative ordering with respect to the mats of fibers shown in Figure 3.25. Filaments were mounted in the microcamera and exposed for 24-72 hours on the RU-200 generator.   The resulting pattern obtained for compound 1, Figure 3.26, exhibited less orientation than the mats of fibers.   Orientation of the filament axis was parallel to the long axis of the photograph.   These patterns clearly show poor orientation as almost concentric rings were observed.   There was some orientation exhibited as demonstrated by the larger equatorial crescents but much less than that exhibited in Figure 3.25.   This behavior was unexpected as thin filaments from a group of fibrils typically exhibit better alignment than the group itself[27].

Figure 3.24: Thin fibers from spin coater as observed under crossed polarizers (200 X)-(10-50 μm diameter fibers)
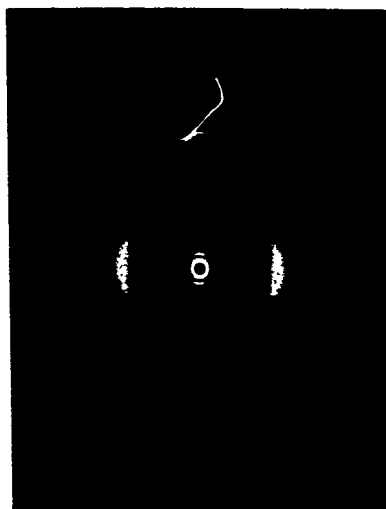
Figure 3.25: Diffraction pattern from group of fibrils of compound 1

Possible explanations include X-ray beam heating which due to the very thin diameters, shrinks and relaxes the fibers. This elastic behavior has been observed with hand-drawn fibers which when heated to 60°C, quickly shrink into a random blob thereby losing their uniaxial order. As discussed previously, TEM/SEM results have indicated that the orientations of fibrils in these shrunken materials were fairly random, similar to a focal-conic texture.

Another possible explanation was the relaxation of the uniaxial order with time. Roughly 6 months had passed from the time when the fibers were accidently drawn and initially examined with the Statton camera and then finally examined with the microcamera. Due to the low T_g's of these materials, perhaps over time the molecules have enough mobility to slowly relax. To date, no more work has been performed on these "cotton" candy samples. Still, the ability of these materials to be drawn into very thin, highly birefringent fibers leads to possible NLO fiber applications.

Figure 3.26: X-ray pattern from an individual filament of compound 1

3.6 Elevated Temperature Diffraction

Powder diffraction patterns for two of these compounds were obtained at a series of elevated temperatures to confirm that the X-ray reflections observed were not a manifestation of the glassy phase. These experiments were done with a home-made heater and there were severe limitations with regard to the thermal stability of the samples and allowable sample-to-film distances. Samples were contained in thin-walled glass capillary tubes. Upon heating into the isotropic phase, the wide-angle halo became very diffuse while all other reflections disappeared. Upon cooling below the clearing point, the reappearance of tne reflections suggests they are indeed due to structure within liquid crystalline phase. A slight lengthening (1.0Å) of the primary d-spacings (as well as the lateral spacings) with temperature was observed for both compounds. Reflections attributed to multiple orders were in general much weaker due to the lack of alignment. No microdensitometric analysis has been performed due to the small sample-to-film distances and the isotropic scattering of the glass capillaries. More details of this work can be found elsewhere[28].

3.7 Summary

Electron microscopy and X-ray diffraction data support a structural model where the cyclic siloxane mesogens organize into a twisted (helicoidal) arrangement having hydrocarbon-rich bilayer-like strata that may be reinforced and delineated by the (immiscible) siloxane component. This phase separation of hydrocarbon and siloxane units on a molecular scale has been proposed before[29-32]. The extension to a macroscopic helicoidal structure is reminiscent of that originally proposed for cholesteryl-containing acrylate and methacrylate side-chain liquid crystalline polymers[23]. A similar type of arrangement has been subsequently proposed by Goodby[33,34]. Strong primary layer spacings and the appearance of periodic meridional reflections indicate a tendency to pack unlike conventional cholesteric phases. A strong dependence of the diffraction patterns on composition was observed. This has been attributed to two types of smectic-like packing structures, one dominant at low x_{chol} and one dominant at high x_{chol}.

It has been shown that this partially layered structure is retained in fibers drawn from the mesophase. Although glassy and brittle, very long length (meters) fibers could be drawn. Contrary to most polymer fibers, the orientation of lamellae was normal to the fiber axis. This may confer unique optical properties to light propagating in such fibers.

3.8 References

(1) Kreuzer, F.H. and Gawhary, G.W., U.S. Patent # 4410570, (1983).

(2) Tsai, M.L., Chen, S.H., and Jacobs, S.D., *Appl. Phys. Lett.*, **54(24)**, 2395-2397(1989).

(3) Pinsl, J., Brauchle, Chr., and Kreuzer, F.H., *J. Mol. Electr.*, **3**, 9-3(1987).

(4) Krishnamurthy, S. and Chen, S.H., *Makromol. Chem.*, **190**, 1407-1412(1989).

(5) Chen, S.H. and Krishnamurthy, S., *Polym. Mat. Sci. Eng.*, **60**, 801-804(1989).

(6) Bunning, T.J., Klei, H.E., Samulski, E.T., Crane, R.L., and Linville, R.J., *Liq. Cryst.*, **10(4)**, 445-456(1991).

(7) Chemie, Wacker, Provisional data sheet provided with the Wacker LC-Silicones, (March 1988).

(8) Demus, D. and Richter, L., *Textures of Liquid Crystals*; Verlag Chemie; Weinheim, (1978).

(9) DeVries, H.L., *Acta. Cryst.*, **4**, 219-226(1951).

(10) Livolant, F. and Bouligand, Y., *Mol. Cryst. Liq. Cryst.*, **166**, 91-100(1989).

(11) Bouligand, Y. and Kleman, M., *J. Phys.*, **31**, 1041-1054(1970).

(12) Voss, J. and Voss, B., *Z. Natureforsch*, **31A**, 1661-1663(1976).

(13) Costello, M. J., Meiboom, S., and Sammon, M., *Phys. Rev. A*, **29(5)**, 2957-2959(1984).

(14) Berreman, D.W., Meiboom, S., Zasadzinski, J.A., and Sammon, M.J., *Phys. Rev. Lett.*, **57(14)**, 1737-1740(1986).

(15) Hara, H., Satoh, T., Toya, T., Iida, S., Orii, S., and Watanabe, J., *Macromolecules*, **21**, 14-19(1988).

(16) Kleman, M., *Rep. Prog. Phys.*, **52**, 555-654(1989).

(17) Davidson, P., Keller, P., and Levelut, A.M., *J. Phys.*, **46**, 939-946(1985).

(18) Davidson, P. and Levelut, A.M., *J. Phys.*, **49**, 689-695(1988).

(19) Decobert, G., Soyer, F., Dubois, J.C., and Davidson, P., *Polym. Bull.*, **14**, 549-556(1985).

(20) Davidson, P. and Levelut, A.M., *Liq. Cryst.*, **11(4)**, 469-517(1992).

(21) Leadbetter, A.J. in *Thermotropic Liquid Crystals*, G.W. Gray, Ed., John Wiley and Sons; NY, **22,** pp 145-170, (1987).

(22) Leadbetter, A.J. in *Thermotropic Liquid Crystals*, G.W. Gray, Ed., John Wiley & Sons; Chichester, **22,** pp 1-27, (1987).

(23) Freidzon, Ya.S., Tropsha, Ye.G., Tsukruk, V.V., Shilov, V.V., Shibayev, V.P., and Lipatov, Yu.S., *Polym. Sci. USSR*, **29(7)**, 1505-1511(1987).

(24) Freidzon, Ya.S., Kharitonov, A.V., Shibaev, V.P, and Plate, N.A., *Eur. Polym. J.*, **21(3)**, 211-216(1985).

(25) Plate, N.A., Freidzon, Ya.S., and Shibaev, V.P., *Pure Appl. Chem.*, **57(11)**, 1715-1726(1985).

(26) Freidzon, Ya. S., Talroze, R.V., Boiko, N.I., Kostromin, S.G., Shibaev, V.P., and Plate, N.A., *Liq. Cryst.*, **3(1)**, 127-132(1988).

(27) Adams, W.W., personal communication with.

(28) Bunning, T.J., Klei, H.E., Samulski, E.T., Adams, W.W., and Crane, R.L., *Characterization of Cholesteric Cyclic Siloxane Liquid Crystalline Materials*, Wright Laboratory, WL-TR-91-4089, (1991).

(29) Diele, S., Oelsner, S., Kuschel, F., Hisgen, B., and Ringsdorf, H., *Mol. Cryst. Liq. Cryst.*, **155**, 399-408(1988).

(30) Diele, S., Manke, S., Weibflog, W., and Demus, D., *Liq. Cryst.*, **4(3)**, 301-307(1989).

(31) Westphal, G., Diele, S., Madicke, A., Kushel, F., Scheim, F., Rohlmann, K., Hisgen, B., and Ringsdorf, H., *Makromol. Chem., Rapid Commun.*, **9**, 489-493(1988).

(32) Percec, V., Hahn, B., Ebert, M., and Wendorff, J.H., *Macromolecules*, **23**, 2092-2095(1990).

(33) Goodby, J.W., Waugh, M.A., Stein, S.M., Chin, E., Pindak, R., and Patel, J.S., *Nature*, **337**, 449-452(1989).

(34) Goodby, J.W., Waugh, M.A., Stein, S.M., Chin, E., Dindak, R., and Patel, J.S., *J. Am. Chem. Soc.*, **111**, 8119-8125(1989).

Section IV

MATERIALS AND SYNTHETIC SCHEMES

This section describes the materials, techniques, and synthetic procedures used in the examination of novel siloxane-based liquid crystalline materials. A number of analogs of the commercial materials examined in Section III were synthesized to examine differences in structure/property relationships for cyclic-siloxane liquid crystals. This section describes the synthetic procedures employed in synthesizing various analogues of these liquid crystals. The syntheses of the catalyst, leader groups, liquid crystalline mesogens, and the siloxane materials are described. Characterization results are presented for all precursors used in the synthesis of the siloxane compounds. Physical properties of the siloxane compounds are discussed separately in Sections V and VI. All materials employed in the synthesis steps were obtained from Aldrich and used as received unless otherwise specified.

4.1 Synthesis Schemes

The synthetic schemes and procedures are discussed separately for the various parts used as building blocks for the final siloxane materials. Great care was taken to produce a final material free of impurities. For effective silanization reactions, a heavy metal catalyst is typically employed. The mechanism will be examined later in the discussion of the hydrosilation reactions. Various heavy metal (transition metal) catalysts[1-3] have been used to effectively couple an Si-H bond and a terminal olefin. For

linear polysiloxanes materials, hexachloroplatinic acid[4,5] has been typically used for the last 10 years. Recently, however, problems with the stability of this catalyst have been discussed[6]. A newer catalyst, dicyclopentadienylplatinum (II) chloride catalyst, was instead chosen for this work.

4.2   Synthesis Of Catalyst[7]

Hydrogen hexachloroplatinic (IV) hydrate, 0.94 g (1.9 mmol), was dissolved in 5ml glacial acetic acid and heated to 70°C. Dicyclopentadiene, 1.5 ml (12.1 mmol) and 10 ml of H_2O were added to the solution. The solution was stirred vigorously for 2-3 hours and the resulting black solution was centrifuged. The solid product was washed once in water and three times with diethyl ether. The product was dissolved in 80 ml dichloromethane and heated to boiling for 15 minutes. The solution was decolorized using both activated carbon and chromatographic grade silica gel. The resulting solution was heated, boiling off the dichloromethane, until the solution started to turn cloudy. The hot solution was poured into 50 ml of petroleum ether yielding a fine white precipitate. The solid was washed several times with petroleum ether and dried giving 277.9 mg (37%). H^1NMR confirmed the structure as $C_{10}H_{12}PtC_{:2}$.

H^1 NMR δ(s): 7.15-6.85 (1H, m), 6.85-6.45 (1H, m), 6.4-5.9 (1H, m), 5.9-5.3 (1H, m), 3.9-3.5 (2H, m), 3.0-2.8 (2H, m), 2.6-1.5 (4H, m).

4.3 Synthesis of Leader Groups

Four separate leader groups, shown in Figure 4.1(a), were chosen to examine the effect on the resulting materials phase behavior. Three of these were synthesized using standard literature techniques[8] shown in Figure 4.1(b). This reaction consists of reacting 4-hydroxybenzoic acid with a given ω-alkenyl bromide in the presence of potassium hydroxide. The fourth leader group, vinylbenzoic acid was obtained from Aldrich. The synthetic details for these three leader groups are listed in detail below.

4.3.1 Synthesis of 4-allyloxybenzoic acid

In a 3-neck 500 ml round bottom flask equipped with a reflux condenser, dropping funnel, and magnetic stirrer, 30 g (0.217 mol) hydroxybenzoic acid was added to 135 ml of methanol. To this, 45 ml of a potassium hydroxide solution (42.9 g KOH/53 ml H_2O) was added dropwise. The resulting solution was heated to reflux for 1 hour. A clean dropping funnel was placed on the flask and used to add 22 ml (0.254 mol) of allyl bromide over a half-hour period. The solution was refluxed for 8 hours, cooled to room temperature and allowed to sit overnight. After 90 ml of methanol was taken off by single stage distillation, the remaining solution was cooled to room temperature and then added to 350 ml distilled water. This was extracted three times with 100 ml diethyl ether. After the remaining aqueous phase was heated to 35°C, 100 ml of 37% HCl was added to precipitate the product. The solid was filtered, washed, and recrystallized three times from ethanol.

111

Yield - 55%; DSC melting point - 165°C (Lit.-167°C)

H^1 NMR δ(s): 8.05(2H, d), 7.0(2H, d), 6.0(1H, m), 5.45(1H, d), 5.35(1H, d), 4.6(2H, d).

4.3.2   Synthesis of 4-penteneoxybenzoic acid

Synthetic procedure was the same as above using 5-bromo-1-pentene.   The solid was filtered, washed, and recrystallized three times from ethanol.

Yield - 51%; DSC-k 124°C n 154°C i(Lit.-k 123°C); k-crystalline; n-nematic; i-isotropic; DSC and POM revealed the presence of more than one crystalline phase.

H^1 NMR δ(s): 8.05(2H, d), 6.95(2H, d), 5.85(1H, m), 5.05(2H, quart), 4.05(2H, tri), 2.25(2H, quart), 1.90(2H, m).

4.3.3 Synthesis of 4-octeneoxybenzoic acid

Synthesized as above using 8-bromo-1-octene.   The solid was filtered, washed, and recrystallized three times from ethanol.

Yield - 29%; DSC k 81°C n 99°C S? 140°C i; No literature values; (Smectic phase is an A or E phase).

H^1 NMR δ(s): 8.05(2H, d), 6.95(2H, d), 5.8(1H, m), 5.00(2H, quart), 4.05(2H, tri), 2.1(2H, quart), 1.8(2H, m), 1.45(6H, m).

1. $CH_2=CH-$⟨⟩$-C\overset{O}{\overset{\|}{O}}H$ VINYLBENZOIC ACID

2. $CH_2=CH-CH_2-O-$⟨⟩$-C\overset{O}{\overset{\|}{O}}H$ ALLYLOXYBENZOIC ACID

3. $CH_2=CH-CH_2-CH_2-CH_2-O-$⟨⟩$-C\overset{O}{\overset{\|}{O}}H$ PENTENEOXYBENZOIC ACID

4. $CH_2=CH-CH_2-CH_2-CH_2-CH_2-CH_2-CH_2-O-$⟨⟩$-C\overset{O}{\overset{\|}{O}}H$ OCTENEOXYBENZOIC ACID

(a)

$CH_2=CH-CH_2-Br$
$CH_2=CH-(CH_2)_3-Br$
$CH_2=CH-(CH_2)_6-Br$

$+$ $HO-$⟨⟩$-C\overset{O}{\overset{\|}{O}}H$ $\overset{2KOH}{\Rightarrow}$ $CH_2=CH-(CH_2)_n-O-$⟨⟩$-C\overset{O}{\overset{\|}{O}}H$

(b)
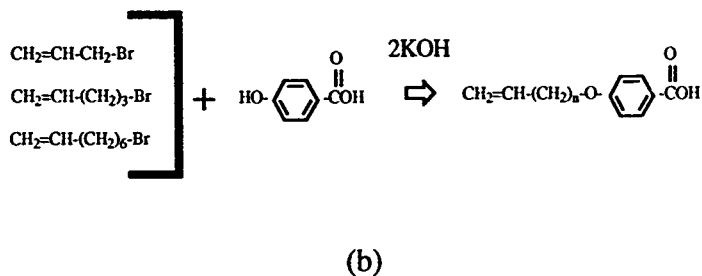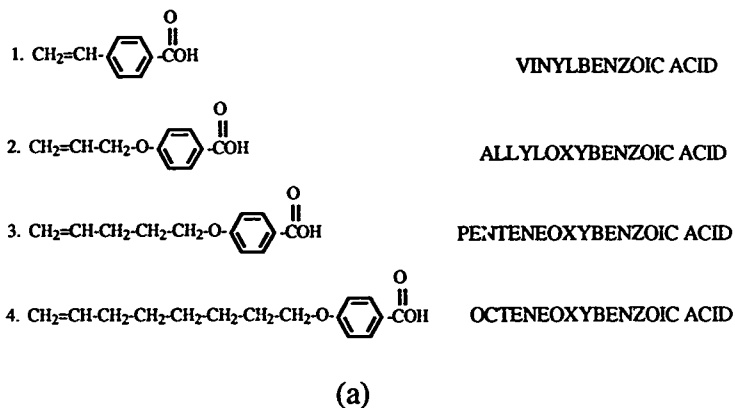
Figure 4.1:   *Four leader groups (a) and the leader group reaction scheme employed (b)*

4.4   Synthesis of Alkene Mesogens

The   synthesis path of the liquid crystalline mesogens was an esterification reaction previously used for peptide bond synthesis[9,10]. The two reactive components, a carboxyl group and either an amino or hydroxyl group couple quantitatively using N,N'-dicyclohexylcarbodiimide (DCCI) and dimethylaminopyridine (DMAP) as the catalyst. The mechanism behind this reaction has been discussed elsewhere[11]. The purification of the product is relatively simple as the DCCI is converted to dicyclohexylurea (DCU) which is insoluble in most aqueous and organic solvents.

Prospective mesogens contained a reactive alcohol group onto which the carboxyl group from the leader compound could attach. The leader group also needed a terminal vinyl group that could later be attached to the Si-H bond on the siloxane core.

Every leader group was attached to two separate materials, hydroxybiphenyl and cholesterol, both of which were present in the Wacker LC-Silicones. The synthesis scheme is shown in Figure 4.2 and the details for the synthesis of each mesogen are listed below. The thermal properties of the eight resulting materials are summarized following the synthetic procedures.

4.4.1   Synthesis of cholesteryl-4-vinylbenzoate: C4VB

In a 200 ml round bottom flask were placed 3.27 g (8.46 mmol) of cholesterol, 1.11 g (7.49 mmol) of vinyl benzoic acid, 1.78 g (8.63 mmol) of DCCI, and 0.21 g (1.72 mmol) of DMAP. Dichloromethane (100 ml) was added, the solution refluxed for 24 hours, and a fine white precipitate, DCU (confirmed using FTIR and
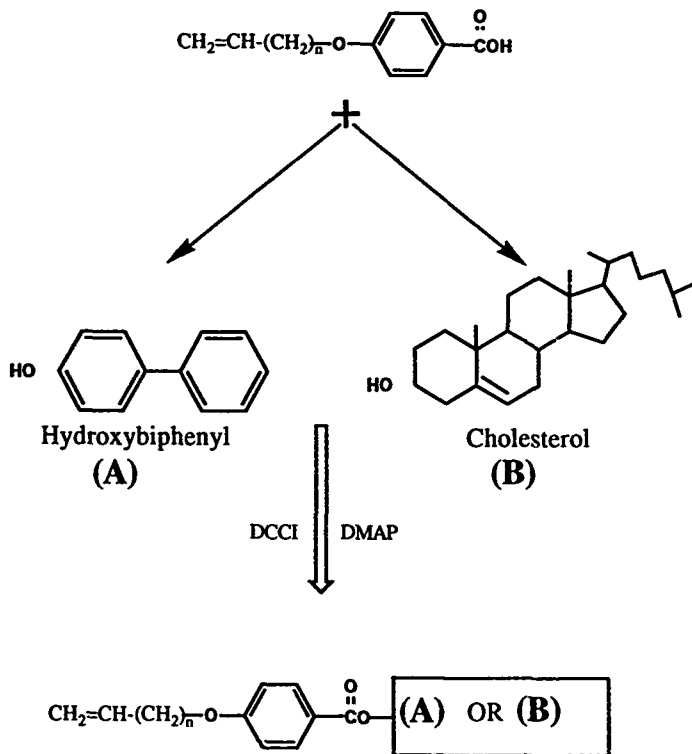
114

Figure 4.2: Esterification reaction used to synthesize biphenyl and cholesterol mesogens
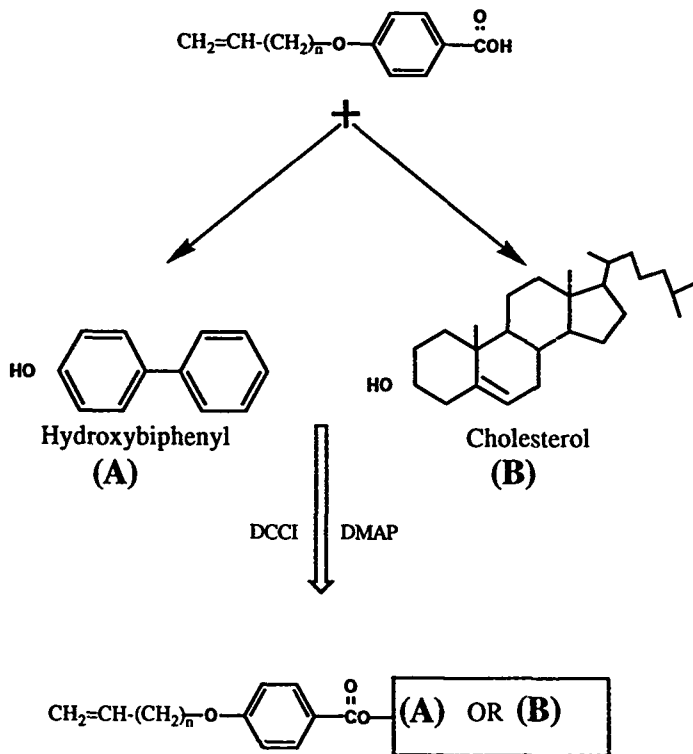
Figure 4.2: Esterification reaction used to synthesize biphenyl and cholesterol mesogens

4.4.3 Synthesis of cholesteryl-4-allyloxybenzoate: C4AB

Synthesis was the same as C4VB above, instead using allyloxybenzoic acid. The product was recrystallized three times from a 1:1 mixture of ethyl acetate/ethanol. Yield (72%). H^1NMR was used to confirm the structure of $C_{37}H_{54}O_3$.

H^1NMR δ(s): 8.00(2H, d), 6.9(2H, d), 6.05(1H, m), 5.50-5.30(3H, d), 4.85(1H, m), 4.6(2H, m), 2.45(2H, d), 1.1(3H, s), 1.00(3H, d), 0.95(6H, d), 0.70(3H, s).

4.4.4 Synthesis of biphenyl-4-allyloxybenzoate: B4AB

Synthesis was the same as B4VB above, instead using allyloxybenzoic acid. The product was recrystallized three times from a 1:1 mixture of acetone/methanol. Yield (88%). H^1NMR was used to confirm the structure of $C_{22}H_{18}O_3$.

H^1NMR δ(s): 8.15(2H, d), 7.70(4H, quart), 7.45(2H,tri), 7.35(1H, tri), 7.25(2H, d), 7.00(2H, d), 6.10(1H, m), 5.45(1H, d), 5.35(1H, d), 4.65(2H, d).

4.4.5 Synthesis of cholesteryl-4-penteneoxybenzoate: C4PB

Synthesis was the same as C4VB above, instead using penteneoxybenzoic acid. The product was recrystallized three times from a 1:1 mixture of toluene/methanol. Yield (52%). H^1NMR was used to confirm the structure of $C_{39}H_{58}O_3$.

H^1NMR δ(s): 8.00(2H, d), 6.90(2H, d), 5.95(1H, m), 5.45(1H, d), 5.05(2H, m), 4.80(1H, m), 2.45(2H, d), 2.15(2H, quart), 0.85(6H, d), 0.70(3H, s).

4.4.6 Synthesis of biphenyl-4-penteneoxybenzoate: B4PB

Synthesis was the same as B4VB above, instead using pentenoxybenzoic acid. The product was recrystallized three times from a 1:1 mixture of toluene/methanol. Yield (57%). H^1NMR was used to confirm the structure of $C_{24}H_{22}O_3$.

H^1NMR δ(s): 8.15(2H, d), 7.60(4H, quart), 7.45(2H, tri), 7.35(1H, tri), 7.25(2H, d), 7.00(2H, d), 5.90(1H, m), 5.10(2H, quart), 4.10(2H, tri), 2.30(2H, quart), 1.90(2H, quart)

4.4.7 Synthesis of cholesteryl-4-octeneoxybenzoate: C4OB

Synthesis was the same as C4VB above, instead using octeneoxybenzoic acid. The product was recrystallized three times from a 1:1 mixture of toluene/methanol. Yield (40%). H^1NMR was used to confirm the structure of $C_{42}H_{64}O_3$.

H^1NMR δ(s): 8.00(2H, d), 6.90(2H, d), 5.80(1H, m), 5.45(1H, d), 5.05(2H, m), 4.85(1H, m), 4.00(2H, tri), 2.45(2H, d), 0.85(6H, d), 0.70(3H, s).

4.4.8 Synthesis of biphenyl-4-octeneoxybenzoate: B4OB

Sythesis was the same as B4VB above, instead using octeneoxybenzoic acid. The product was recrystallized three times from a 1:1 mixture of toluene/methanol. Yield (32%). H^1NMR was used to confirm the structure of $C_{27}H_{28}O_3$.

H^1NMR δ(s): 8.15(2H, d), 7.60(4H, quart), 7.45(2H, tri), 7.35(1H, tri), 7.25(2H, d), 7.00(2H, d), 5.85(1H, m), 5.00(2H, m), 4.05(2H, tri), 2.10(2H, quart), 1.85(2H, m), 1.60-1.40(6H, m).

118

4.4.9 Summary of Alkene Properties

The thermal transitions for all eight compounds are shown in Table 4.1. Where possible the literature values have been reported for comparison. All cholesterol-containing materials exhibited a cholesteric liquid crystalline phase as a typical Grandjean texture appeared when the top slide was shifted with respect to the bottom slide. The longer length cholesterol derivatives exhibited a smectic phase consistent with literature[12,13]. The shorter biphenyl-containing materials were not liquid crystalline and exhibited sharp melting points. B4OB exhibited a nematic liquid crystalline phase. Both B4VB and C4VB were observed to thermally polymerize upon initial melting and thus second heating scans were not possible. For C4VB, this polymerization masked the clearing temperature.

Table 4.1

Thermal transitions as reported by DSC

Compound	Transitions (^{o}C) [a]	Literature values [b]
B4VB	k 163 i	NR
C4VB	k 171 n* ?	k 169 n* 203 i
B4AB	k 137 i	k 139 i
C4AB	k 121 n* 237 i	k 124 n* 226 i
		k 120 n* 243 i
B4PB	k 151 i	NR
C4PB	k 135 n* 239 i	NR
B4OB	k 101 n 121 i	NR
C4OB	k 123 S_A 160 n* 215	NR

[a] k-crystalline; n-nematic; S_A-smectic-A; n*-cholesteric; i-isotropic
[b] NR- unreported; C4VB and C4AB[14,15]; B4AB[16]

Elemental analysis was performed on all eight compounds. As Table 4.2 shows, there was good agreement between the theoretical and measured percentages. The measured values were the average of two separate measurements.

Table 4.2

Elemental analysis results

Compound	Molecular formula	Theoretical %C	Measured %C	Theoretical %H	Measured %H
B4VB	$C_{21}H_{16}O_2$	83.97	83.21	5.37	5.41
C4VB	$C_{36}H_{52}O_2$	83.67	83.74	10.14	10.30
B4AB	$C_{22}H_{18}O_3$	79.97	79.86	5.50	5.51
C4AB	$C_{37}H_{54}O_3$	81.27	81.41	9.95	9.76
B4PB	$C_{24}H_{22}O_3$	80.42	80.51	6.19	6.26
C4PB	$C_{39}H_{58}O_3$	81.48	81.49	10.17	10.1
B4OB	$C_{27}H_{28}O_3$	80.97	81.01	7.05	7.17
C4OB	$C_{42}H_{64}O_3$	81.76	82.05	10.46	10.25

Thin layer chromatography was used to check the purity of all eight compounds. Only one spot was identified for each compound using silica gel plates and an eluent of 1:1 ethyl acetate/hexane mixture. R_f values using dichloromethane as the eluent are shown in Table 4.3 for future comparison to the final silanization products whose TLC were run exclusively in dichloromethane following the procedure of Nestor[17].

Table 4.3

Rf values for alkenes

Alkene	R_f
B4VB	0.84
C4VB	0.88
B4AB	0.81
C4AB	0.83
B4PB	0.77
C4PB	0.79
B4OB	0.83
C4OB	0.83

4.5 Hydrosilation Reactions

Hydrosilation reactions have been performed extensively in the literature with linear polysiloxane backbones[18,19]. The methodology employed in this work was analogous to that used with the linear siloxane systems. Certain modifications of reaction monitoring were needed when working with small siloxane units. These will be discussed in detail where pertinent. Basic methodology was obtained under the tutelage of Drs. Cary Veith and Edward T. Samulski, Dept. of Chemistry, University of North Carolina.

4.5.1 Mechanism

As mentioned earlier, a hydrosilation reaction is typically catalyzed by a transition metal complex, a dicyclopentadienylplatinum (II) chloride catalyst in this case. Figure 4.3 shows a schematic of the proposed mechanisms for these

121

reactions[2]. The mechanism can be rationalized, as described by Chalk and Harrod[20,21], such that all the chemical changes take place within the coordination sphere of the transition metal. Initially, compound (I) is stabilized by a terminal olefin after it has been reduced initially by the silane. This reduction period is typically observed as an "induction" period when a reaction is first started. This structure (II) readily undergoes oxidative addition as the Si-H compound attacks the platinum catalyst to form compound (III). The next step, the rearrangement from an olefin π- to an alkyl σ- complex, has been suggested to be rate determining. The alkyl σ- complex (IV) reacts with more olefin thus regenerating compound (II) and forming the hydrosilated product. When great care is taken to use pure reagents, 10^{-7} moles of Pt/mole product causes hydrosilation to occur rapidly near room temperature for low molecular weight siloxane materials.
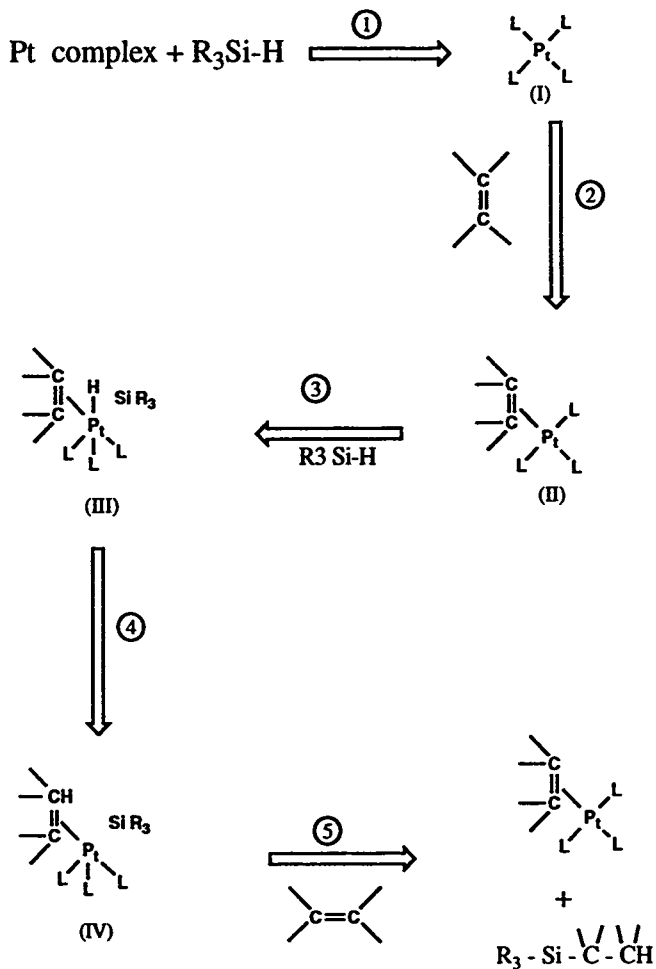
Figure 4.3: Proposed mechanism for hydrosilation reactions using a transition metal complex catalyst

123

4.5.2   Siloxane Materials

Seven different siloxane cores examined are shown in Figure 4.4 along with abbreviations for each that will be referred to in the discussion.   Two of these siloxane materials were cyclic rings, C4 and C5, similar to those used as a precursor in the Wacker LC-Silicones.   A third material, a "star" ST siloxane, closely resembled these materials.   Three low molecular weight linear compounds were examined, a trisiloxane monomer (M) containing one terminal Si-H bond, a trisiloxane dimer (TD) containing two terminal Si-H bonds, and a disiloxane dimer (DD) also containing two terminal Si-H bonds.   A linear polysiloxane backbone, siloxane P, was also chosen for comparison purposes.   Great care was taken to use pure siloxane materials in the reaction mixture.   All compounds except the linear polysiloxanes were checked for purity using GC techniques.   The cyclic compounds were vacuum distilled and checked periodically with GC to ensure no breakdown had occurred. The monomer compound, M, was distilled prior to use.   The "star" (ST) and disiloxane (DD) compounds were obtained from Dr. Christ Tamborski of Fluidics Company.   The linear polysiloxane backbone was obtained from Aldrich.   All other siloxane materials were obtained from Huls America.   The structure of the linear siloxane is based on a molecular weight of 1,800 obtained verbally from Aldrich.
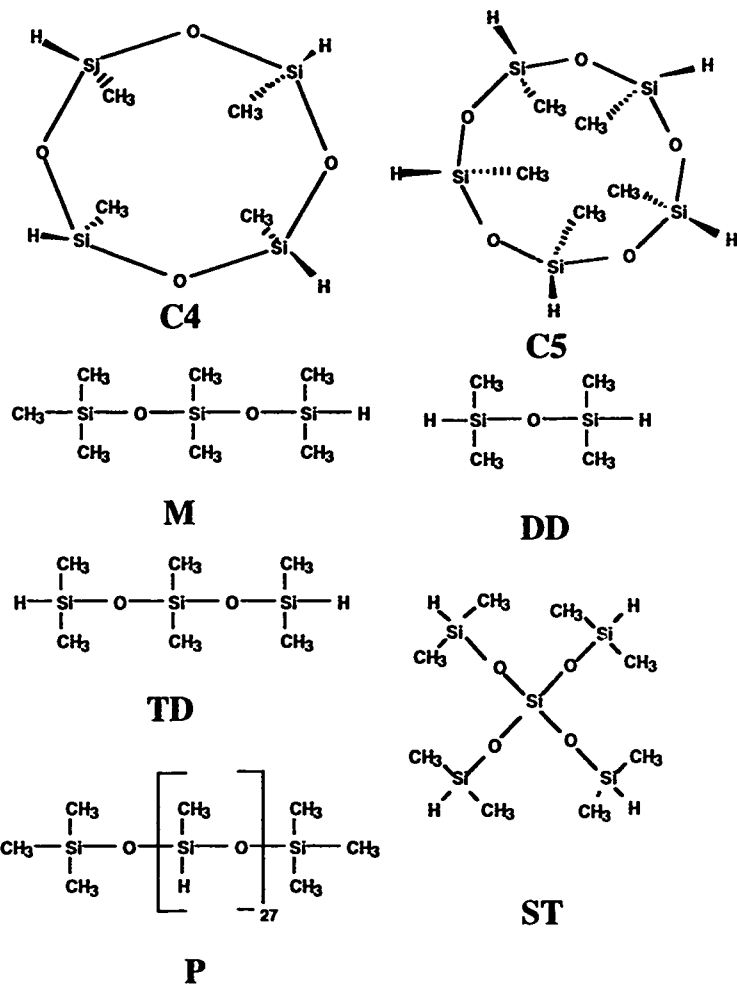
Figure 4.4: The seven siloxane cores examined

125

4.5.3   A Typical Hydrosilation Reaction

A typical reaction consisted of first drying 10 mole % excess alkene per mole of Si-H for four hours at a reduced pressure of 0.5 mm mercury.   The alkene was then placed in a 100 ml 3-neck round bottom flask equipped with a thermometer and a condenser column.   Toluene (20-40 ml) was added and the solution was heated to 70-80°C while being stirred.   The siloxane was added with a micropipette and allowed to mix for 5 minutes at which time the catalyst solution was also added.   Enough catalyst solution (in methlene chloride) was added to obtain a mole ratio of 1:10^3 to 10^6 of Pt/alkene.   The reaction vessel was blanketed with dry Ar through a valve on top of the condenser tube during the entire reaction sequence.   All ground glass joints were sealed using Teflon stoppers rather than vacuum grease.   Preliminary results indicated vacuum grease poisons the catalyst solution as well as contaminating the resulting product[22].

The reaction was allowed to proceed until no Si-H peak was present in the IR spectra (discussed below).   This time period varied greatly depending on the type of siloxane used and the length of the leader group.   For most cases, the reaction was allowed to sit for 24-36 hours.   However, for the low molecular weight siloxane materials, the reaction typically proceeded very quickly within the first few hours.   The linear polysiloxanes required more time and were allowed to sit for 48-72 hours.   An induction period, discussed earlier in 4.5.1, was observed for some reactions.

126

When complete, the reaction mixture was filtered into methanol (typically 5:1 methanol/toluene ratio) which resulted in the precipitation of the product. The solid product was collected by vacuum filtration and precipitated at least three more times from methanol/toluene solutions until TLC showed no residual alkene present in the product. This method was chosen as Nestor [17] has shown TLC to be very sensitive to any excess alkene present in the products. Some of the low molecular weight siloxanes would not precipitate and subsequently were recrystallized from suitable solvents. Products were dried in a vacuum oven.

4.5.4   FTIR   Reaction   Monitoring

Typical hydrosilation reactions with linear polysiloxane backbones are monitored by watching the disappearance of the Si-H band with FTIR or H^1NMR. For this work, FTIR was the analytical tool of choice as it has been shown[17] to be more sensitive than NMR.   Ten microliters of the reaction mixture were taken periodically from the flask and applied to a silver chloride plate. The solvent was allowed to dry and the resulting thin film was examined with FTIR.   Monitoring of the reaction with a liquid aliquot was difficult due to the dilute concentration of Si-H bonds in the reaction mixture.   Due to the excess of alkene in the reaction mixture, complete disappearance of the Si-H peak occured.   Figure 4.5 shows FTIR data from a representative reaction where the Si-H peak (2155 cm^{-1}) completely disappears from the spectra.   All siloxane starting materials were volatile and thus at time zero no Si-H peak was observed.   However, after the reaction had

proceeded for a short time, the Si-H peak appeared (due to involatile partially substituted product on the salt plate) and was monitored. Compounds M, DD, and TD did not exhibit any appreciable Si-H peak during the reaction. Instead a shift of the relative intensities of the 1272 to 1250-1200 peak and a broadening of the 1000-1100 cm^{-1} region during the first two hours indicated reaction progress as shown in Figure 4.6. These were attributed to both Si-CH$_2$ and Si-O-Si stretches, respectively. Monitoring of the terminal alkene bands, 990 and 910 cm^{-1} was difficult due to the complexity of the spectra.
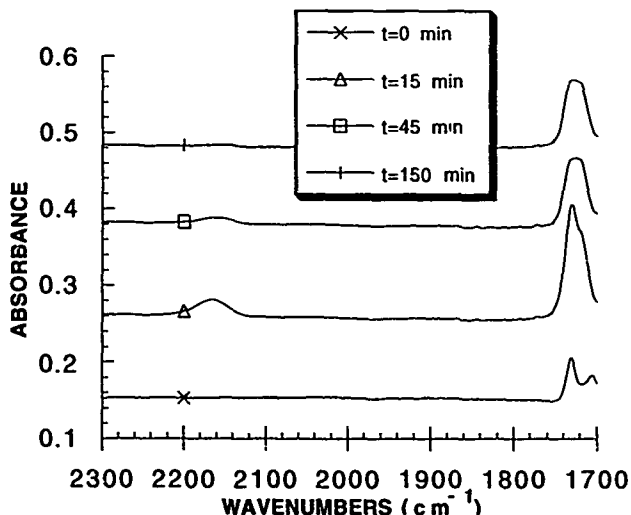
Figure 4.5: Disappearance of characteristic Si-H band at 2150 cm^{-1}
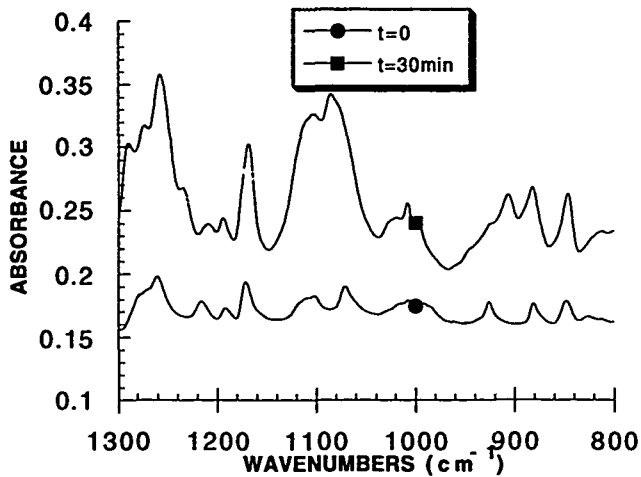
Figure 4.6: Broadening of 1200-1000 cm^{-1} region of FTIR spectra as reaction proceeds

4.5.5   Reactions Performed

The physio-chemical results of the synthesized siloxane materials will be discussed separately in the Sections V and VI. A number of siloxane materials were synthesized to examine changes in their properties as the ring size, leader length, mole fraction cholesterol, and type of siloxane core were varied. Shown in Table 4.4 is a listing of all silanization reaction products. They are grouped into several subsets. Included in this list are several siloxane materials containing mesogens other than the biphenyl and cholesterol units discussed above. These include NLO chromophores, new photochromic mesogens, and nonsteroidal chiral mesogens. The structures of these mesogens and the structure/property relationships of the product siloxanes are discussed in Section VI. All materials were examined with FTIR, DSC, NMR, optical microscopy, and TLC for general characterization. Elemental analysis was performed on certain select materials as was SEM/TEM. X-ray diffraction was performed on all materials.

Table 4.4

Siloxane compounds synthesized

Compound #	Siloxane [a]	Leader [b] Group	X_{chol} (%) [c]
	Mole Fraction Cholesterol		
1	C5	allyl	0
2	C5	allyl	15
3	C5	allyl	30
4	C5	allyl	50
5	C5	allyl	60
6	C5	allyl	70
7	C5	allyl	85
8	C5	allyl	100
	Linear Polysiloxanes		
9	P	allyl	0
10	P	allyl	25
11	P	allyl	50
12	P	allyl	75
13	P	allyl	100
	Leader Group/Ring Size		
14	C5	vinyl	50
4	C5	allyloxy	50
15	C5	penteneoxy	50
16	C5	octeneoxy	50
17	C5	vinyl	0
18	C5	vinyl	100
19	C4	vinyl	50
20	C4	allyl	50

Table 4.4 (con't)

	Low Molecular Weight Siloxanes		
21	M	allyl	100
22	M	allyl	0
23	TD	allyl	100
24	TD	allyl	0
25	DD	allyl	100
26	DD	allyl	0
	Star Siloxanes		
27	ST	allyl	0
28	ST	allyl	50
29	ST	allyl	100
30	ST	vinyl	0
	Other Siloxanes		
31 [d]	C5	allyl	45
32 [c]	C5	allyl	25
33 [f]	C5	allyl	80
34 [g]	C5	allyl	0

[a] - As listed in Figure 4.3

[b] - As listed in Figure 4.1

[c] - Mole fraction cholesterol within siloxane; Remainder is biphenyl mesogen

[d] - This siloxane contained 10 mole % of a photochromic spiropyran mesogen attached with allyloxy leader groups with 45% each of C4AB and B4AB.

[e] - This siloxane contained 50 mole % of a photochromic spiropyran mesogen attached with allyloxy leader groups with 25% each of C4AB and B4AB.

[f] - This siloxane contained 20 mole % of NLO chromophore based on MAONS. The remainder is 80% C4AB.

[g] - This siloxane contained 50 mole % of a nonsteroidal, chiral mesogen with 50% B4AB.

4.5.6 Proton NMR of Siloxane Materials

Reactions involving more than one type of mesogen were statistical in nature. H^1 NMR was employed to verify the composition of the synthesized materials. This allowed for independent verification that the hydrogen belonging to the Si-H bond was entirely reacted and that the resulting products were free of excess mesogen. Ratios of characteristic chemical shifts for key bonds within the cholesterol and biphenyl side chains were calculated and compared to the theoretical values. For all cases listed in Table 4.4, this procedure confirmed the theoretical mesogen ratio.

Recently[23], side reactions have been reported for hydrosilation reactions when using allyloxy derivatives. This reaction is characterized by the splitting of the CO bond, elimination of propene, and direct attack of the silicon to oxygen as shown in Figure 4.7. This can be observed with NMR as the chemical shift of the Si-CH$_3$ protons move downfield for the side product. No attempt at quantitating this shift was reported[23].

Evaluation of the siloxane materials synthesized in this study revealed differences in the extent of this side reaction depending on the nature of the siloxane core. The ring systems, both 4 and 5, show approximately 10-15% of propene elimination product in the final mixture. Numerical values were obtained by comparing the downfield chemical shift at 0.35 ppm to the sum of the peaks at 0.35 and 0.15 ppm. The hydrosilation reactions performed with the vinyl terminated mesogens revealed no indication of a side reaction taking place as expected.

133
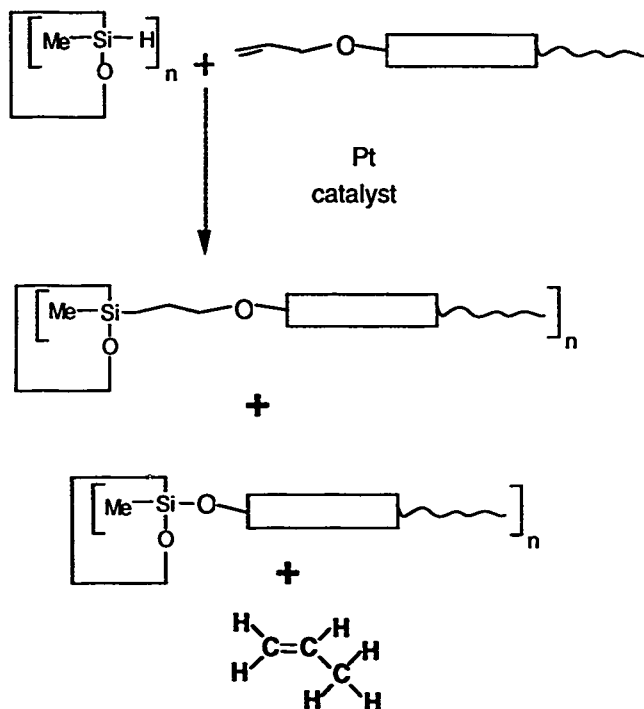
Figure 4.7: Schematic of normal hydrosilation reaction and propene elimination side reaction with allyloxy derivatives

Surprisingly, when the linear polysiloxanes and trisiloxanes reacted with allyloxy derivatives, they suffered the side reaction to different degrees. Linear samples exhibited 5-7% of the undesirable side product while no side reaction occurred for the low molecular weight siloxane compounds. It is unclear at this time what causes these differences.

134

4.5.7 Thin Layer Chromatography of Siloxane Materials

Not surprisingly, most ring siloxane products exhibited two spots, one which was due to the side reaction product as shown in Table 4.5.

Table 4.5

R$_f$ values for ring siloxane materials

Compound #	X$_{chol}$	R$_{f1}$	R$_{f2}$
1	0	0.185	0.35
2	15	0.17	0.35
3	30	0.16	0.37
4	50	0.165	0.35
5	60	0.16	0.34
6	70	0.14	0.32
7	85	0.13	0.29
8	100	0.115	0.27

The higher R$_f$ value spot was due to the undesired side product while the lower spot was due to the product. No indication of any unreacted alkene was observed. The trend of smaller R$_f$ values with increasing cholesterol content was a consequence of the larger molecular weights obtained. The ring systems with vinyl terminated mesogens showed only one spot which was consistent with the NMR data, suggesting no alkene elimination side reaction. Four membered ring systems exhibited slightly higher Rf values than their corresponding 5-membered rings probably due to the lower molecular weight. Linear polysiloxanes all showed the expected R$_f$ value of 0.0 as suggested in the literature[17].

4.6   Summary

An inert atmosphere/vacuum system has been utilized in synthesizing a heavy metal catalyst, all precursors, and a number of siloxane analogs of the commercial materials examined in Section III.   All precursor materials were thoroughly characterized using NMR, FTIR, elemental analysis, and thermal techniques.   These were used to synthesize a number of siloxane compounds which were also thoroughly characterized using the above techniques.   A consistent method to monitor the hydrosilation reactions using FTIR was developed.   Proton NMR of the siloxane products indicate the presence of a side reaction whose extent was dependent on the nature of the siloxane core.   The structure/property relationships of these compounds are investigated in Sections V and VI.

4.7   References

(1)   Speier, J.L., *Adv. Organo. Chem.*, **17**, 407-447(1979).

(2)   Cundy, C.S., Kinpton, B.M., and Lappert, M.F. in *Advances in Organometallic Chemistry*, F. G. A. Stone and R. West, Ed., Academic Press; New York,   pp 253-330, (1973).

(3)   Rylander, P.N.,   *Organic Synthesis with Noble Metal Catalysts*; Academic Press; New York, pp 275-293, (1973).

(4)   Speier, J.L., Zimmerman, R., and Webster, J., *J. Am. Chem. Soc.*, **79**, 974-978(1957).

(5)   Speier, J.L., Zimmerman, R., and Webster, J., *J. Am. Chem. Soc.*, **78**, 2278-2281(1956).

(6)   Gray, G.W., Lacey, D., Nestor, G., and White, M.S., *Makromol. Chem., Rapid Commun.*, **7**, 71-76(1986).

(7)   Drew, D. and Doyle, J.R. in *Inorganic Synthesis*, F. A. Cotton, Ed., McGraw-Hill; New York, **XIII,** pp 47-55, (1971).

(8)   Ringsdorf, H. and Schneller, A., *Makromol. Chem., Rapid Commun.*, **3**, 557-562(1982).

(9)   Sheehein, J.C. and Hess, C.P., *J. Chem. Phys.*, **77**, 1067(1955).

(10)   Gnanou, Y. and Rempp, P., *Makromol. Chem.*, **188**, 2111-2119(1987).

(11)   Hassner, A. and Alexian, V., *Tetrah. Lett.*, **46**, 4475-4478(1978).

(12)   Kasuga, K., Hatakeyama, H., and Hatakeyama, T., *Mol. Cryst. Liq. Cryst.*, **147**, 1-14(1987).

(13)   Dave, J.S. and Vora, R.A., *Liquid Crystals and Ordered Fluids*, , 477(1970).

(14)   Janini, G.M., Lamb, R.J., and Shaw, T.J., *Makromol. Chem., Rapid Commun.*, **6**, 57-63(1985).

(15) Adams, N.W., Bradshaw, J.S., Bayong, J.M., Markides, K.E., and Lee, M.L., *Mol. Cryst. Liq. Cryst.*, **147**, 43-60(1987).

(16) Apfel, M.A., Finkelmann, H., Janini, G.M., Laub, R.J., Luhmann, B.H., Price, A., Roberts, W.L., Shaw, T.J., and Smith, C.A., *Anal. Chem.*, **57**, 651-658(1985).

(17) Nestor, G., White, M.S., Gray, G.W., Lacey, D., and Toyne, K.J., *Makromol. Chem.*, **188**, 2759-2767(1987).

(18) Finkelmann, H. and Rehage, G., *Makromol. Chem., Rapid Commun.*, **1**, 733-740(1980).

(19) Finkelmann, H. and Rehage, G., *Makromol. Chem., Rapid Commun.*, **1**, 31-34(1980).

(20) Harrod, J.F. and Chalk, A.H., *J. Am. Chem. Soc.*, **(86)**, 1776(1964).

(21) Chalk, A.H. and Harrod, J.F., *J. Am. Chem. Soc.*, **87**, 16(1965).

(22) Hsu, C.S. and Perec, V., *Makromol. Chem., Rapid Commun.*, **8**, 331-337(1987).

(23) Kreuzer, F.H., Andrejewski, D., Haas, W., Haberle, N., Riepl, G., and Spes, R., *Mol. Cryst. Liq. Cryst.*, **199**, 345-378(1991).

SYNTHESIZED SILOXANE LIQUID CRYSTALLINE MATERIALS
(Results and Discussion)

In order to investigate the packing structures proposed in Section III, the structure/property relationships for a number of synthesized materials were examined. The results have been separated into sections due to the large number of compounds synthesized. All compounds are listed by number in their respective groups as defined in Table 4.4. Three separate variables which have been shown independently to induce layer packing in liquid crystalline structures were investigated. These included the variation of the size and shape of the siloxane core, the leader group length, and the molar composition of cholesterol within a given molecule. The phase behavior, microscopic and macroscopic packing structures, optical properties, and fiber drawing abilities as a function of these variables are investigated in this section. X-ray diffraction results were used to deduce the molecular architectures of the ring and linear siloxane compounds. These are compared to the models proposed in Section III. Models for the packing structures of the low molecular weight compounds are also proposed.

5.1 Effect of Mole Fraction Cholesterol

To examine the effect of cholesterol on the packing behavior, the phase diagram was formulated using a pentasiloxane ring with cholesterol contents ranging from 0 to 100%. Although Kruezer's

139

group[1] has recently reported on several compositions, no systematic examination of the complete phase behavior for these cyclic siloxane systems has been performed. The initial examination of the commercial systems reported in Section III indicated the cholesterol content had a substantial effect on the resulting molecular packing behavior. Table 5.1 lists eight compounds, all based on cholesteryl-4-allyloxybenzoate and biphenyl-4-allyloxybenzoate mesogens, synthesized to examine the phase behavior, optical properties, and X-ray diffraction behavior.

Table 5.1

Properties of pentasiloxane ring with various

percentages of the two base mesogens

#	X_{chol}	Thermal Transitions	λ_{max} (nm)
1	0.00	k_1 115 k_2 135 n 175 i	n/a
2	0.15	g 47 n^* 180 i	1050
3	0.30	g 50 n^* 208 i	647
4	0.50	g 50 n^* 220 i	514
5	0.60	g 50 S_A 120 n^* 230 i	n/a
6	0.70	g 61 S_A 200 n^* 245 i	n/a
7	0.85	g 60 S_A 210 n^* 244 i	n/a
8	1.00	g 61 S_A 228 n^* 246 i	n/a

k-crystalline; n-nematic; n*-cholesteric; S_A-smectic-A; i-isotropic; g-glassy; n/a-not applicable (did not exhibit selective reflection from cholesteric glasses)

5.1.1   Phase Behavior

As Figure 5.1 indicates, the phase behavior for these mixed mesogens was complex as five different phases were present. Compound 1 exhibited a nematic phase with a lower temperature crystalline phase. Extensive DSC measurements indicated the exact location of the crystalline to nematic temperature was very dependent on the thermal history of the sample. Cooling curves did not exhibit crystallization peaks while heating curves exhibited one or two first order transitions both below 120°C. The temperature and magnitudes of these peaks were dependent on annealing conditions. This may be indicative of domain size changes of the ordered regimes or small changes in the packing arrangement of differently ordered domains[2]. Optical microscopy only revealed a nematic phase upon cooling from the isotropic transition which contained a large number of characteristic disclination lines as shown in Figure 5.2. No sign of crystallinity was observed as these textures were frozen into a glassy state upon cooling to room temperature.
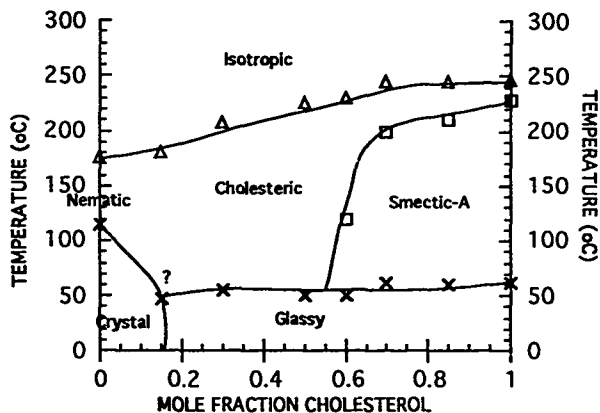
Figure 5.1   Phase diagram for pentasiloxane ring with varying percentages of cholesteryl-4-allyloxybenzoate and biphenyl-4-allyloxybenzoate mesogens

The left half of the phase diagram indicates a single cholesteric phase with a lower temperature glassy phase.   The selective reflection wavelengths for the glassy cholesteric films are shown in Table 5.1.   The thermal and optical properties of compounds 2, 3, and 4 agree well with the reported data[1].   Compounds containing more than 50% cholesterol formed a lower temperature smectic-A phase in addition to a narrow upper temperature cholesteric phase. This indicates the tendency of cholesterol moiety to pack in layers and thus form smectic phases[3-5].   Large homeotropic areas[6], characteristic of smectic-A phases, were observed with POM.

Figure 5.2: Characteristic nematic texture observed for compound 1 (200X)

Sheared films of the cholesteric materials had very good optical clarity throughout the visible region. Compound 1, a nematic mesophase, exhibited a foggy texture due to light scattering from random microdomains. Compounds 7 and 8 formed homeotropic glasses with very good optical clarity. Compounds 5 and 6 formed highly scattering films due to random orientations of

the molecules. As will be shown later, X-ray diffraction results indicate the macroscopic orientation for these two compounds was somewhere between a true planar or homeotropic orientation.

The clearing temperatures rose with increasing amounts of cholesterol as did the glass transition temperatures. It should be noted that the cholesterol-rich samples were observed to degrade under an air atmosphere near 200°C with microscopy and DSC. This would limit the upper working temperatures for these materials in air, although degradation was not observed until much higher temperatures (300°C) with helium and nitrogen.

5.1.2 SEM/TEM Results

Preliminary examinations with electron microscopy indicate these materials were relatively free of the macroscopic debris present in the commercial samples. SEM conducted on uncoated samples revealed the lamellar fracture surface characteristic of cholesteric materials for compounds 2-4 and a featureless fracture morphology for the smectic-A materials. Higher magnification SEM reveals some fine structure within the lamellar fracture surfaces due to fracture inconsistencies arising from misalignment of the cholesteric axes[7] for compounds 2-4. A pitch length of 330 nm was measured for compound 4 which yields a refractive index of 1.56 based on Equation 3.1. There was also a pronounced absence of surface granularity observed for the coated samples in Section III.

TEM also indicated morphologies free of foreign debris. No residual platinum was observed for these materials although it has

been seen with other siloxanes[8]. TEM was found useful to distinguish different liquid crystalline phases, as the typical banded texture, characteristic of a cholesteric phase, was absent for the smectic phases. This may serve as an additional technique for distinguishing liquid crystalline mesophases. One can observe a residual characteristic cholesteric morphology residing on edges of thin films from compounds 5 and 6. Being cooled the quickest, the edges retain remnants of the lamellar structure present in the cholesteric phase while the interior, which cools slower, exhibits a nonbanded morphology as shown in Figure 5.3.

Figure 5.3: TEM micrograph showing residual cholesteric behavior at the edge of a quenched smectic film (9 mm=500 nm)

5.1.3 X-ray Diffraction Results

A strong dependence of the diffraction patterns on composition was observed. The d-spacings of the reflections will be discussed later. Compound 1 exhibited a high number of reflections on the meridian for an edge orientation of a thin film. Although the reflections were periodic, there was no sign of crystallinity indicating the liquid crystalline order was frozen into a glass. The meridional layer reflections indicate a planar orientation of the molecules with respect to the thin film surface. Diffraction patterns taken normal to the surface of thin films exhibited a series of rings with the same d-spacings as the edge reflections. Compounds 2, 3, and 4 had diffraction patterns similar to those discussed in Section III for the commercial cholesteric materials. The fiber and edge diffraction patterns exhibited a series of periodic reflections in addition to a low-angle reflection on the meridian and large equatorial crescents which also indicates a planar orientation of the molecules. The normal diffraction patterns exhibited a series of equal intensity azimuthal rings of the same d-spacings. Diffraction patterns from the high x_{chol} samples (compounds 7 and 8) contained large crescents on the meridian and a large number of reflections on the equator. The 90° rotation of the mesogenic director with respect to the film surface is characteristic of a homeotropic orientation. This type of orientation was not observed for compound 5 or 6 although they also exhibited smectic-A phases. Their edge diffraction patterns resembled those from compounds 2-4 which indicates a preferential planar orientation of the molecules. Normal diffraction patterns of compound 5 exhibited equal

intensity rings while the behavior of compound 6 was somewhat different. Both the edge and normal diffraction patterns as a function of composition are shown schematically in Figure 5.4. Edge and normal refer to the geometries as shown in Section II. Combined, these two patterns give an indication of the macroscopic orientation of the molecules as a function of composition and indicate whether there was a twisting of the molecules present. The behavior of compund 6 is indicated in pattern (c) where both the edge and normal patterns exhibited orientation. Its normal patterns did not always show meridional alignment but always possessed an orthogonal relationship between the primary layer and wide-angle spacings. This indicates multiple domains with the molecules having a preferential planar orientation within these domains. The even intensity azimuthal rings exhibited by compound 5 suggests a twisted phase or random microdomains. The low smectic-A to cholesteric transition may indicate that a fully developed homeotropic packing could not form. No evidence of a smectic-C* phase was observed with microscopy. Attempts made at controlled shearing while in the smectic state for both compounds 5 and 6 resulted in diffraction patterns exhibiting features similar to those from compounds 3 and 4.
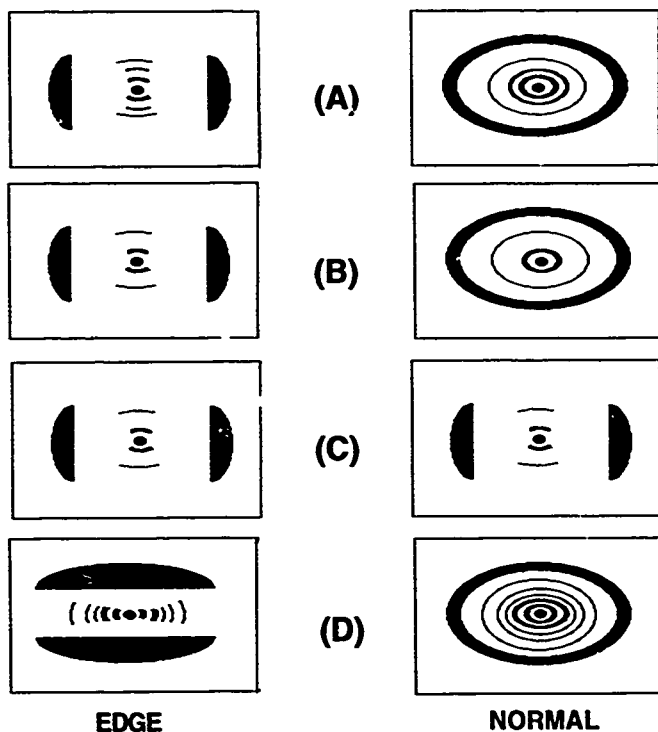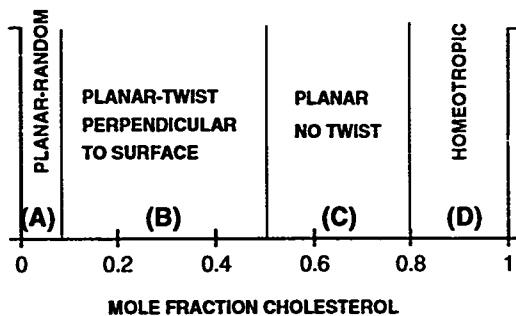
Fig 5.4: Macroscopic orientation versus composition with corresponding diffraction patterns

148

Fibers were obtainable only from mesophases of certain compounds. The relative ease with which filaments drew and their lengths were used as a basis of comparison. That is, if only a 1 mm long filament was obtained for compound X, its fiber drawing ability would be considered poor compared to compound Z which repeatedly drew 2 m long filaments. The cholesteric compounds drew very long fibers and no dependence on composition was observed. The higher x_{chol} smectic compounds did not readily draw fibers. Compound 5 did not draw as well as the cholesteric compounds. Compound 1 did not draw into glassy fibers, as partially crystalline filaments, discussed later, were obtained. These fibers were only weakly birefringent where those from compounds 2-5 were strongly birefringent. Fiber diffraction patterns were obtainable from compounds 1-5. Patterns from compounds 2-5 resembled thin film edge diffraction patterns of the same compound as the same reflections were present. Diffraction patterns from compound 1 indicate a partially crystalline packing behavior. This will be discussed later. Alignment of the molecules was parallel to the chain direction, which as discussed in Section III, is unusual for layered structures[9,10].

Two trends with respect to composition were observed in the thin film edge diffraction patterns. The primary layer spacings increased linearly with composition throughout the entire phase diagram as shown in Figure 5.5. Measured primary layer spacings ranged from 21 to 29Å. These can be compared to those calculated using the rule of additivity proposed by Diele[11-14] for mixed mesogenic systems. The calculated values were obtained using

149

Equation 5.1 with the mole fractions given in Table 5.1 and the extended molecular lengths of 18.8Å and 27.2Å (L_1 and L_2) for the biphenyl and cholesterol mesogens, respectively. These were calculated from the minimized structures (Chem3D software) by measuring the distance from an attached Si atom to the end of a fully extended mesogen. A constant of 4.5Å was added to take into account the diameter of the ring. The linear dependence of the primary d-spacing with respect to composition indicates the mesogens are statistically packing as a single entity.

$$x_1 * L_1 + x_2 * L_2 + constant = \text{d-spacing} \qquad \text{Eq. 5.1}$$
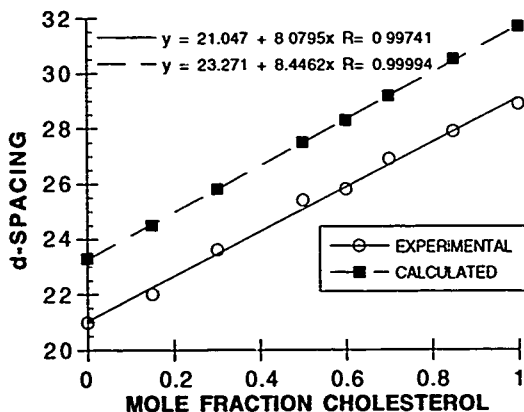
Figure 5.5: *Experimental versus calculated d-spacings as a function of x_{chol}. R=corr. coeff.*

The experimental d-spacings exhibited the same slope as the calculated values but are offset to a lower value by a constant. This

is typical for most interdigitated structures as d-spacings 10-15% smaller than the calculated values are usually obtained[6,15]. However, only by assuming a constant interface of siloxane (4.5Å) is present is this argument valid.. This supports the hypothesis that there may be a finite contribution to the experimental lamellae thickness from the siloxane ring itself as suggested in Section III. This is consistent with recently published results[16-18] which suggest that the formation of microphase separated regions caused by chemically different backbone and mesogenic groups is possible. Molecular modeling was used to examine the conformation of the siloxane ring within the lamellae and these results will be discussed in Section VII. A strong increase of the wide-angle spacings with composition was also observed. This increase, from 4.7 to 5.8Å with composition, was expected due to the larger rotational volume of the cholesterol-based mesogen.

The primary layer reflection observed in the cholesteric mesophase was sharp unlike most nematic-like compounds. For unaligned samples, the difference between nematic and smectic layer reflections is shown in Figure 5.6. Most nematics do not show a low two-theta reflection in an unaligned configuration. For nematic samples that do, this reflection is typically very broad and weak in intensity compared to the large two-theta reflection. This is indicative of the nonexistent or weak positional order among molecules. This is contrary to smectic structures whose small two-theta reflections are typically strong and sharp. In addition, multiple-order reflections sometimes arise from this reflection.
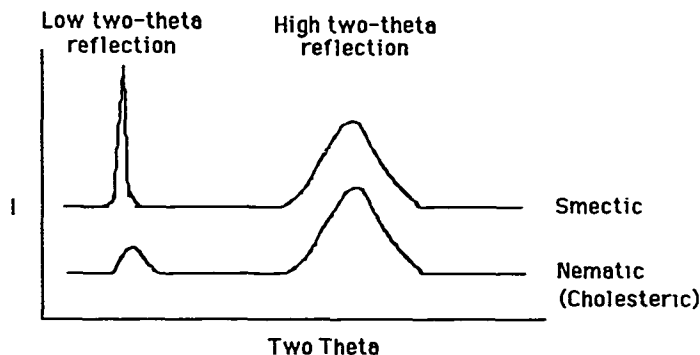
Figure 5.6: Schematic of unaligned diffraction pattern from nematic and smectic structures

Examination of unaligned diffraction results from throughout the phase diagram suggests a tendency to layer pack which is partially due to the cholesterol moiety. This is shown in Figure 5.7 which reveals very little difference in the low two-theta reflection with regard to the phase. In fact, compounds 2, 3, and 4, which exhibit only a cholesteric phase, also show a strong reflection indicative of a layered packing structure. This suggests that the typical model of a twisted nematic for conventional cholesteric phases does not hold here. Instead a layered-like molecular structure is present which is macroscopically twisted as suggested in Section III and previously by Freidzon[4,5,19,20].
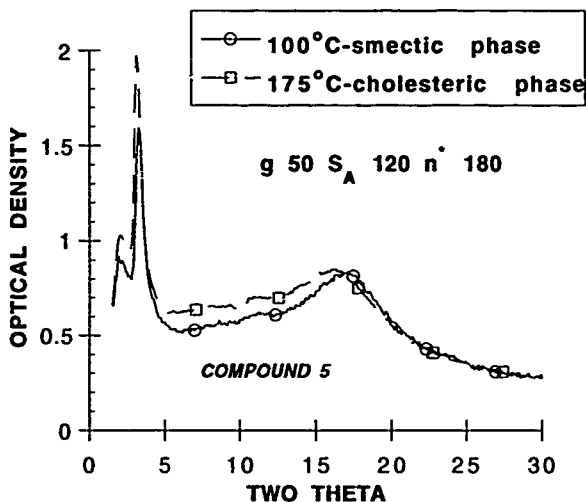
Figure 5.7: Unaligned diffraction from compound 5 in smectic and cholesteric phase

This tendency to layer pack and the similarity in the calculated and experimental d-spacings supports the model for the low x_{chol} compounds proposed in Section III. This is also consistent with the layered-like structure proposed by Freidzon. This behavior was attributed to the tendency of the cholesterol molecule to layer pack. This, however, cannot be the sole driving force as the unaligned diffraction pattern of compound 1 (no cholesterol) also possessed a strong small two-theta reflection.

As observed in Section III, a strong dependence of the intensity of the low-angle reflection with composition was noted. No low-angle reflection was observed for compounds 1 or 2. As

153

x_{chol} increased, the intensity of this reflection steadily increased as shown schematically in Figure 5.8. These values are the ratio of the primary layer intensity (I_{pls}) to the low-angle intensity (I_{las}) corrected for background scatter. A steady decrease of this ratio was observed as the low-angle reflection becomes stronger at higher cholesterol compositions. Also noted was a slight increase in the low-angle spacing with composition (46Å for compound 3 to 50Å for compound 8).
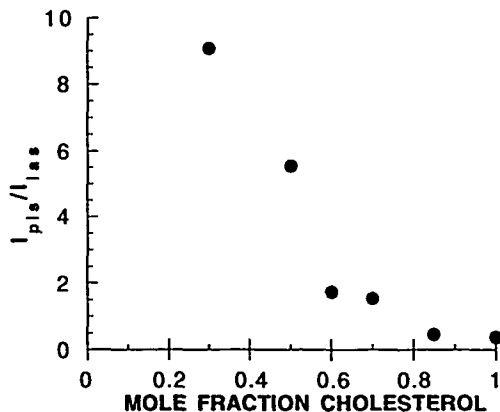
Figure 5.8: Primary layer intensity to low-angle intensity ratio as a function of composition

In Section III, the cause of the low-angle reflection was proposed as regions of partially interdigitated cholesterol molecules. Examination of the thin film X-ray patterns from compounds 7 and 8 further support this hypothesis. Unaligned diffraction patterns

from compounds 7 and 8 reveal three reflections of 50, 28.9, and 19.0Å, which are not periodic with one another. These reflections have been attributed to a packing structure similar to the dual packing scheme proposed in Section III. Two major lamellae are present as shown in Figure 5.9, one due to a highly interdigitated structure, responsible for the 28.9Å spacing, and the second due to a partially interdigitated structure which gives rise to the low-angle spacing. The spacing of these two structures is statistical in nature and not alternating as shown in Figure 5.9. The first packing scheme is analogous to the S_{Ad}-like structure proposed for the cholesterol-poor samples. As more and more cholesterol is added, the partially interdigitated structure becomes more and more dominant as indicated in Figure 5.8. Only above 80% cholesterol does the third reflection of 19.0Å appear. These three reflections, (a), (b), and (c) have previously[5,20] been seen for homopolymers of cholesterol derivatives. The relative amount of the (c) to (b) reflection could be controlled by the flexibility of leader group. It is unclear why two commensurate packing schemes are prevalent with only one molecular species. This indicates there are strong mesogenic interactions dictating the packing behavior. Under favorable circumstances, the cholesterol molecules have enough flexibility to interdigitate while under other circumstances they can't. This leads to interesting speculations about possible domain formation. No investigation into possible microphase separation of different packing schemes has been investigated.
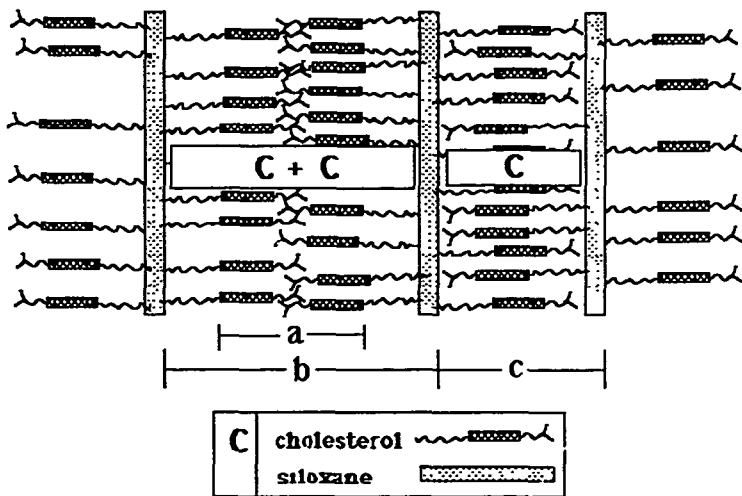
Figure 5.9: Packing scheme for compounds 7 and 8

Examination of all meridional d-spacings exhibited by these eight compounds is more revealing. Figure 5.10 shows all reflection spacings from an edge orientation of thin films where the legend data corresponds to Figure 5.9. Shown is a strong dependence of the primary layer spacing along with a much weaker dependence of the low-angle spacing. The periodic reflections originally observed for the commercial compounds in Section III[21,22] were present for all compositions (listed as unknown reflections in Fig. 5.10) although above $x_{chol}=0.80$, other multiple order reflections become evident. These diffuse reflections have previously been attributed to uncorrelated periodic columns of mesogens plus backbones[23,24].
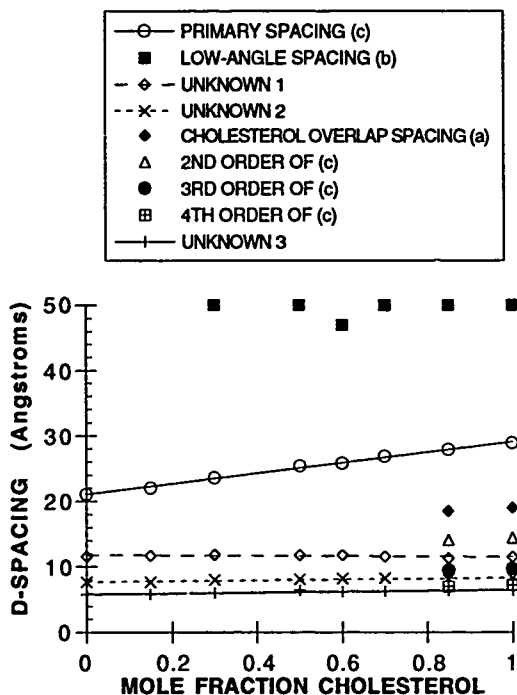
Figure 5.10: All reflections from an edge orientation of thin film edges as a function of composition

Adib[23] observed reflections in linear siloxane compounds corresponding closely to the 2nd and 3rd orders of the extended molecular lengths of the pendant mesogens. His compounds, however, exhibited layer spacings 1.4 times the extended molecular length and therefore those reflections could not be due to multiple order reflections. A recent review of X-ray diffraction from

157

mesomorphic polymers gives some insight into the origin of these reflections[25]. Two types of diffuse reflections due to short-range order can be present. The first are wide, curved diffuse streaks which do not correspond to the layer periodicity. These are due to intramolecular interferences. The second type are straight, diffuse lines on the meridian which are periodic with respect to the primary layer spacing. These are due to uncorrelated columns of molecules which exhibit longitudinal disorder as shown schematically in Figure 5.11(a). The presence of large aligning fields or strong intermolecular interactions among mesogens causes the nematic molecules to form strings of molecules. The corresponding diffraction pattern then consists of equally spaced diffuse lines on the meridian where the distance is proportional to the molecular length and the thickness of the reflection is related to the distance over which these strings occur. The similarity in periodicity of these reflections and Bragg multiple orders necessitates highly aligned samples to differentiate (Figure 5.11 (b)) between highly ordered monodomains and those which have a tendency to form strings of molecules with longitudinal disorder.
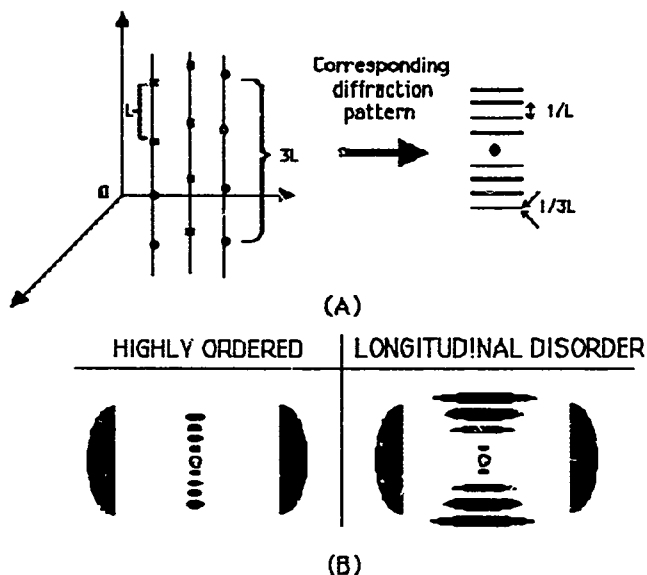
*Figure 5.11: Longitudinal disorder among chains of molecules (a)
and diffraction patterns for a highly aligned monodomain and a
layered structure exhibiting a tendency to form strings (b)*

The number of reflections observed was maximum at both
ends of the phase diagram. Compounds 4 and 5 (x_{chol}=0.5 and 0.6,
respectively) exhibited the weakest diffuse lines. Compound 1 and
compound 8 showed the greatest number of reflections as shown in
Figures 5.12 and 5.13 where both the SAXS and WAXS patterns
from both compounds are shown. Note the difference in orientation
with regard to composition as previously discussed in Figure 5.4.
This indicates that rings with only one type of mesogen attached
pack more efficiently. Compound 1 exhibited six periodic
reflections on the meridian while compound 8 exhibited several

periodic reflections on the equator. A substantial amount of arcing was present for both compounds indicating better alignment was possible. The large number of periodic reflections present indicates a strong tendency to form strings of molecules. The appearance of some of these reflections in unaligned samples indicates a portion may be due to intramolecular interferences. A layered-like structure consistent with the models previously proposed can be envisioned as shown in Figure 5.14. The strong tendency to pack into strings, however, indicates that mesogenic interactions may be more important in the development of the layer-like structure than previously envisioned. As already shown, compounds containing the steroid derivatives displayed a tendency to layer pack indicating strong steric interactions among these molecules. The large number of reflections for the all-biphenyl compound, however, suggests this cannot be the sole cause of this behavior. The proposed model, discussed in Section III for the cholesterol-poor compounds, a S_{Ad}-like bilayer with extensive association is therefore still valid. The much larger d-spacings than those calculated and the strength of the periodic diffuse lines both support a pseudo-layering not present in conventional nematic or cholesteric compounds.
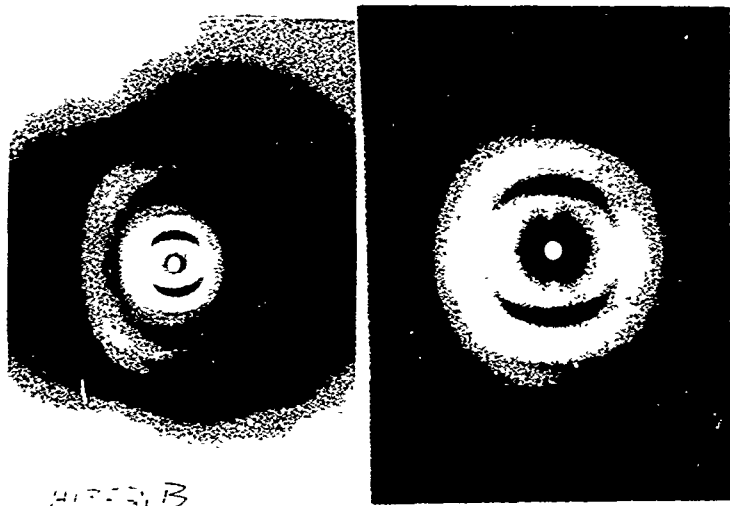
Figure 5.12: WAXS and SAXS patterns from a thin film edge of compound 1
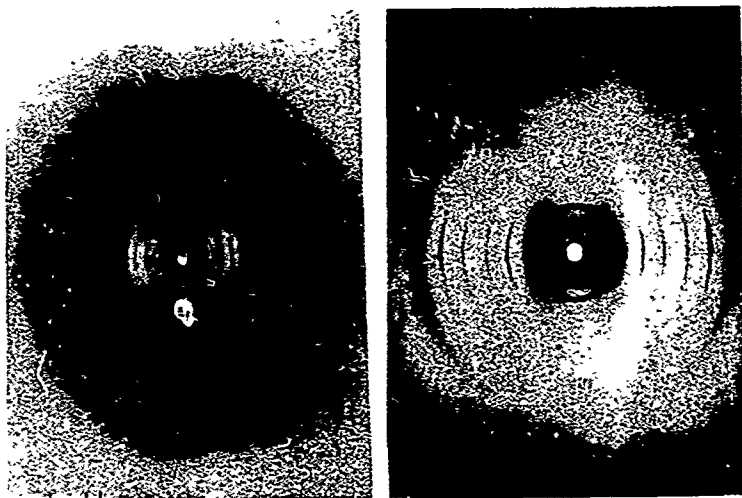
Figure 5.13: WAXS and SAXS patterns from a thin film edge of
compound 8
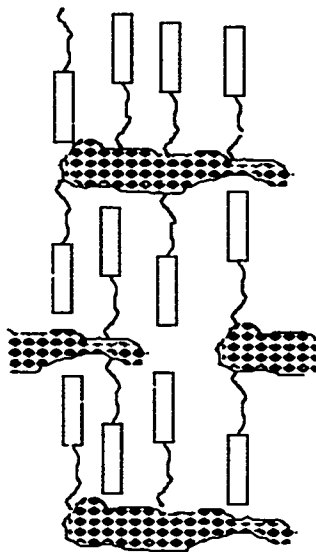
Figure 5.14: Schematic of string-like layered nematic-like structure of cyclic siloxanes

Elevated temperature diffraction patterns of unoriented bulk samples exhibited much less order as evidenced by the fewer number and weaker intensity of reflections. Strong reflections at low angles, primary layer reflections, and a wide-angle halo were observed for all compounds. No low-angle reflections were observed for compounds 1 and 2. In addition, the 8.0Å and/or 6.4Å reflections were noticed on a number of compounds including compounds 7 and 8 further suggesting they were not due to multiple order reflections from a single layer spacing. The appearance of these reflections in unaligned samples may indicate a small contribution due to intramolecular interferences[25]. The

163

primary d-spacings showed little dependence with temperature as shown in Figure 5.15. This was true for compounds exhibiting any of the three liquid crystalline phases and is contrary to what has been reported for highly interdigitated structures[26]. In some instances, there was a slight difference in d-spacing between the glassy room temperature value and that obtained at elevated temperatures. A slight shortening of the low-angle spacing was also observed as the temperature was increased. This indicates better packing efficiency among the cholesterol molecules. The diffraction patterns of compound 4 (cholesteric) were very similar to those taken of compounds 5 and 6 in their lower temperature smectic phase. This supports the proposition that the low x_{chol} compounds exhibit a smectic-like packing structure.
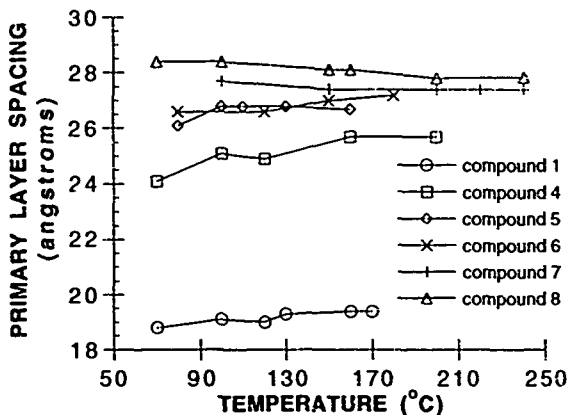
Figure 5.15: Primary layer spacing versus temperature

The intensity of the primary layer reflections increased with temperature indicating a better order parameter of the layers. For smectic compounds, the diffraction maxima depend on the order parameter of the smectic layers (τ_l) and the form factor of the mesogenic units (F) as:

$$I \propto (\tau_l \; F)^2 \qquad\qquad \text{Eq. 5.2}$$

If (F) is taken to be constant, the order parameter is proportional to the square root of the intensity[27]. Above a certain temperature, the intensity of these reflections decreased as the isotropic region was approached. More revealing was the dependence of the primary layer intensity to the low-angle intensity (I_{pls}/I_{las}) ratio on temperature as shown in Figure 5.16. The low-angle reflection clearly became weaker relative to the primary layer reflection with temperature for all smectic compounds and, therefore, this ratio increases as shown. This trend indicates that the elevated temperature supplies enough energy for the sterically hindered cholesterol molecules to become interdigitated. This is also supported by the slight decrease in the low-angle spacing which suggests some partial bilayer regions are transformed to a more efficiently packed structure. The wide-angle spacings also increase substantially with temperature as shown in Figure 5.17.

165
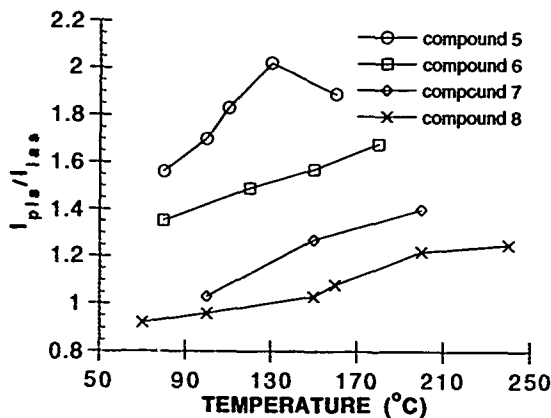
Fig 5.16: *Primary layer intensity versus low-angle intensity as a function of temperature*
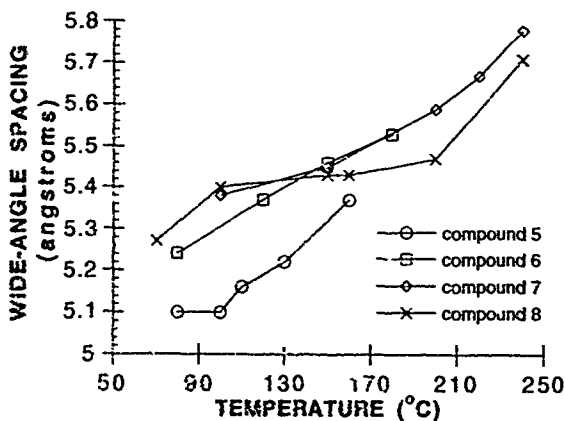
Figure 5.17: Wide-angle spacing as a function of temperature

As mentioned earlier, thin films of compound 1 exhibited frozen liquid crystalline diffraction patterns although being crystalline at room temperature. This is consistent with DSC data which indicate a glass transition upon cooling. Diffraction patterns taken from these thin films after one year of storage at room temperature indicate the frozen liquid crystalline phase was stable. Normal diffraction patterns exhibited a series of rings with the same d-spacings as the edge reflections. This was attributed to the random orientation of microdomains rather than a macroscopic cholesteric twist as previously discussed. As stated earlier, the large number of reflections was unusual for conventional nematic phases.

Crystalline diffraction patterns were obtained from powder samples that had been annealed for 48 hours at 120°C and from hand-drawn fibers. These patterns, shown in Figures 5.18 and 5.19, exhibit a number of reflections. Surprisingly, drawing of fibers induces partial crystallization as evidenced by the large number of reflections present. The large wide-angle crescents indicative of a liquid crystalline phase were present. However, a number of sharp meridional reflections were present in addition to those present on the thin film edge diffraction patterns. All of the reflections exhibited orientation on the meridian. No attempt at determining the unit cell parameters has been performed.
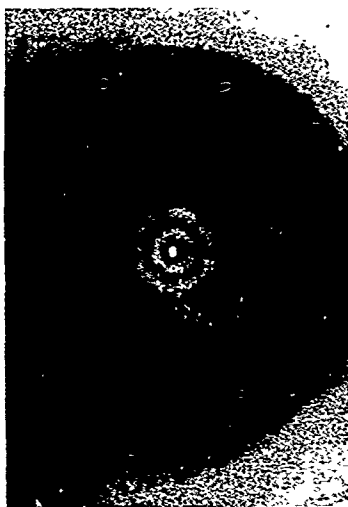
Figure 5.18: Powder diffraction pattern obtained from compound 1

HI' FIB7R
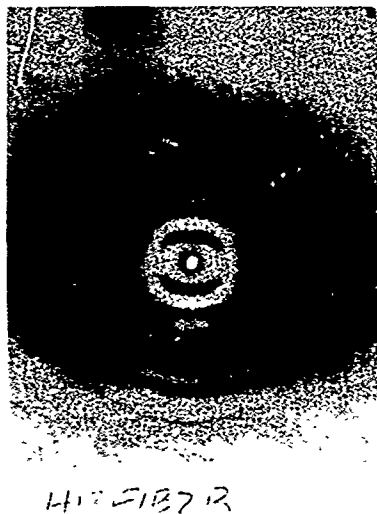
Figure 5.19: WAXS pattern from fibers of compound 1 drawn from
the melt

169

5.1.4 Summary

The dependence of the packing structure on x_{chol} was determined for all compositions. Large changes in the molecular packing in addition to macromolecular packing tendencies were observed. Above 50% cholesterol, a smectic-A mesophase region was present which adopted a homeotropic alignment in sheared thin films. The all-cholesterol material exhibited multiple molecular packing schemes consistent with the literature. Cholesterol served both to disrupt the molecular packing homogeneity and to increase the tendency to form layered smectic structures. Cholesterol-rich samples were also thermally unstable. The results support the proposed models of molecular packing discussed in Section III. The all-biphenyl material exhibited numerous reflections from a S_{Ad}-like structure consisting of highly interdigitated biphenyl mesogens. Although crystalline at room temperature, thin films exhibiting frozen liquid crystalline textures were formed. Fibers could be drawn from the melt although semi-crystalline diffraction patterns were obtained.

The cholesteric compounds exhibited diffraction patterns similar to those discussed in Section III. The cholesteric compounds have a tendency to layer pack which was attributed to the cholesterol moiety. The cholesteric phases of these compounds should not be thought of as a twisted nematic as conventional cholesteric compounds are. Instead, a psuedo-layered structure on the molecular level is twisted on the macroscopic level to give rise to the helicoidal twist responsible for the unique optical properties exhibited by these compounds. X-ray diffraction reflections

170

previously attributed to multiple order reflections are now thought to be due to uncorrelated periodic columns, as observed by others[23,25,28-30]. The tendency to form strings of molecules may be important with regard to the fiber forming capabilities. This indicates strong mesogenic interactions among molecules. Fibers could easily be drawn from the cholesteric compounds. The thermal and optical properties of the cholesteric compounds were consistent with those published previously[1]. The packing scheme of these compounds lies intermediate to that of the all-cholesterol and all-biphenyl samples. Elevated temperature diffraction confirmed these trends with respect to composition. Changes in the ratio of intensities due to the two packing schemes indicates thermal energy is sufficient to induce changes in the packing structures. The lack of a dependence of the primary layer spacings with temperature was unusual in light of the interdigitation proposed[26]. Changes in the intensity of the smectic layer reflections with temperature indicated an increase of order. Optical clarity was good for the cholesteric materials and the homeotropic smectic thin films. The cholesteric materials formed nice glasses exhibiting selective reflection from the visible to the NIR and birefringent fibers were obtained. The inability to draw fibers from most of the smectic compounds is a consequence of their layered structure.

5.2   Polysiloxane Liquid Crystalline Materials

5.2.1   Thermal Properties

Five linear polysiloxane analogs of the corresponding cyclic materials are listed in Table 5.2. In general, there was little difference in the thermal properties between cyclic and linear compounds containing the same composition of mesogens. This is contrary to what has been reported for cyano-based mesogens as markedly different thermal properties between cyclic and linear analogs were observed[31]. Compound 9 exhibited a slightly lower crystalline transition than had been reported previously[32] although this transition was highly dependent on the thermal history of the sample. In general, there were only slight differences in the glass transition temperatures although there were substantial differences in the clearing temperature.

Table 5.2

Linear polysiloxane thermal data

Compound	X_{chol}	Thermal Transitions (^oC)
9	0	k 120 n 175 i
10	25	g 50 n* 210 i
11	50	g 62 n* 230 i
12	75	g 50 S_A >230 dec
13	100	g 72 S_A > 250 dec

k-crystalline;   n-nematic;   n*-cholesteric, S_A-smectic-A;   dec-decomposed

In general, identification of the liquid crystalline phases was difficult with POM due to the increased viscosity of the linear compounds. Compounds 12 and 13 exhibited undetermined smectic phases. Based on the phase diagram reported for the cyclic materials and the similarities between thermal transitions, this phase is most likely a smectic-A phase. Small focal-conic regions characteristic of smectic-A phases were observed when annealed above 200°C for a few hours. Decomposition set in before the clearing temperatures could be obtained. There was no indication of the upper temperature cholesteric phase present in the cyclic analogs. Compound 9 exhibited nematic droplets although there was a pronounced absence of the disclination lines observed for compound 1. Compounds 10 and 11 were colored and exhibited Grandjean disclination lines indicative of a cholesteric phase upon shearing. Also noted was the appearance of a mosaic phase within a very small temperature regime near the isotropic transitions. This was characterized by large mosaic platelets with a brown, rust, or blue coloring. It is unclear whether this was a dynamic texture in the formation of the cholesteric phase or an indication of a blue phase. Sheared, glassy thin films of these two linear compounds exhibited much poorer optical quality than films from their analogs. The selective reflection wavelength could not be obtained, as highly scattering films were formed. The selective reflection wavelength, estimated from the general color exhibited by these films, was in the blue region for compound 11 and in the red region for compound 10. Also noted was a much poorer ability of the linear compounds to draw into fibers. Only short segments of fibers from

173

compounds 9, 10, and 11 were obtained and attempts to draw long continuous fibers failed.

5.2.2   X-ray Diffraction Results

There were few differences in the reflection spacings for edge and normal diffraction patterns from cyclic and linear analogues of the same composition as indicated in Table 5.3.   Slightly larger spacings were observed for the linear compounds.   There were substantial differences in the relative orientation and intensities of similar reflections, however.

Table 5.3

Measured d-spacings for linear and cyclic
thin film edge geometries

100% Cholesterol	
Cyclic (Å)-compound 8	Linear (Å)-compound 13
50.0	51.5
28.9	29.4
1 9	19.1
14.4	14.5
11.5	11.5
9.7	9.7
8.2	8.3
7.2	7.2
6.4	- -
Crescent-5.8	Crescent-5.8

Table 5.3 (con't)

100% Biphenyl

Cyclic (Å)-compound 1	Linear (Å)-compound 9
21.0	22.1
11.6	11.7
7.7	7.8
5.7	5.8
4.7	4.8
3.9	--
Crescent-4.4	Crescent-4.5

50/50 Material

Cyclic (Å)-compound 4	Linear (Å)-compound 11
46.9	46.9
25.6	26.2
12.1	12.6
8.1	8.1
6.4	--
Crescent-5.0	Crescent-5.0

Diffraction patterns from compound 9 exhibited five reflections of similar spacings as compound 1. Edge diffraction patterns resembled powder patterns with a slight preferential alignment on the equator. It is surprising that very little orientation of the mesogens was observed in light of the strong meridio.al alignment exhibited by compound 1. Fiber patterns exhibit reflections preferentially aligned on the equator indicating the siloxane backbones were aligned along the direction of draw with the mesogens lying preferentially perpendicular to the fiber axis. As with the edge patterns, very little orientation was

observed. This equatorial orientation is typical for layered polymer liquid crystalline structures[9] in fiber geometries. The switch in alignment indicates the strong effect the backbone structure and conformation has on the packing behavior. No signs of partial crystallinity were observed for these fibers although semi-crystalline fibers from compound 1 were formed. Edge diffraction patterns from compounds 10 and 11 agree with the diffraction patterns originally observed for the Wacker materials. The edge patterns show planar orientation with multiple reflections on the meridian while the normal patterns exhibit uniform intensity rings of the same d-spacings. No 6.4Å reflection was present for compound 11. Fiber diffraction patterns from these two compounds exhibited a 90° rotation of the mesogens as compared to their cyclic counterparts. Edge diffraction patterns from compounds 12 and 13 showed the large number of reflections observed for the ring compounds 7 and 8. These reflections resided on the equator indicating homeotropic alignment of the molecules. The relative degree of azimuthal intensity distributions was also similar.

Elevated temperature diffraction revealed slight differences between linear and cyclic analogs. The low-angle reflection was much stronger than the primary reflection for compound 13 than for compound 8. The 20Å reflection, attributed to correlated diffraction from the interior of the partially interdigitated cholesterol molecules, was also stronger in intensity than for compound 8. Both these factors indicate the mer gens on the linear compond did not have the same flexibility as when attached to the cyclic siloxane core. As the temperature increased, the I_{pls}/I_{las} ratio

decreased substantially for compound 13 as shown in Figure 5.20 which may indicate reduced flexibility of the cholesterol molecules. All cyclic smectic compounds showed increasing ratios with temperature. Very little changes in the reflection spacings were observed for the linear compounds. There was little difference between compounds 11 and 4 except for the presence of the hazy halo at 10-15Å discussed earlier for the linear compound. This was also true of compound 9. Elevated temperature diffraction was not performed on compounds 10 or 12.
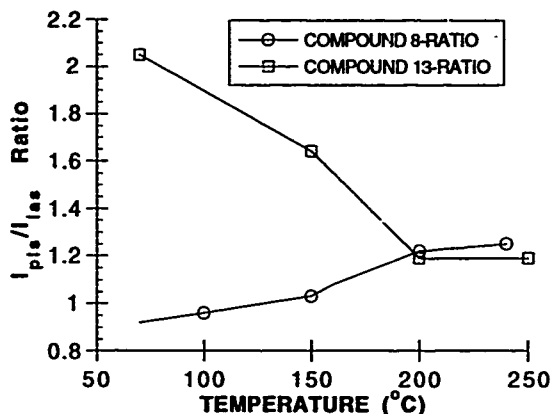
Figure 5.20: I_{pls}/I_{las} ratio dependence on temperature

The similarities of the d-spacings indicate the linear compounds possess similar packing schemes to those proposed for the cyclic compounds. The only difference observed was the macroscopic orientation of the mesogens in thin film and fiber

177

geometries. Differences in the ability to form fibers and optically clear thin films were attributed to different flexibilities. All thin-film diffraction compositional dependences for the cyclic compounds were exhibited by the linear compounds.

5.3 Effect of Leader Group

Several analogs of the ring systems discussed earlier were synthesized with various length leader groups to examine their effect on the resulting packing structure and phase behavior. Four different length leader groups were incorporated into the ring system with a 50/50:biphenyl/cholesterol ratio as shown in Table 5.4. Homopolymers with vinyl leader groups were also synthesized. Leader groups are shown in Figure 4.1.

Table 5.4

Leader group examination

#	Leader	X_{chol}	Thermal Transitions
14	vinyl	50	g 80 n* 204 i
4	allyloxy	50	g 50 n* 220 i
15	penteneoxy	50	g 41 S_C^* 130 S_A 198 n* 228 i
16	octeneoxy	50	g 32 S_A 210 i
17	vinyl	0	g 76 n 155 i
18	vinyl	100	g 76 S_A 247 i

n-nematic; n*-cholesteric; S_A-smectic-A; S_C^*-chiral smectic C
i-isotropic; g-glassy

5.3.1 Phase Behavior

As Table 5.4 indicates, there was a strong dependence of phase behavior on the length of the leader group. The glass transition temperature increased with shorter leader groups as compound 14 (vinyl) exhibited a T_g of 80°C while compound 16 (octeneoxy) exhibited a T_g of 32°C. This is expected due to a decoupling of motions between the mesogens and the cyclic backbones[33]. The selective reflection capabilities of the cholesteric phases were also affected as compound 14 exhibited a much different λ_{max} (694 nm) and $\Delta\lambda_{max}$ (139 nm) than compound 4 (514nm and 67nm). Materials with longer leader groups exhibited higher order mesophases; compound 15 exhibited smectic-C*, smectic-A, and cholesteric phases while compound 16 exhibited a smectic-A phase. Identification of the smectic-A phase was facilitated by the formation of large homeotropic areas. The smectic-C* phase manifested itself as a grey, slightly birefringent texture attributed to a pseudo-homeotropic texture[6]. The appearance of the chiral smectic phase is promising due to its applications as a optical material[34-36]. Homopolymers with vinyl leader groups generally exhibited much higher glass transition temperatures with corresponding lower clearing temperatures. An exception was compound 15 where no upper temperature cholesteric phase was observed although a similar clearing temperature to compound 8 was observed. Fibers could not be drawn from the smectic materials while compounds 14 and 4 drew into nice fibers. The optical clarity of the homeotropic films was comparable to that exhibited by compound 8. Compounds 15 and

179

17 exhibited foggy thin films which scattered light. The cholesteric films again exhibited good clarity outside the reflection bandwith.

5.3.2 X-ray Diffraction Results

Diffraction patterns from compounds 14, 4, and 15 exhibited meridional layer spacings indicating planar orientation while compound 16 exhibited equatorial reflections indicating homeotropic orientation of the molecules. Sheared film diffraction patterns revealed a strong dependence of the degree of order, d-spacings, and small-angle intensity on the leader group length. Table 5.5 lists the observed d-spacings for the four compounds containing $x_{chol}=0.50$.

Table 5.5

Trends with respect to leader group

spacings in Å

Compound 14	Compound 4	Compound 15	Compound 16
Vinyl	Allyloxy	Penteneoxy	Octeneoxy
44.1	46.9	NONE	NONE
24.5	25.6	25.2	31.3
11.5	12.1	12.6	15.6
7.5	8.1	8.8	10.5
	6.4	6.7	7.8, 6.4
5.2[a]	5.0[a]	4.8[a]	4.8[a]

a- Wide-angle reflection

There was a steady increase of the primary layer spacing with leader group length in addition to a decrease of the small-angle intensity. Compounds 15 and 16 did not exhibit a small-angle reflection. Again, reflections were present which resembled multiple order reflections as initially described for compound 4. These diffuse reflections were very weak for compound 14 and there was an absence of the 6.0Å reflection observed for compound 4. Compound 15 exhibited two reflection orders which both gave an indication of splitting as shown in Figure 5.21. Using the splitting angle of 30°, shown in Figure 5.22, a molecular length of 29Å can be calculated. For all cases, the measured d-spacings were larger than the calculated values using the rule of additivity discussed earlier as shown in Table 5.6. The average difference was 3.0Å which was similar to the diffferences observed in the composition study. Compound 16 exhibited a strong primary equatorial reflection at 31.3Å, a weaker second-order spacing at 15.6Å, and three weak, diffuse lines as shown. It also exhibited a very weak equatorial arc at 64Å as shown in Figure 5.23. As discussed later, this reflection was not present at elevated temperature. All four compounds exhibited wide-angle crescents orthogonal to the layer reflections. These spacings slightly decreased with increasing leader group lengths.

Table 5.6

<u>Calculated and measured primary layer reflections for compounds</u>
<u>with different length leader groups (Å)</u>

Compound	Measured	Calculated	Difference
14	24.5	20.9	3.6
4	25.6	23.0	2.6
15	29.0[a]	25.6	3.4
16	31.3	28.9	2.4

[a] - Using molecular length based on splitting angle
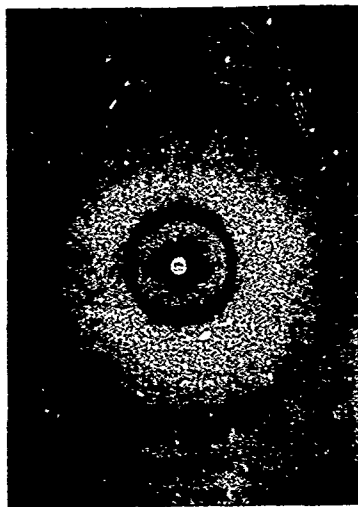
Figure 5.21: SAXS pattern of compound 15
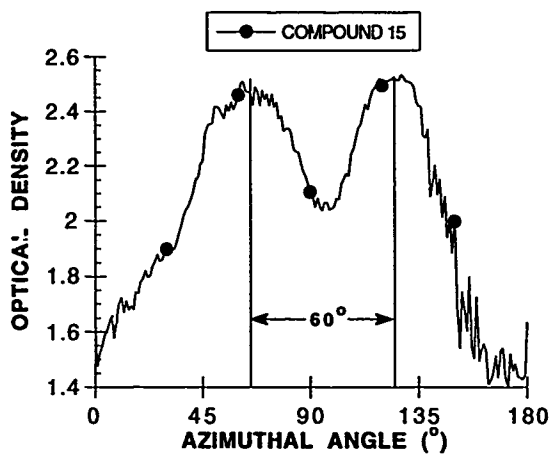
Figure 5.22: *Splitting of the first-order reflection for compound 15*

183

Figure 5.23: SAXS pattern of compound 16

Differences in the diffraction patterns have been attributed to the different flexibility of the mesogens depending on the length of the leader group. This is readily apparent when comparing compounds 14 and 4 as shown in Figure 5.24. Compound 4 exhibited a much weaker small-angle reflection than compound 14 and no low-angle reflection was observed for compound 15. In addition, the primary layer reflection of compound 4 was moderately diffuse and misoriented (broad χ angle) compared to that of compound 14. The lower flexibility of the vinyl leader groups did not allow the mesogens to become highly interdigitated. Mesogens that have become interdigitated were more or less locked in by their lower flexibility and therefore, their primary layer reflection became less diffuse and misoriented. The longer leader groups of compounds 15 and 16 allowed enough flexibility to become fully interdigitated and no low-angle reflection was observed.
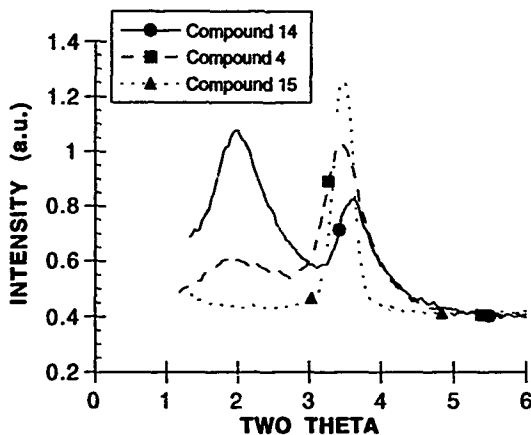
Figure 5.24: Low-angle region for compounds 14, 4, and 15

Comparison of the homopolymers containing vinyl and allyloxy leader groups also revealed differences attributed to the flexibility of the spacer unit. Compound 17 did not exhibit any primary layer spacing instead only showing a wide-angle halo. Attempts to orient by shear failed as thin film edge patterns were unoriented. Also present was the 8.0Å reflection observed for the other compounds although it was very weak in intensity. Compound 18 exhibited similar patterns to compound 8 although its spacings were shorter as shown in Table 5.7. All reflections exhibited smaller d-spacings except the wide-angle reflection which was slightly larger for the vinyl compounds. This indicates the decreased flexibility present for the shorter leader groups. The change in the low-angle and primary layer spacings can be

186

expected as the leader group is a building block of both. A decrease in the overlap spacing of the partially interdigitated cholesterol molecules from 19.0Å to 17.3Å was also observed. One would expect this spacing to be constant regardless of leader group although its intensity should vary. The first three reflections were strong but the remaining reflections were weak compared to compound 8. The low-angle intensity was stronger relative to the primary layer intensity for compound 8 indicating more of the partially overlapped structure was present.

Table 5.7

D-spacings of compounds 8 and 18(Å)

Compound 18	Compound 8
vinyl	allyloxy
46.0	50
26.2	28.9
17.3	19.0
13.1	14.4
10.6	11.5
8.8	9.7
7.6	8.2
	7.2
Wide-angle-6.0	Wide-angle-5.7

Elevated temperature diffraction indicated little dependence of the primary layer spacing for compounds 14, 4, and 16 but a strong dependence for compound 15 on temperature as shown in Figure 5.25. This is typical for a smectic-C* compound which shows increasing d-spacings with temperature as the smectic-A phase is approached. No other compounds examined exhibited such a strong dependence of d-spacing with temperature. The second-order reflection was not observed at elevated temperature although the 6.7 and 8.8Å reflections were present throughout the mesophase. No dependence of these reflections on temperature was observed.
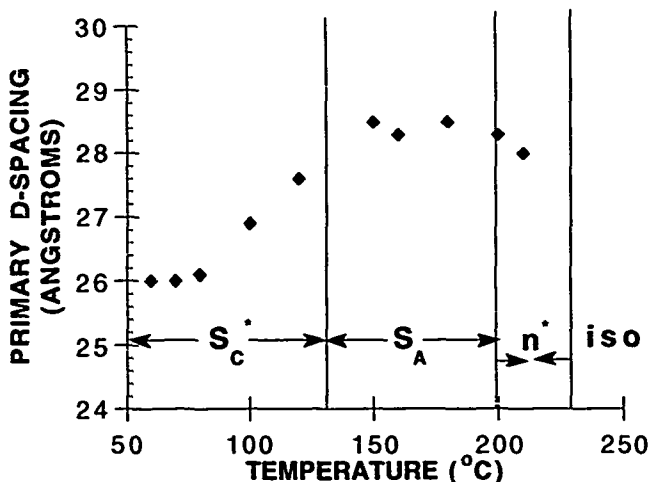
Figure 5.25: D-spacings versus temperature for compound 15

Compound 16 exhibited the first two reflection orders, the wide-angle halo, and a diffuse halo at 10.3Å. No sign of the weak 64Å reflection was observed throughout the mesophase. The intensity of the second-order reflection increased with temperature. This indicated an increase in the smectic ordering of the molecules as temperature was increased. The intensity and d-spacing of the wide-angle halo also increased with temperature.

Compound 18 exhibited different thermal behavior than compound 8 as shown in Figure 5.26. The ratio of I_{pls}/I_{las} was constant with temperature for this compound where it steadily increased for compound 8. This is indicative of the decreased flexibility of the vinyl leader groups. Not enough mobility was possible to allow the partially interdigitated structure to become more efficiently packed. The strong intensity of the 18Å spacing for compound 18 also indicates the dominance of the partially overlapped structure in analogy to compound 13. No elevated temperature diffraction was done on compound 17 as there was no primary layer spacing intensity to monitor.
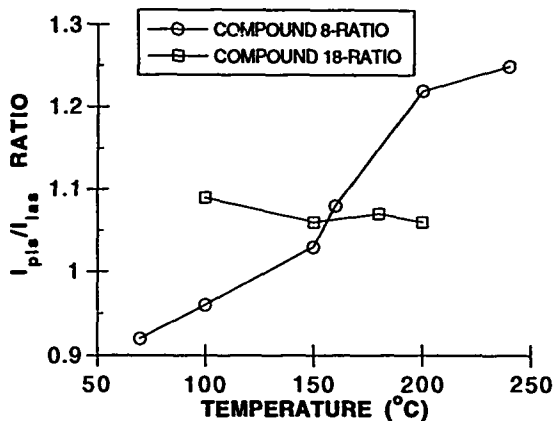
Figure 5.26: Primary layer to low-angle intensity ratio for compounds 8 and 18

Lengthening of the leader group effectively has the same effect on the packing structure as does decreasing x_{chol}. Longer leader groups allow sufficient flexibility for the mesogens to become fully interdigitated into a smectic structure rather than a S_{Ad}-like structure proposed for the cholesteric compounds. Compounds with vinyl leader groups showed a much weaker tendency to layer pack. The presence of diffuse periodic lines was observed regardless of the leader group length. Their spacings and intensities were highly dependent on the leader group. In addition, the glass transition temperature decreased substantially with longer leader groups due to a decoupling of the dynamic side-chain and main-chain motions. Fiber drawing was possible for the poorly

packed vinyl compounds while the layered penteneoxy and octeneoxy compounds did not draw fibers at all. The assumption that strong lateral interactions induced by a high degree of interdigitation is responsible for the fiber drawing capabilities needs to be examined further. The inability of the smectic compounds and the poor ability of the nematic compounds to draw fibers indicate this ability may be a function of the viscosity of the cholesteric phase.

5.3.3   Ring Size Variation

Two compounds, shown in Table 5.8, were synthesized with 4-membered siloxane rings. Their X-ray diffraction patterns were similar to their 5-membered ring counterparts. There was little change in the glass transition and clearing temperatures as expected[1]. There was, however, a strong effect on the reflection wavelength and bandwidths as shown in Table 5.8 for the allyloxy-containing compounds but not for the vinyl analogs. This is consistent as the helical twisting power of the chiral component weakens as the ring size decreases[1].

Table 5.8

Effect of ring size

Compound	Ring	T_g (°C)	T_{cl} (°C)	λ (nm)	$\Delta\lambda_{max}$ (nm)
		Vinyl Leader Groups			
14	D5	74	204	694	139
19	D4	73	204	695	134
		Allyloxy Leader Groups			
4	D5	50	220	520	67
20	D4	55	230	638	150

More ring sizes are needed to fully examine the effect on structure/property relationships. The relative insensitivity of the thermal transitions was unexpected as very strong dependence on the thermal behavior with ring size has been observed for cyanoester siloxane-ring systems[31]. The clearing temperatures steadily rose with ring sizes ranging from 4 to 24 while a minimum in glass transition temperature was observed for a 13-membered ring. It is thought this is due to the siloxane ring adopting a low energy, all trans conformation at x=11.

5.4 Low Molecular Weight Siloxane Liquid Crystals

Six low molecular weight siloxanes (LMWS) were synthesized to act as model compounds for investigating the interplay of the siloxane moiety and the pendant mesogens. Two consisted of a

disiloxane (DD) with all biphenyl or cholesterol on each end, two consisted of a trisiloxane (TD) with all biphenyl and cholesterol on each end, and two consisted of a trisiloxane (M) with either a biphenyl or cholesterol molecule on one end attached with allyloxy leader groups. The molecular structures of the siloxanes are shown in Figure 4.4 of Section IV. Their thermal properties are listed in Table 5.9. The thermal transitions of the two mesogens are listed for comparison. The two compounds containing the DD siloxanes are still under investigation.

Table 5.9

Low molecular weight siloxanes investigated as model compounds

Compound #	Siloxane	X_{chol}	Thermal Transitions (^{o}C)
21	M	100	k 88 S_A 150 i
22	M	0	k 30 S_E^a 65 i
23	TD	100	k 80 S_A 225 i
24	TD	0	k_s 76 k_{s1} [b]118 i i 94 n 89 S_A 64 i
25	DD	100	unknown
26	DD	0	unknown
B4AB			k 139 i
C4AB			k 121 n^* 237 i

k-crystalline; n-nematic; S_A-smectic-A; S_E-smectic-E; i-isotropic; n^*-cholesteric
[a]- See discussion in text
[b]- Two crystal forms were present

5.4.1   Phase   Behavior

The phase behavior of these compounds was much different than the cyclic or linear compounds. All four materials had lower temperature crystalline phases with some exhibiting multiple crystalline forms. The two cholesterol derivatives exhibited a single smectic-A phase. The two biphenyl compounds exhibited a variety of liquid crystalline phases. Lowering of the crystalline-to-mesophase and mesophase-to-isotropic transitions for compound 21 as compared to C4AB was expected. Addition of a siloxane tail to the end of the cholesterol molecule effectively increased the length of the flexible leader group thereby minimizing the influence of the attached mesogen. This has been observed previously for cholesterol esters[37,38]. The addition of a second cholesterol mesogen (compound 23) had little effect on the crystalline temperature but increased the clearing point substantially.

The all-biphenyl materials exhibited much more complicated phase behavior. Compound 22 exhibited what appeared to be a smectic-E phase as a high degree of continuous arcing across the back of focal-conic fans was observed. This is a characteristic texture for this type of smectic phase[6,39]. The formation of this phase directly below the isotropic phase is unusual[6] as very few materials have exhibited this phase paramorphotically. The focal-conic texture indicates the presence of an upper temperature smectic-A mesophase although it was not observed. Compound 24 exhibited monotropic smectic-A and nematic phases in addition to multiple crystal structures.

5.4.2   X-ray   Diffraction   Results

Sheared film diffraction patterns only yielded information regarding the crystalline phase. Crystal structure analyses have not yet been performed. Compounds 21 and 23 showed only a first-order reflection in addition to the wide-angle halo at elevated temperature. There was little change in the d-spacing with temperature although there were changes in the wide-angle intensity and spacings similar to the cyclic compounds. Interestingly upon cooling compound 23 to room temperature, a diffraction pattern consisting of a series of equally spaced rings was obtained as shown in Figure 5.27. The sharpness of the wide-angle reflection indicates its crystalline nature. It is peculiar, however, that the only reflections present were multiple order with respect to the primary layer. Similarly, shear aligned films of compound 23 exhibited the same d-spacings except there was preferential homeotropic alignment of the molecules as shown in Figure 5.28. These thin films were optically clear.

Compound 22 exhibited what appeared to be three diffraction orders as shown in Figure 5.29 in the mesophase region. In addition, broad diffuse reflections were present at 7.2Å and 4.7Å as shown. The wide-angle reflection was sharper for this compound than for the smectic-A compounds examined. Upon cooling below the crystalline transition temperature, a typical powder pattern was exhibited as shown in Figure 5.30. The other two biphenyl-containing compounds exhibited strong first-order reflections and wide-angle halos. The wide-angle spacings were 4.7Å for the biphenyl compounds and 5.8Å for the cholesterol compounds.
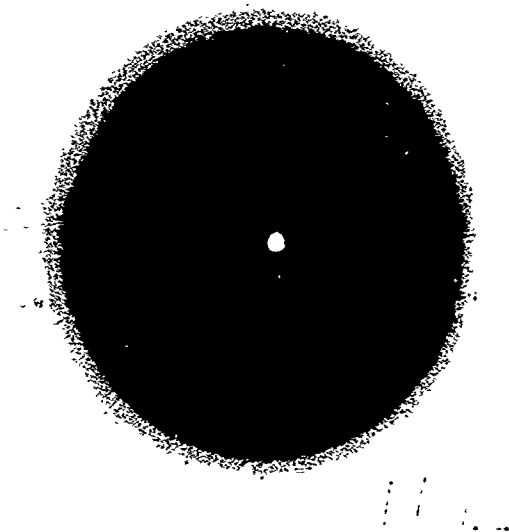
Figure 5.27: Diffraction pattern from thin film of compound 23 at room temperature
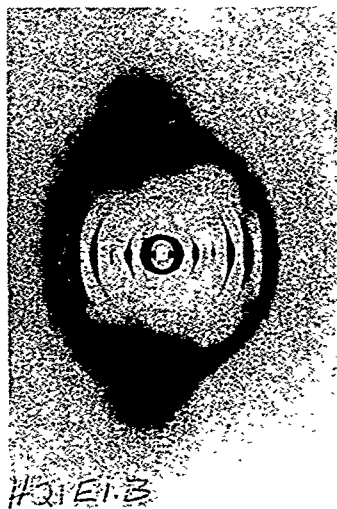
Figure 5.28: Sheared thin film diffraction pattern of compound 23
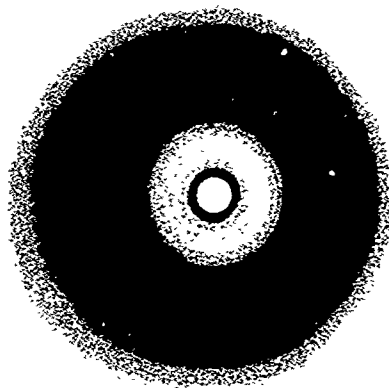
Figure 5.29: Compound 22 at 55°C
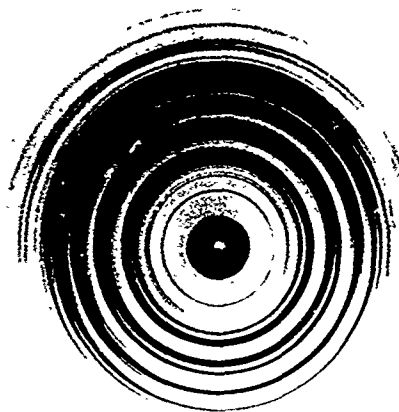
Figure 5.30: Compound 22 at room temperature

The measured first-order reflections for all four compounds (Table 5.10) can be compared to the calculated extended molecular lengths shown tabulated in Table 5.11. Molecular lengths were calculated from all-trans extended molecules using software (CHEM3D) generated models.

Table 5.10

Measured first order spacing for LMWS

Biphenyl Compounds	Cholesterol Compounds
M - #22 - 28.2Å	M - #21 - 37.0 Å
TD - #24 - 24.1 Å	TD - #23 - 32.0 Å
DD - #26 - not measured	DD - #25 - not measured

Table 5.11

Calculated molecular lengths for LMWS

A	B	extended length[a]	fully interdigitated[b]
M siloxane 7.6 Å	biphenyl 18.6 Å	44.8 Å	26.2 Å
M siloxane 7.6 Å	cholesterol 26.8	61.2 Å	34.4 Å
TD siloxane 5.8 Å	biphenyl 18.6 Å	43.0 Å	24.4 Å
TD siloxane 5.8 Å	cholesterol 26.8	59.4 Å	32.6 Å
DD siloxane 2.8 Å	biphenyl 18.6 Å	40.0 Å	21.4 Å

[a]. Assuming no interdigitation-A + B + B
[b]. Assuming full interdigitation- A + B

The calculated fully interdigitated lengths of 24.4 and 32.6Å for the trisiloxane dimers (TD) of biphenyl and cholesterol, respectively, were close to measured first-order reflections of 24.1 and 32.0Å. This indicates a fully interdigitated packing structure as shown in Figure 5.31 consisting of two layers, siloxane (A) and mesogen (B). The measured values of 28.2 and 37.4Å for the monomer (M) compounds were slightly larger than the calculated values of 26.2 and 34.4Å. For both these cases, the aliphatic tails of the cholesterol mesogens have been factored into the lengths of the cholesterol unit. The resulting packing scheme for the monomer siloxanes, shown in Figure 5.32, is very similar to that shown for the TD siloxanes except that slightly larger d-spacings were observed due to steric crowding of the terminal methyl groups on the free end of the siloxane with the aliphatic tails of the cholesterol. The slight difference in the monomer spacings implies some mixing of the terminal methyl unit on the siloxane core with these aliphatic tails.
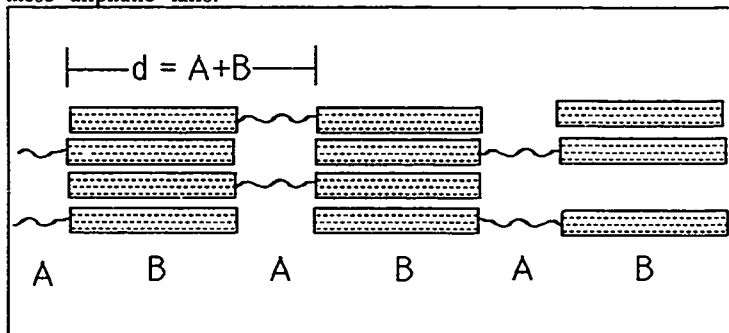
Figure 5.31: Packing scheme of TD siloxanes with pendant mesogenic groups. A and B refer to lengths tabulated in Table 5.11
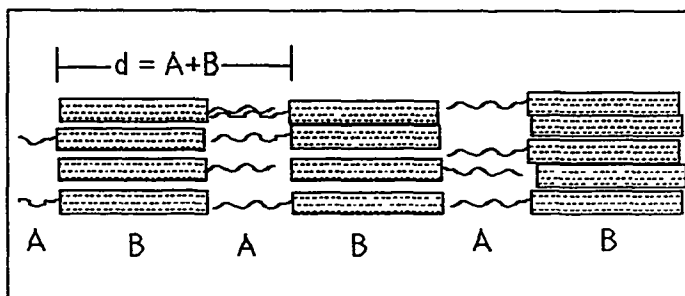
Figure 5.32: Packing scheme of M siloxanes with pendant mesogenic groups. A and B refer to lengths tabulated in Table 5.11

Preliminary results indicate that the flexibility of the interior core substantially affects the packing behavior of the pendant groups. Very small changes in chemical structure lead to strong differences in the packing behavior. The inclusion of the siloxane moiety into a repeat unit indicates, that although highly flexible, it has to be considered separately. Large changes in the packing behavior brought about due to small changes in the chemical structure indicate that intermolecular interactions are very important. Further information about the structural properties of these low molecular weight compounds is discussed in Section VIII which describes preliminary real-time diffraction experiments.

These six compounds were initially synthesized to act as model compounds in the understanding of siloxane/hydrocarbon interactions. Slight changes in the chemical makeup resulted in large changes in the molecular packing schemes and the thermal properties. Not all compounds exhibited a highly interdigitated packing structure; instead this was observed to be a function of the

202

flexibility of the siloxane core and aliphatic/siloxane component interactions.

5.5 Star Siloxanes

A seventh siloxane core, a "star" molecule, was obtained to examine the importance of coupled mesogenic interactions inherently present for the cyclic siloxane rings. The crowded crown-shaped[40] siloxane may add constraints to intramolecular interactions in addition to the typical rotational and translational motions of the mesogens. Several attempts made using the same hydrosilation chemistry employed previously have yielded no success. Products obtained, compounds 27, 28, 29, and 30 exhibited reproducible thermal and structural (X-ray) properties. NMR and elemental analysis did not yield chemical verification of the products, however. NMR indicates the allyloxy side reaction discussed in Section IV may greatly affect the product stoichiometry. FTIR also indicated much different reaction kinetics as the reaction proceeds to completion within the first 5 minutes. All other hydrosilation reactions take place over the course of 4-24 hours. A reaction, compound 30, involving vinyl leader group mesogens has been recently performed to eliminate the variable of the allyloxy side reaction. Analysis of this compound is underway.

5.6 Summary

The packing structure proposed for the commercial materials has been investigated by examining all compositions. The all-biphenyl ring compound exhibited a S_{Ad}-like packing structure

although exhibiting an apparent nematic phase. The large number of diffuse meridional reflections indicates a tendency to form strings of molecules indicating dominant mesogenic interactions. The all-cholesterol ring compound exhibited two packing structures, a S_{Ad} and S_{A2} layering scheme, which gave rise to a number of reflections in sheared thin films. Major phase behavior and organizational changes were observed as a function of composition. Four-membered cyclic compounds exhibited the same thermal transitions but much different optical properties than their 5-membered analogs. The leader group length greatly affected the order and mesophase behavior. These differences were attributed to changes in the flexibility of the pendant groups. Compounds with longer length leader groups exhibited well-ordered smectic phases. Uncorrelated multiple reflections were also present and exhibited a strong dependence of their spacings and intensity on the length of the leader group. The ability to form optical quality glasses was worse for the linear compounds. In addition, fiber drawing was possible but much more difficult than for the cyclic analogs. Diffraction patterns exhibiting similar d-spacings to the cyclic analogs but much different orientation and relative intensities were obtained. Fibers could primarily be drawn from materials exhibiting cholesteric phases. Smectic-A and C* compounds, although exhibiting a high degree of interdigitation, did not draw. This indicates the rheological properties may be of prime importance rather than the microscopic packing structure. The chiral nature of the cholesteric phase may also be of importance. Optical clarity was good for homeotropic smectic-A and cholesteric

204

phases only. Lengthening the leader group yielded compounds with much poorer optical quality. The model compounds exhibited large changes in their thermal properties and molecular packing schemes with slight changes in structure. The flexibility of the siloxane core affected the degree of interdigitation possible for these compounds.

5.7 References

(1) Kreuzer, F.H., Andrejewski, D., Haas, W., Haberle, N., Riepl, G., and Spes, R., *Mol. Cryst. Liq. Cryst.*, **199**, 345-378(1991).

(2) Zugenmaier, P. and Menzel, H., *Makromol. Chem.*, **189**, 2647-2655(1988).

(3) Finkelmann, H. and Rehage, G., *Makromol. Chem., Rapid Commun.*, **3**, 859-864(1982).

(4) Freidzon, Ya.S., Kharitonov, A.V., Shibaev, V.P, and Plate, N.A., *Eur. Polym. J.*, **21(3)**, 211-216(1985).

(5) Freidzon, Ya.S., Tropsha, Ye.G., Tsukruk, V.V., Shilov, V.V., Shibayev, V.P., and Lipatov, Yu.S., *Polym. Sci. USSR*, **29(7)**, 1505-1511(1987).

(6) Gray, G.W. and Goodby, J.W.G., *Smectic Liquid Crystals-Textures and Structures*; Leonard Hill; Glasgow, pp 224, (1984).

(7) Livolant, F. and Bouligand, Y., *Moi. Cryst. Liq. Cryst.*, **166**, 91-100(1989).

(8) Klei, H.E., Observed with other materials; specifically was looking at hydrosilation products using PBLG. When examining thin films with TEM, observed particles within the films that was determined to be platinum using EDAX.

(9) Zentel, R. and Strobl, G.R., *Makromol. Chem.*, **185**, 2669-2676(1984).

(10) Freidzon, Ya. S., Talroze, R.V., Boiko, N.I., Kostromin, S.G., Shibaev, V.P., and Plate, N.A., *Liq. Cryst.*, **3(1)**, 127-132(1988).

(11) Diele, S. and Sackman, H., *Ber. Bunsenges. Phys. Chem*, **93**, 467-477(1989).

(12) Diele, S., Nasta, L., and Sackmann, H., *Krist. Techn.*, **12**, 1063(1977).

(13) Diele, S., Baumeister, U., and Demus, D., *Z. Chem.*, **21**, 267(1981).

(14) Diele, S., Billich, K., and Przedmulski, J., *Z. Chem*, **26**, 26(1986).

(15) Basu, S., Rawas, A., and Sutherland, H.H., *Mol. Cryst. Liq. Cryst.*, **132**, 23-28(1986).

(16) Davidson, P., Levelut, A.M., Achard, M.F., and Hardouin, F., *Liq. Cryst.*, **4(5)**, 561-571(1989).

(17) Percec, V., Hahn, B., Ebert, M., and Wendorff, J.H., *Macromolecules*, **23**, 2092-2095(1990).

(18) Diele, S., Oelsner, S., Kuschel, F., Hisgen, B., and Ringsdorf, H., *Mol. Cryst. Liq. Cryst.*, **155**, 399-408(1988).

(19) Shibaev, V.P. and Freidzon, Ya. S. in *Side Chain Liquid Crystal Polymers*, C.B. McArdle, Ed., Blackie; Glasgow, pp 260-286, (1989).

(20) Freidzon, Y.S. in *Polymeric Liquid Crystals*, A. Blumstein, Ed., Plenum Press; New York, (1985).

(21) Bunning, T.J., Klei, H.E., Samulski, E.T., Crane, R.L., and Linville, R.J., *Liq. Cryst.*, **10(4)**, 445-456(1991).

(22) Bunning, T.J., Klei, H.E., Samulski, E.T., Adams, W.W., and Crane, R.L., *Characterization of Cholesteric Cyclic Siloxane Liquid Crystalline Materials*, Wright Laboratory, WL-TR-91-4012, (1991).

(23) Adib, Z. A., Ph.D. Thesis, University of Hull, (1987).

(24) Sutherland, H.H., Adib, Z.A., Gasgous, B., and Nestor, G., *Mol. Cryst. Liq. Cryst.*, **155**, 327-336(1988).

(25) Davidson, P. and Levelut, A.M., *Liq. Cryst.*, **11(4)**, 469-517(1992).

(26) Richardson, R.M. and Herring, N.J., *Mol. Cryst. Liq. Cryst.*, **123**, 143-158(1985).

(27) Leadbetter, A.J. and Wrighton, P.G., *J. Phys.*, **3**, 234-242(1979).

(28) Decobert, G., Soyer, F., Dubois, J.C., and Davidson, P., *Polym. Bull.*, **14**, 549-556(1985).

(29) Davidson, P., Keller, P., and Levelut, A.M., *J. Phys.*, **46**, 939-946(1985).

(30) Davidson, P. and Levelut, A.M., *J. Phys.*, **49**, 689-695(1988).

(31) Richards, R.D.C., Hawthorne, W.D., Hill, J.S., White, M.S., Lacey, D., Semlyen, J.A., Gray, G.W., and Kendrick, T.C., *J. Chem. Soc., Chem. Commun.*, , 95-97(1990).

(32) Apfel, M.A., Finkelmann, H., Janini, G.M., Laub, R.J., Luhmann, B.H., Price, A., Roberts, W.L., Shaw, T.J., and Smith, C.A., *Anal. Chem.*, **57**, 651-658(1985).

(33) Portugall, M., Ringsdorf, H.. and Zentel, R., *Makromol. Chem.*, **183**, 2311-2321(1982).

(34) LeBarny, P. and Dubois, J. C. in *Side Chain Liquid Crystal Polymers*, C. B. McArdle, Ed., Blackie; Glasgow, pp 130-158, (1989).

(35) Griffin, A. C. and Bhatti, A. M., **69**, 295-300(1989).

(36) Kapitza, H., Paths, H., and Zentel, R., **44**, 117-125(1991).

(37) Kasuga, K., Hatakeyama, H., and Hatakeyama, T., *Mol. Cryst. Liq. Cryst.*, **147**, 1-14(1987).

(38) Dave, J.S. and Vora, R.A., *Liquid Crystals and Ordered Fluids*, , 477(1970).

(39) Hsu, C.S. and Lu, Y.H., *J. Polym. Sci. Part A: Polym. Chem.*, **29**, 977-986(1991).

(40) Hahn, B. and Perec, V., *Mol. Cryst. Liq. Cryst. Inc. Nonlin. Opt.*, **157**, 125-150(1988).

azobenzene and its derivatives have been observed[2-6]. Cholesteric liquid crystal siloxanes containing azobenzene moieties have potential applications in reversible holographic optical data storage media[6]. The combination of photochromic and liquid crystalline properties in the same molecule renders the material useful for many practical applications including imaging technology, optical storage materials, integrated optical devices, laser optical media, and nonlinear optical (NLO) materials. Synthesis of materials exhibiting both photochromic and liquid crystalline properties is challenging as their combination usually results in the loss of one of these properties.

Recently, there have been reports of nematic liquid crystal polymers in which the side chains were partially composed of spiropyran or spiroxazine units[7-11]. Irradiation of these copolymer liquid crystalline films with UV radiation turned the films blue due to the formation of the merocyanine structure as shown in Figure 6.1. This process was reversible with the application of heat and light (>500 nm)[7-11]. The noncentrosymmetric geometry of the merocyanine structure also leads to possible second order $\chi^{(2)}$ nonlinear optical applications. Previous work has shown that the merocyanine form of spiropyran in liquid crystal polymers can be aligned by poling in an electric field with a resulting second order nonlinear response[11].

azobenzene and its derivatives have been observed[2-6]. Cholesteric liquid crystal siloxanes containing azobenzene moieties have potential applications in reversible holographic optical data storage media[6]. The combination of photochromic and liquid crystalline properties in the same molecule renders the material useful for many practical applications including imaging technology, optical storage materials, integrated optical devices, laser optical media, and nonlinear optical (NLO) materials. Synthesis of materials exhibiting both photochromic and liquid crystalline properties is challenging as their combination usually results in the loss of one of these properties.

Recently, there have been reports of nematic liquid crystal polymers in which the side chains were partially composed of spiropyran or spiroxazine units[7-11]. Irradiation of these copolymer liquid crystalline films with UV radiation turned the films blue due to the formation of the merocyanine structure as shown in Figure 6.1. This process was reversible with the application of heat and light (>500 nm)[7-11]. The noncentrosymmetric geometry of the merocyanine structure also leads to possible second order $\chi^{(2)}$ nonlinear optical applications. Previous work has shown that the merocyanine form of spiropyran in liquid crystal polymers can be aligned by poling in an electric field with a resulting second order nonlinear response[11].

Table 6.1

Photochromic siloxane compounds

Compound #	C4AB/B4AB/ABNS	Thermal Transitions (°C)
31	45/45/10	g 51 n* 210 i
32	25/25/50	g 80 i

g-glassy; n*-cholesteric; i-isotropic
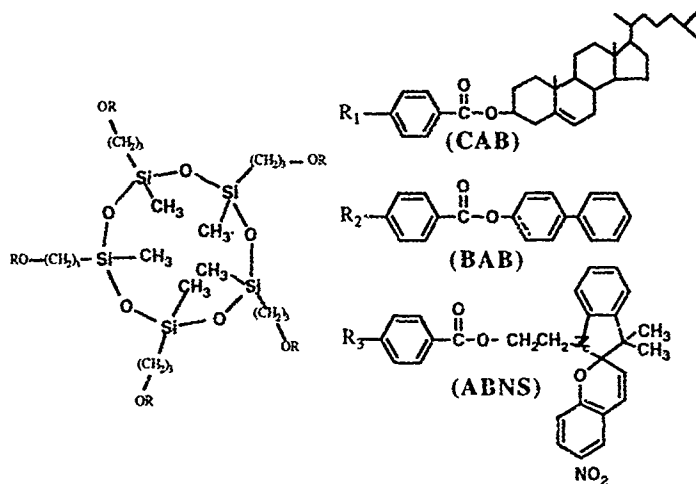
Figure 6.2: The chemical structure of compound 31

Table 6.1

Photochromic siloxane compounds

Compound #	C4AB/B4AB/ABNS	Thermal Transitions ($^{\circ}$C)
31	45/45/10	g 51 n* 210 i
32	25/25/50	g 80 i

g-glassy; n*-cholesteric; i-isotropic

Figure 6.2: The chemical structure of compound 31

212
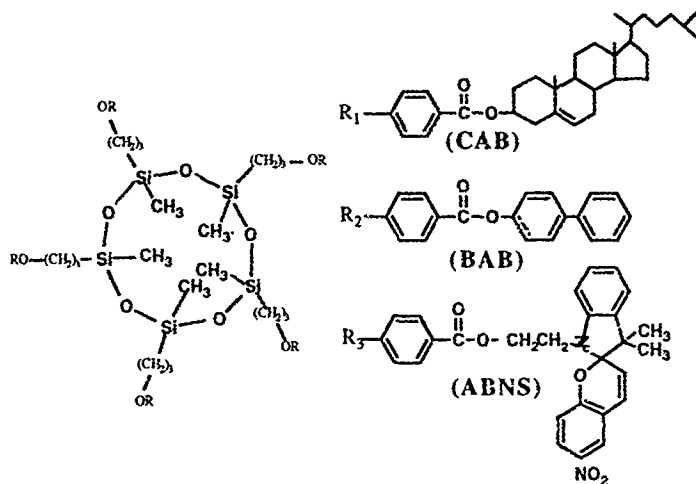
Compound 31 exhibited two thermal transitions as observed with differential scanning calorimetry (DSC). A glass transition temperature of 51°C followed by a clearing temperature of 210°C were obtained from second heating runs with a heating rate of 10°C/min. Polarized optical microscopy (POM) confirmed the liquid crystalline phase present between these temperatures was cholesteric. Upon cooling from the isotropic phase, a tight focalconic texture characteristic of cholesteric materials was observed[13]. Displacement of the top cover glass slip resulted in the reorientation of the random helices perpendicular to the glass substrates causing a macroscopically aligned planar texture which selectively reflects circularly polarized light[14]. It is interesting to note the similarities of the thermal transitions to compound 4 discussed in Section V. The addition of only 10% spiropyran drastically decreases the clearing temperature with little effect on the glass transition temperature. This implies that the presence of the laterally attached mesogen disrupts the intermolecular interactions needed to form a liquid crystalline phase. This is further evidenced when increasing the spiropyran composition to 50%. Compound 32 did not exhibit any liquid crystalline behavior. A glass transition of 80°C was observed above which a sticky, rubbery substance formed that did not readily flow until 200°C.

The glassy nature of compound 31 allowed for the cholesteric structure to be frozen into thin films. Shearing the liquid crystal between glass plates at 150°C followed by cooling to room temperature yielded a glassy film exhibiting a selective reflection band centered at 514 nm as shown in Figure 6.3(a). The

213

corresponding absorption spectra, Figure 6.3(b), also reveals this selective reflection bandwidth as well as the characteristic UV absorption maxima of spiropyran at 340 nm.

Upon irradiation of the thin film with UV light (365 nm), the glassy liquid crystalline film turns blue in less than ten seconds due to the characteristic ring-opening reaction (Figure 6.1) of the spiropyran molecule which is now transformed to the merocyanine structure. This absorption peak, centered at 594 nm, is clearly evident in the absorption spectrum but is absent from the reflection spectra. No changes in the reflection wavelength or bandwidth were observed upon irradiation. The blue color disappears slowly in the dark over a period of 20 hours. The color fading reaction involves the ring closure of the zwitterionic merocyanine form. The energy barrier for the dark back reaction is known to be influenced by substituents in the spiropyran ring, polarity of solvents, and environmental conditions. In highly viscous solvents and polymer matrices, the ring closure in dark has been shown to proceed slowly[15]. Heating of the thin film to 45-50°C eliminates the blue color in a matter of seconds. The blue color formation and disappearance are reversible, thus demonstrating the photochromic nature of this liquid crystalline siloxane. The thin films were also resistant to photofatigue.
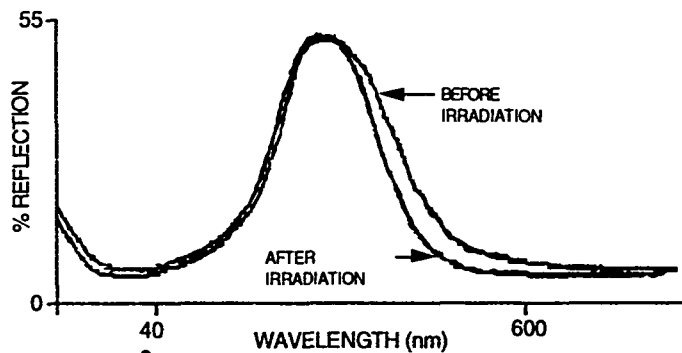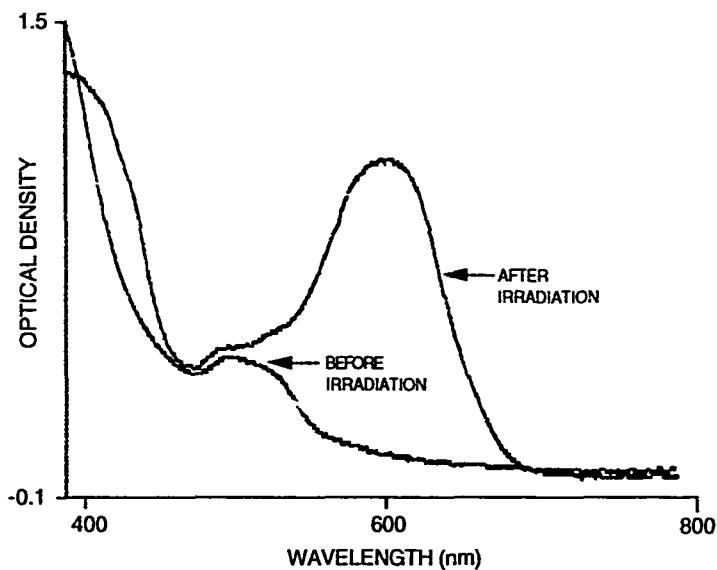
Figure 6.3: Reflection spectra (a) and absorption spectra (b) of compound 31

Upon heating to the isotropic phase, the thin film of liquid remains clear (absence of red color) indicating no aggregration of the spiropyran molecules, unlike the nematic copolymers synthesized by Krongauz[7-11]. Krongauz observed that upon heating into the isotropic phase, the isotropic melts exhibited a red color indicating the formation of aggregated merocyanine structures which led to the physical crosslinking of the polymeric backbones. The absence of this behavior for compound 31 may be attributed to steric factors. Once covalently attached to the siloxane core, the mobility of these spiropyran molecules becomes restricted since each ring has five large pendant groups attached. Examinations of spiropyran-doped siloxanes containing only CAB and BAB pendant groups indicate aggregation was possible. The liquid crystal siloxane is also photochromic in solvents such as toluene and dichloromethane, exhibiting the same absorption spectra as in thin films upon irradiation. The thermal fading of the blue color in toluene solutions occurs in approximately 20 seconds and follows first order kinetics characteristic of spiropyrans[15]. Compound 32 did not form optically clear thin films due to contamination present in the ABNS sample. This compound was photochromic in solution and thin films exhibiting the same kinetics as compound 31.

X-ray diffraction studies on thin glassy films of compound 31 agree well with similar cholesteric cyclic siloxane liquid crystals without spiropyran units attached[16]. This was unexpected as the attachment of the spiropyran units was lateral. Steric disruptions to the liquid crystalline packing are regulated by the flexibility of the allyloxy leader group. However, with the small percentage

attached, no disruption was observed contrary to compound 32. No differences in the small- or wide-angle scattering patterns were observed for films before and after irridiation with UV (365 nm) light. Although the film clearly turned blue indicating an opening of the spiropyran molecule, no observable changes in the diffraction patterns were observed.

Compound 31 was drawn into long fibers from the liquid crystalline mesophase. At room temperature, these fibers were glassy but maintained their liquid crystalline order. The orientation of the lamellae within these fibers was perpendicular to that of the typical transverse orientation in conventional polymeric liquid crystalline fibers[17]. Fibers from this compound were easily drawn from the melt, highly birefringent, and photochromic. When irradiated with UV (365 nm) light, the fibers exhibited an intense blue color which disappeared slowly (20 hours) in the dark. These irradiated fibers were also birefringent. Preliminary experiments performed on fibers drawn from the siloxane liquid crystal containing only CAB and BAB (compund 4) indicate they propagate radiation from an He-Ne laser (633 nm) light. Based on these observations, experiments are now in progress to quantitatively evaluate the transmittance of the spiropyran-containing siloxane before and after irradiation with UV light. Upon irradiation, it is expected that the blue fiber will attenuate the propagation of He-Ne radiation and thus act as a fiber optic filter. Recent results also indicated these compounds can be used to form diffraction gratings. Radiation of the photochromic molecule with two laser beams induces a periodic amplitude in the conformation of the spiropyran.

The ease with which these liquid crystalline siloxanes are shear aligned, the order frozen at room temperature, and the high optical quality of the glasses formed make them good matrices for incorporating NLO chromophores.

6.2 NLO Siloxanes

In recent years, organic materials[18,19] exhibiting strong nonlinear optical behavior have received considerable interest because of their applicability in a variety of optical devices. These materials are expected to play a major role in optical communication and computing in addition to active and passive switching and limiting media. Inorganic single crystalline materials have several inherent drawbacks including difficult processing, low damage thresholds, crystal quality, and poor responses at optical frequencies. Organic materials are promising as they can be engineered to exhibit desired thermal and mechanical properties. They are inherently easier to process into thin films or fibers. Nonlinear molecules can be combined with polymer systems in a number of ways including guest/host systems, covalent attachment to glassy polymer backbones, and incorporation into liquid crystalline phases. To be practical, organic NLO materials must exhibit large and temporally stable nonlinear signals, processing ease, and good optical quality (low losses) in addition to specific device requirements.

The primary applied interest in the cyclic siloxane compounds lie in their formation of well-ordered films with a control over the molecular packing in a planar, Grandjean, or homeotropic

orientation. In addition, the fiber drawing capability previously demonstrated is a unique characteristic of these low molecular weight compounds. The two base mesogens examined in this report, biphenyl and cholesterol, do not possess any significant NLO activity. They may, however, be easily replaced by mesogens exhibiting nonlinear activity which will facilitate the formation of large $\chi^{(2)}$ and/or $\chi^{(3)}$ glasses. For $\chi^{(2)}$ materials, an external poling technique must be used to remove the centrosymmetric behavior as discussed in Section I.

To demonstrate the feasibility of using these siloxane glasses as carriers for NLO materials, a NLO chromophore (Figure 6.4) based on a derivative of MMONS (3-methyl-4-methoxy-4'-nitrostilbene)[20-22] was synthesized by Drs. M. Jin and E. Samulski of the University of North Carolina (UNC). This chromophore, MAONS shown in Figure 6.4, contained a terminal vinyl bond which facilitated its attachment to the siloxane ring. Compound 33 contained 80% C4AB and 20% MAONS on a five-membered siloxane ring. This ratio was chosen as previously synthesized compounds with large cholesterol compositions exhibited preferential homeotropic alignment of the molecular director. This orientation was sought as it minimized light scattering and enabled second harmonic generation measurements with an in-situ poling device.
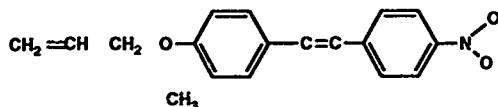
Figure 6.4: NLO chromophore, MAONS, used in compound 33

The resulting compound exhibited both smectic-A and cholesteric phases as shown in Table 6.2. The clearing temperature of 245°C and T_g of 53°C are close to those exhibited by compounds 6 and 7, containing 70 and 85% cholesterol, respectively. The S_A-cholesteric transition is somewhat higher at 230°C than those exhibited by these two compounds. Compound 33 exhibited a slight yellow color in bulk and solution. In chloroform, the absorption edge of the attached chromophore was shifted to a lower wavelength as shown in Figure 6.5. This blue shift is indicative of a decrease in conjugation resulting from the attachment of the terminal vinyl bonds of MAONS. For both cases, there is no absorption at 532 nm thereby allowing nonresonant second harmonic generation effects to be observed.

Table 6.2

Physical properties of compound 33

Compound	C4AB/MAONS Ratio	Thermal Transitions (°C)
33	80/20	g 53 S_A 230 n* 245 i

g-glassy; S_A-smectic-A; n*-cholesteric; i-isotropic
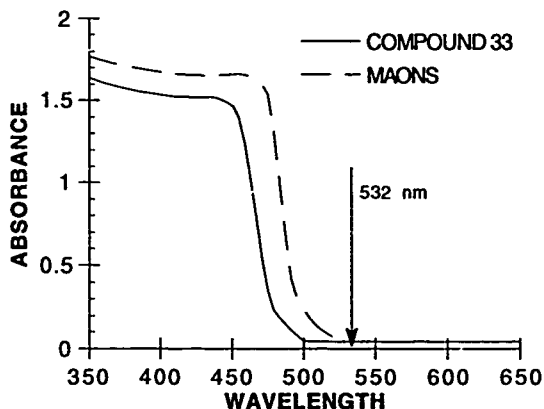
Figure 6.5: Absorption spectra of MAONS and compound 33

Edge diffraction patterns (Figure 6.6) were similar to those obtained for the high x_{chol} ring compounds. A low-angle reflection is again observed at 50Å along with multiple-order reflections of the 27.4Å primary layer reflection. Large meridional crescents indicate a homeotropic packing behavior. No indication of the 20Å reflection attributed to structural order among partially overlapped cholesterol mesogens observed for componds 7 and 8 was observed. This may indicate that below 85% cholesterol, this type of packing is not sufficiently correlated. Weak, diffuse reflections at 8.0 and 6.3Å were also present. These reflections indicate a tendency to form columns of molecules as discussed earlier[23]. At elevated temperature, unaligned samples show only the low-angle and primary layer spacings along with the wide-angle halo. The layer

221

spacing of 27.4Å fits nicely into the layer spacing dependence on x_{chol} discussed in Section V. This is expected due to similarities in extended molecular lengths of MAONS and B4AB (17.2 and 18.8Å, respectively) and the small amount attached.

Figure 6.6: X-ray pattern from thin film edge of compound 33

An initial NLO examination was performed at UNC on a thin film sheared onto indium-tin oxide treated glass slides. To remove the centrosymmetry of the NLO chromophores, the thin film was corona poled using a tungsten needle while the measurement took place. A Q-switched Nd-YAG laser with a pulse length of 10 nsec and pulse frequency of 10 Hz was employed. Details of the experimental setup have been presented elsewhere[24]. Initial experiments indicate a temperature dependence of the SHG signal as shown in Figure 6.7. Two increases in the SHG signal were observed upon heating; one on initially turning the field on and heating to the glass transition temperature. This indicates that although the sample was in the glassy state, there was sufficient free volume for the chromophores to realign with the applied field. Above the T_g, a large change in the SHG signal was observed until heated to 100°C where a large drop in signal was observed. This has been attributed to a decrease in the charge density at the surface due to increased mobility of ions from within the bulk of the film[25]. Upon cooling very little change in the remaining signal was observed. The ending SHG signal was approximately 25% that of the maximum value obtained during the experiment. One problem observed was the formation of a highly scattering texture at elevated temperature with the applied field. This was attributed to the formation of domain structures where molecular and ionic motion at boundary walls caused a highly scattering texture.
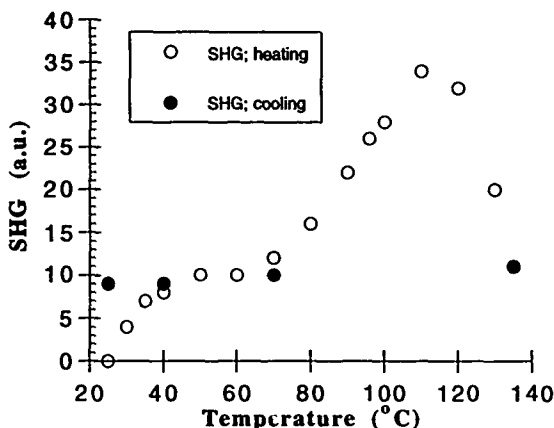
Figure 6.7: SHG response of compound 33

No systematic study of the temporal stability of the NLO response has been performed. Due to the low glass transition temperatures, molecular motion of the mesogens is expected in the glassy state. Nevertheless, the feasibility of incorporating a nonlinear chromophore into these siloxane compounds has been demonstrated. Variation of the chemical composition should allow for fibers to be drawn, giving rise to the possibility of organic nonlinear fibers. Examinations into the temporal stability and compositional variations are underway.

6.3 Nonsteroidal, Chiral Mesogens

As discussed in Sections III and V, packing models from high x_{chol} compounds indicate a partial interdigitation of the cholesterol units at the 17th carbon position. This sterically hindered packing scheme was shown to disrupt the fully interdigitated S_{Ad}-like packing of the biphenyl molecules. Addionally, these high x_{chol} compounds exhibited a reduced ability to form transparent films and continuous fibers. They were also shown to be more susceptible to thermal degradation in air.

In an attempt to increase compatibility among mesogens, the cholesterol mesogen was replaced with a smaller chiral molecule. This work was done in conjunction with Dr. Steve Pollack, University of Cincinnati. A heterocyclic, optically active compound, shown in Figure 6.8, was designed and experimental details are presented elsewhere[26]. Unfortunately, only enough of this compound was obtained to perform one hydrosilation reaction with a five-membered siloxane ring.
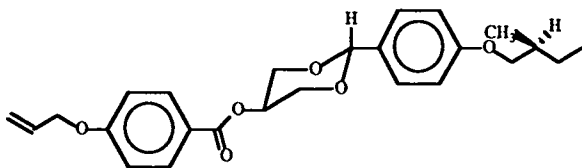
Figure 6.8: Heterocyclic, optically active olefin

Table 6.3

Physical properties of compound 34

Compound	B4AB/Olefin Ratio	Thermal Transitions (°C)
34	50/50	g 75 n* 150 i

g-glassy; n*-cholesteric; i-isotropic

The final product, compound 34, had 50% B4AB and 50% of the above shown olefin. It exhibited a glass transition temperature of 75°C and a clearing temperature of 150°C. Optical microscopy indicated a cholesteric phase whose selective reflection wavelength was in the ultraviolet region of the spectrum. The thermal transitions were very similar to those exhibited by compound 1 although compound 34 contained only 50% B4AB. The thin film and fiber diffraction patterns were also similar to those of compound 1. Fibers were drawn more easily from this compound than compound 4 which contained the same percentage of cholesterol-based mesogens. A series of reflections were observed on the meridian with two broad reflections on the equator. There were indications that the first-order reflections were split as shown in Figures 6.9 and 6.10.

The primary reflection of 21.0Å was considerably shorter than its cholesterol-containing analog, compound 4, of 24.5Å. The observed primary reflection spacing is also lower than the calculated layer spacing based on the extended molecular lengths of the two mesogens. The 24.6Å and 18.8Å lengths of the olefin and

226

B4AB, respectively, yield a calculated spacing of 21.7Å. However, since the compound was cholesteric and did not exhibit any appearance of a smectic-C^* phase. the splitting of the first-order reflection must arise from a cybotactic-like packing structure.
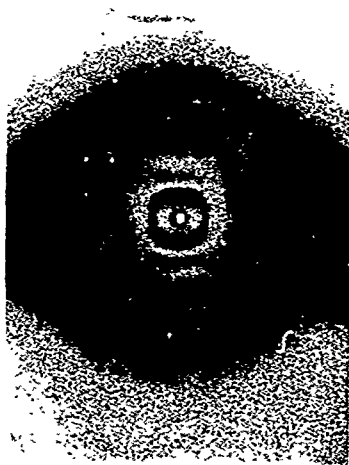
Figure 6.9: WAXS pattern of fiber from compound 34
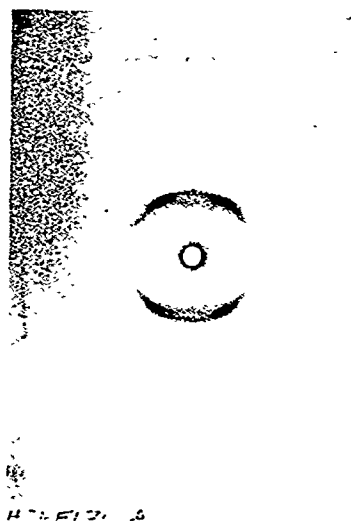
Figure 6.10: SAXS pattern from fiber of compound 34

Using a tilt angle of 32° as shown in Figure 6.11 and the measured d-spacing of 21Å, a fully extended d-spacing of 24.8Å can be calculated. The wide-angle crescents showed no signs of splitting as would be expected for a smectic-C* phase and the relative alignment was greater for this compound than its cholesterol-containing analog as shown in Figure 6.12. No low-angle peak was observed indicating only an S_{Ad}-like packing structure was present.
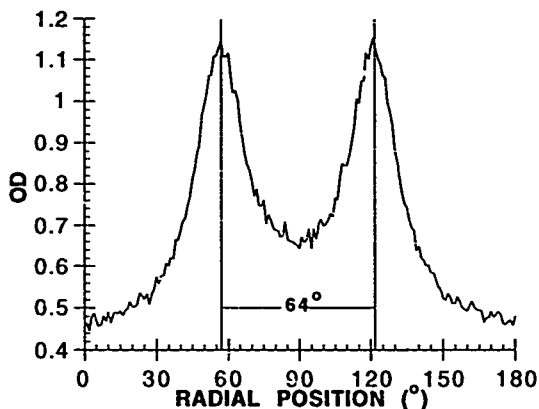
Figure 6.11: Radial intensity of primary reflection for compound 34
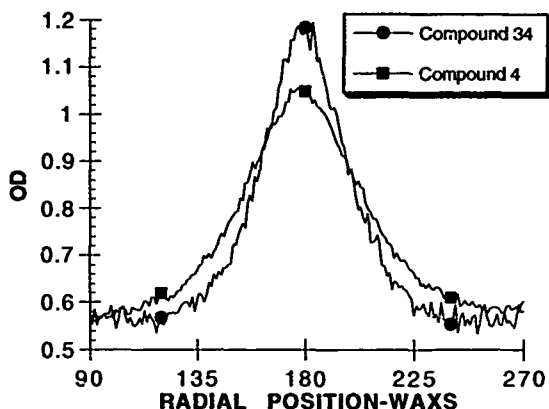
Figure 6.12: WAXS radial intensity for compounds 4 and 34

Although the incorporation of this olefin does not lead to multifunctional materials, it has shown the dominance of the cholesterol moeity in the other compounds examined. The absence of the low-angle reflection and the similarities to compound 1 show the incompatibility of the biphenyl-based mesogens with cholesterol-based mesogens. Improving the packing efficiency eliminates the partially interdigitated packing structure observed for high x_{chol} compounds. The strong ability to draw fibers is promising. More compositions are needed to fully examine the interplay between biphenyl and these two mesogens. It is expected that at higher concentrations of this olefin, a chiral smectic-C phase will form in place of the smectic-A mesophase region observed for the cholesterol compounds.

230

6.4 Summary

Due to the ease of attachment, synthesis of functional siloxanes is readily obtainable. Three separate examples have been demonstrated. A novel class of photochromic, cholesteric liquid crystalline materials was synthesized. These materials are truly multifunctional as they exhibit photochromism, thermochromism, and nonlinear activity. Photochromic thin films and fibers can be readily formed in addition to holographic gratings. Nonlinear optical activity was also demonstrated by the attachment of an NLO chromophore. This compound exhibited SHG although there were initial problems with domain formation and subsequent light scattering. Results from the incorporation of a nonsteroidal, chiral molecule indicate better compatibility among molecules. The removal of the large, bulky cholesterol group had substantial effects on the packing structure and the fiber drawing capabilities. All three systems are still currently under investigation.

6.5 References

(1) Cabrera, I., Dittrich, A., and Ringsdorf, H., *Angew. Chem., Int. Ed. Engl.*, **30(1)**, 76-78(1991).

(2) Ikeda, T., Kurihara, S., Karanjit, D.B., and Tazuke, S., *Macromolecules*, **23**, 3938(1990).

(3) Tazuke, S. and Ikeda, T. in , American Chemical Society; Washington, **ACS Symp. Series 412,** pp 209-223, (1989).

(4) Ikeda, T., Miyamato, T., Kurihara, S., Tsukada, M., and Tazuke, S., *Mol. Cryst. Liq. Cryst.*, **182**, 357(1990).

(5) Pinsl, J., Brauchle, Chr., and Kreuzer, F.H., *J. Mol. Electr.*, **3**, 9-13(1987).

(6) Ortler, R., Brauchle, C., Miller, A., and Riepl, G., *Makromol. Chem., Rapid Commun.*, **10**, 5-8(1989).

(7) Shragina, L., Buchholtz, F., Yitzchaik, S., and Krongauz, V., *Liq. Cryst.*, **7(5)**, 643-655(1990).

(8) Cabrera, I., Krongauz, V., and Ringsdorf, H., *Mol. Cryst. Liq. Cryst.*, **155**, 221(1988).

(9) Cabrera, I., Krongauz, V., and Ringsdorf, H., *Angew. Chem., Int. Ed. Engl.*, **26(1)**, 1178-1180(1987).

(10) Yitzchaik, S., Cabrera, I., Bucholtz, F., and Krongauz, V., *Macromolecules*, **23**, 707(1990).

(11) Yitzchaik, S., Berkovic, G., and Krongauz, V., *Macromolecules*, **23**, 3539-3541(1990).

(12) Natarajan, L.V., Bunning, T.J., Klei, H.E., Crane, R.L., and Adams, W.W., *Macromolecules*, **24(24)**, 6554-6556(1991).

(13) Gray, G.W., *Molecular Structure and the Properties of Liquid Crystals*; Academic Press; NY, pp 61, (1962).

(14) DeVries, H.L., *Acta. Cryst.*, **4**, 219-226(1951).

232

(15) Bertelson, R.C. in *Photochromism*, G. H. Brown, Ed., Wiley-Interscience; NY, pp 45-294, (1971).

(16) Bunning, T.J., Klei, H.E., Samulski, E.T., Crane, R.L., and Linville, R.J., *Liq. Cryst.*, **10(4)**, 445-456(1991).

(17) Freidzon, Ya. S., Talroze, R.V., Boiko, N.I., Kostromin, S.G., Shibaev, V.P., and Plate, N.A., *Liq. Cryst.*, **3(1)**, 127-132(1988).

(18) *Nonlinear Optical Properties of Organic Molecules and Crystals*, Chemla, D.S. and Zyss, J., Ed., Academic Press; NY, **I & II**, (1987).

(19) *Nonlinear Optical Properties of Organic and Polymeric Materials*, Williams, D.J., Ed., American Chemical Society; Washington, **ACS Symp. Ser. 233**, pp 212, (1985).

(20) Tam, W., Guerin, B., Calabrese, J.C., and Stevenson, S.H., *Chem. Phys. Lett.*, **154**, 93(1989).

(21) Bierlein, J.D., Cheng, L.K., Wan, Y., and Tam, W., *Appl. Phys. Lett.*, **56**, 423(1990).

(22) Eaton, D. F., **253**, 281-287(1991).

(23) Davidson, P. and Levelut, A.M., *Liq. Cryst.*, **11(4)**, 469-517(1992).

(24) Pauley, M.A., M.S. Thesis, University of North Carolina, (1991).

(25) Hampsch, H.L., Yang, J., Wong, G.K., and Torkelson, J.M., *Macromolecules*, **23(15)**, 3640-3647(1990).

(26) Pollack, S.K., *Synthesis and Characterization of Chiral Mesogens for use in Cyclic Siloxane Liquid Crystalline Materials*, AFOSR Summer Technical Report, University of Cincinnati, (1991).

MOLECULAR MODELING

As discussed in Sections III and V, the exact details of the cyclic siloxane global molecular conformation and possible intermolecular arrangements among the pendant mesogens are unknown. To examine different possibilities, a series of semi-empirical, molecular mechanics, and molecular dynamic simulations were performed. Simulated X-ray patterns were also obtained which allowed for comparison to the experimental data. This work was done in collaboration with Dr. Ruth Pachter, Wright-Patterson AFB.

Computational studies of cyclic and linear polydimethyl-siloxanes have been reported[1,2], and the columnar stacking of a disc-like model of similar polymeric cyclic siloxane-based liquid crystals but with mesogens attached has been simulated[3,4]. However, no theoretical studies based on the cyclic penta(methylsiloxane) molecular system have been attempted. Molecular simulations of this class of compounds are important in obtaining an understanding of the arrangement and organization of the pendant mesogens within these materials, in addition to outlining a general strategy for a molecular modeling approach for such a large molecular system. Further, a comparison of linear and cyclic siloxane-based macromolecules, various mesogen modeling, and taking into account internal structural changes to be used for a statistical average for the diffraction pattern calculations may enable the derivation of a general modeling strategy to be used in

future molecular design studies of materials. This work is ongoing and results are preliminary. Presented below are summaries of some initial results obtained for characteristic geometries in addition to calculated X-ray scattering data for the cyclic siloxane with mixed mesogens. The computational details will not be discussed in detail as they have been presented elsewhere[5].

7.1   Mixed Mesogens Molecular Modeling

7.1.1   Global Molecular Topology

It is intriguing to examine types of molecular conformations that are compatible with the lamellar arrangement shown in Section V. The arrangement of pendant mesogenic cores relative to one another may assume some rather different global shapes as shown in Figure 7.1. In Figure 7.1(a), a disc-like shape is depicted where the pendant mesogens are splayed out radially about a siloxane-rich centroid. As discussed in Section V, a finite interface of siloxane may be present which aids in the formation of a layered-like structure. However, to fit the cyclic siloxane molecule into lamellae keeping the pendant mesogens normal to the layers, two possible conformations are shown in Figures 7.1(b) and (c). The cylinder model, Figure 7.1(b), may be envisioned with the steroid and biphenyl separated on opposite ends of a cylinder. An extreme global conformation of this topology can be envisioned with the steroid and biphenyl units separated on opposite ends of the siloxane ring. Such intramolecular aggregation might derive from intermesogen packing preferences. A conical shape (with a siloxane-rich nose-cone) can also be envisioned for these

235

compounds. All these shapes would permit the observed mesogen to pack in lamellae and allow for a siloxane-rich interface and therefore were studied theoretically.

The cyclic penta(methylsiloxane) molecular system was built by using the geometry parameters of the molecular modeling option of the Quanta/CHARMm molecular design program[6]. Six isomers are possible where the methyl groups are positioned either axial or equatorial relative to the ring. The isomer in which all methyl groups were axial was the least favored energetically of the six possible isomers. Molecular models containing two cholesterol units and three biphenyl units were constructed using standard geometry parameters. This ratio was chosen to compare to the experimental fiber diffraction patterns. The cholesterol and biphenyl mesogens were constructed by using standard geometry parameters followed by subsequent merging with an optimized siloxane ring. Although the computational method minimizes the possibility of calculating a local minimum in the potential energy surface, no systematic conformational space search was performed. The three global topologies discussed earlier were constructed as shown in Figures 7.2, 7.3, and 7.4. The energies of the disk, cylinder, and cone were 297.5, 259.5, and 308.9 kcal/mol, repectively. Thus, the cylinder model is more favorable energetically than the other two structures.
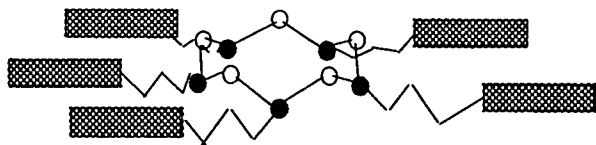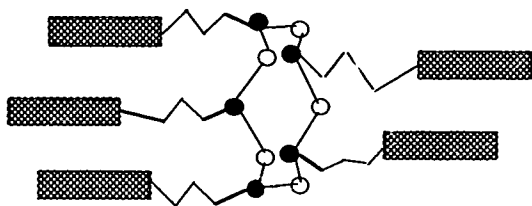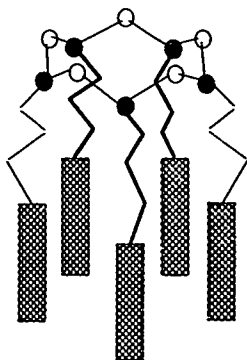
Figure 7.1. General global conformations examined for ring systems: disk (a), cylinder (b), and cone (c) conformation
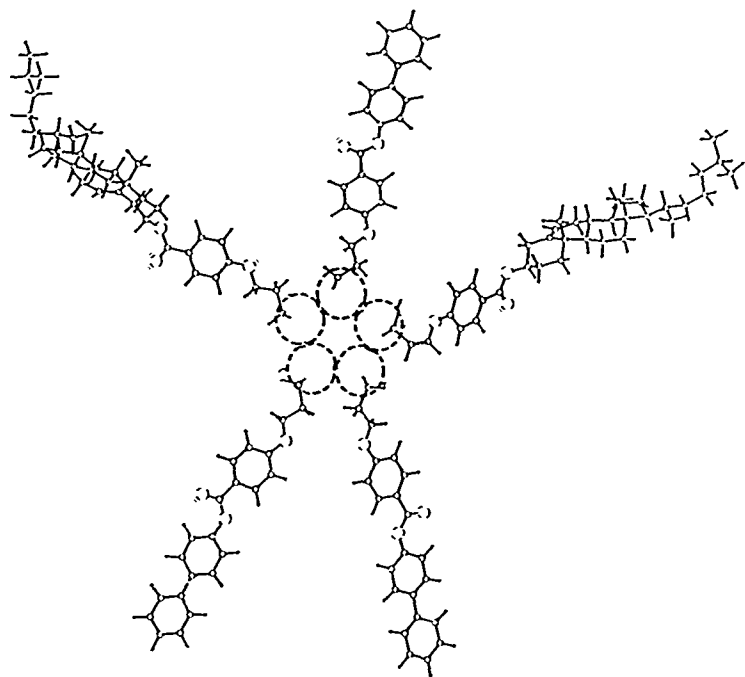
Figure 7.2: Minimized disk global topology with derivatized mesogens

238
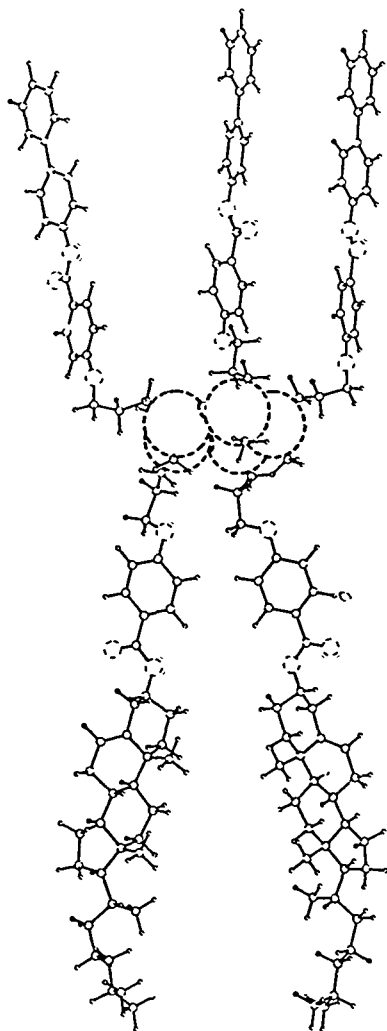
Figure 7.3: Minimized cylinder global topology with derivatized mesogens
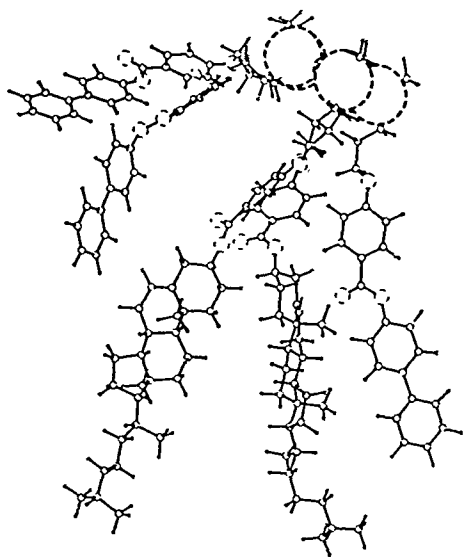
Figure 7.4: Minimized cone global topology with derivatized mesogens

7.1.2 Intermolecular Ordering

Seven different intermolecular ordering patterns were initially considered based on the interdigitation of mesogen structural supposition derived from experimental data[7,8]. These are shown in Figures 7.5-7.11 with their intermolecular arrangements shown in Table 7.1. Four molecules of each were fixed at their minimum energy geometry. Details have been presented elsewhere[5].

Table 7.1

Ordering patterns for the cyclic siloxane liquid crystal models

Model	Ordering Patterns[a]	Interdigitation
IIIa	{B}{s1}{C}{C}{s2}{B} {B}{s3}{C}{C}{s4}{B}	phase-separated
IIIb	{B}{s1}{C}{B}{s2}{C} {B}{s3}{C}{B}{s4}{C}	maximal
IIIc	{B}{s1}{C}{B}{s2}{C} {B}{s3}{C}{B}{s4}{C}	phase-separated
IIIA	{B}{s1}{C}{B}{s2}{C} {B}{s3}{C}{B}{s4}{C}	maximal
IiIB	{B}{s1}{B}{B}{s2}{B} {B}{s3}{B}{B}{s4}{B}	maximal
I		partial
II		none

[a] - {B} and {C} correspond to biphenyl- and cholesterol-based mesogens; {s} corresponds to the siloxane ring

Figure 7.5: Intermolecular arrangement IIIa

242

Figure 7.6: Intermolecular arrangement IIIb

243

Figure 7.7: Intermolecular arrangement IIIc
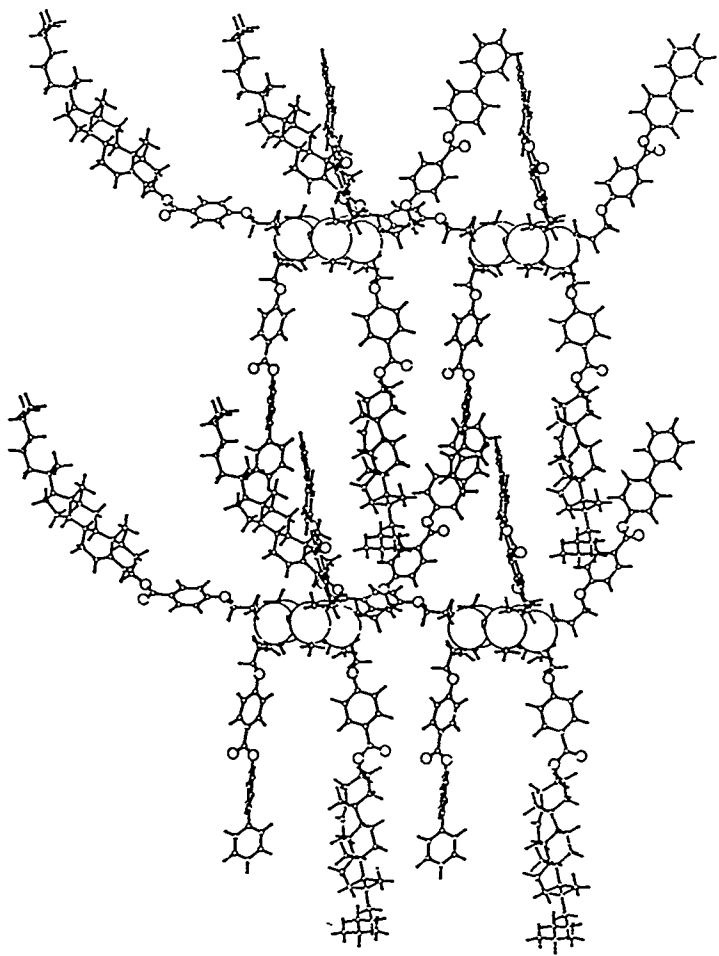
Figure 7.8: Intermolecular arrangement IIIA
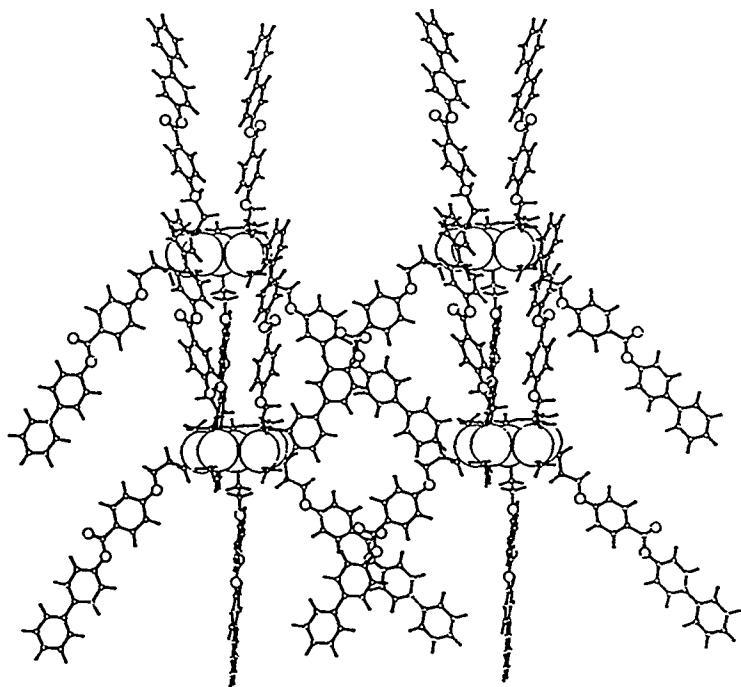
Figure 7.9: Intermolecular arrangement IIIB
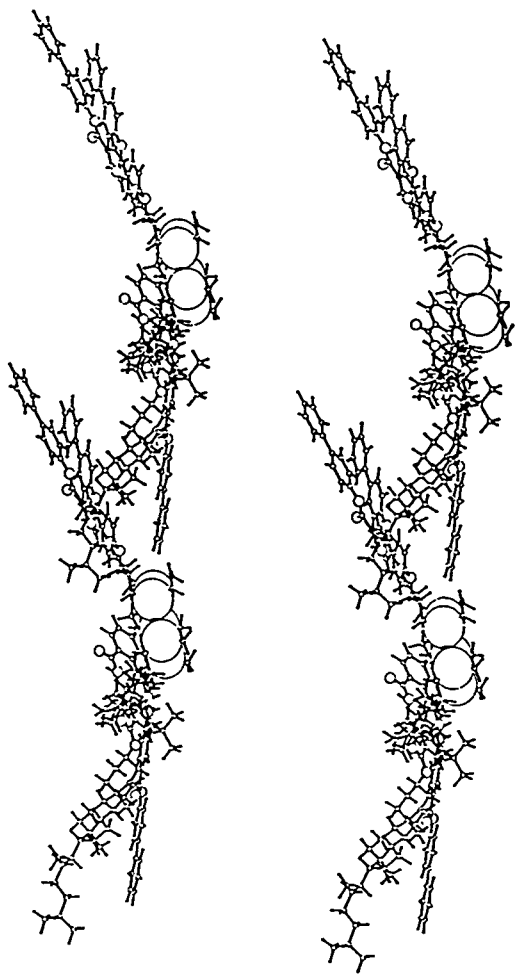
Figure 7.10: Intermolecular arrangement 1
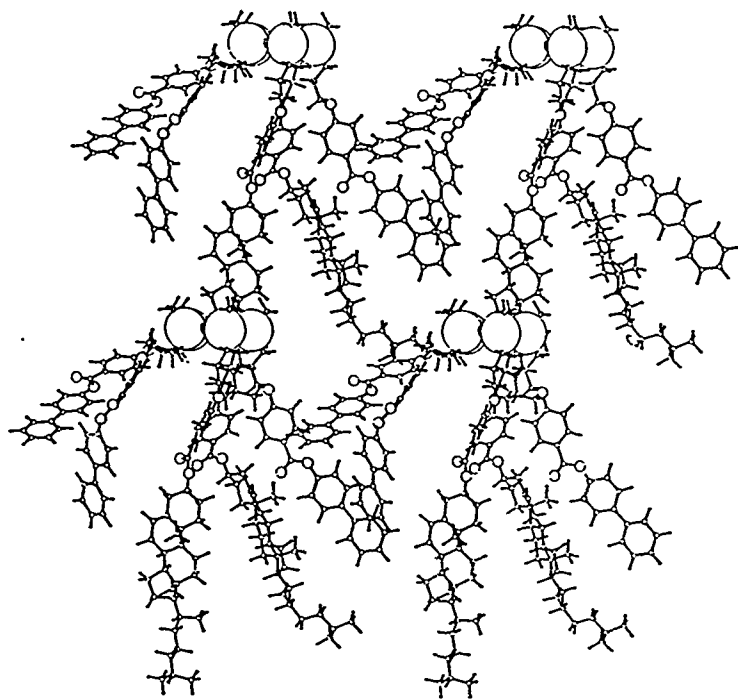
Figure 7.11: Intermolecular arrangement II

7.1.3 Diffraction Simulations

Cylindrically averaged scattering is the most common technique for modeling scattering from an anisotropic material oriented with fiber cylindrical symmetry without needing to assume any crystalline ord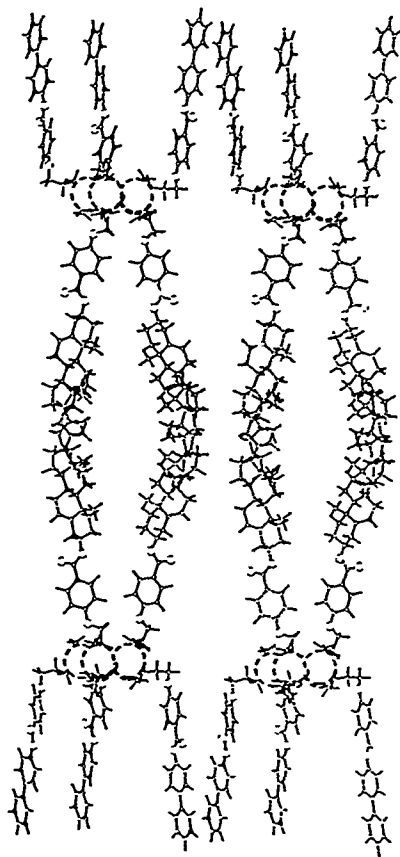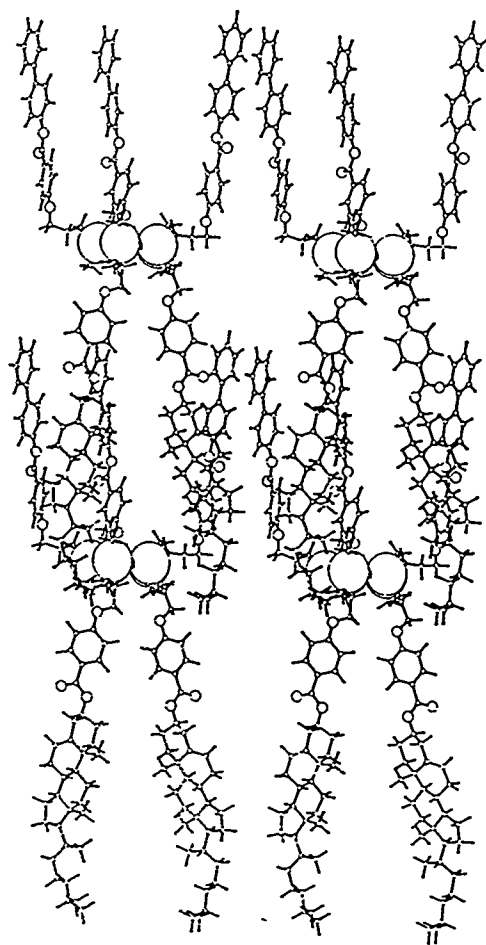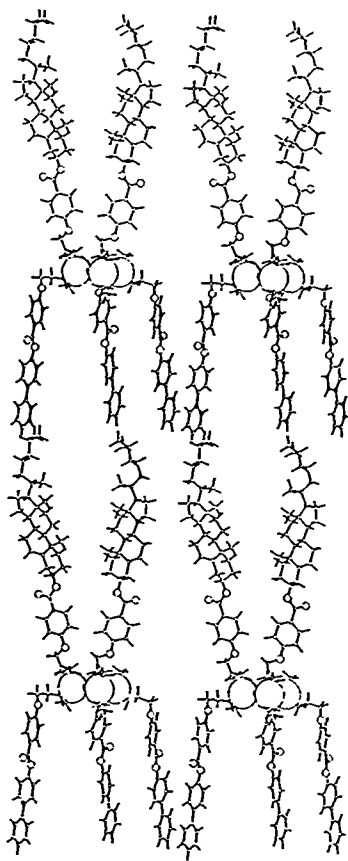er[9]. The diffraction patterns of these molecular structures were calculated using the Cerius simulation program[10]. The computational techniques are described elsewhere[5]. The data presented previously[5] were calculated with an earlier version (version 2.1) of Cerius. A low-angle reflection caused by a model correction parameter has been eliminated from all plots. Although there were slight differences between versions, the qualitative conclusions were the same. The calculated meridional scattering sections for the intermolecular models with various phase separations and degrees of interdigitation, Figure 7.12, indicate the importance of intermolecular as well as intramolecular orientations of the pendant mesogens by showing that there are considerable differences in the relative intensities of the 2θ maxima as well as their position. Although the relative effect of various parameters is difficult to discern and a quantitative interpretation of the simulated scattering patterns cannot be achieved at this stage of the simulation, some qualitative conclusions can be drawn. The interdigitation of the mesogens (ordering **IIIb** vs. **IIIc**) results in fewer reflections with the maximal interdigitated layer spacings approaching the experimentally observed magnitude of the primary d-spacings[8]. The large number of reflections for **IIIa** and **IIIc** are attributed to contributions from both cholesterol and biphenyl mesogens where

249

IIIb containing interdigitated mesogens exhibits fewer reflections. Rather different meridional scattering sections result when changing the relative configuration of the mixed mesogens (ordering **IIIA** vs. **IIIb**) as well as when changing the constituent mesogens within the siloxane ring (ordering **IIIB** vs. **IIIA**). On the other hand, the degree of interdigitation of mesogens along the z a: is in **IIIb** causes the simulated scattering sections for systems consisting of two, four, seven, and twelve cylinders of this type to show slight differences in the 2θ maxima, and also in their relative intensities. Note that a small error due to the conformational flexibility in the system not taken into account at this stage of the calculation may be propagated for a large number of interacting molecules, and thus quantitatively incorrect trends may be revealed in such a comparison. These effects occur since there is no interdigitation between the cholesteryl-4'-allyloxybenzoate mesogens at one end of the packed structure and the biphenyl-4'-allyloxybenzoate mesogens at the other. Indeed, increasing the number of molecular systems for the phase separated packing geometry (ordering pattern **IIIc**) has no effect on the 2θ maxima as both the interior and exterior mesogens are not interdigitated.
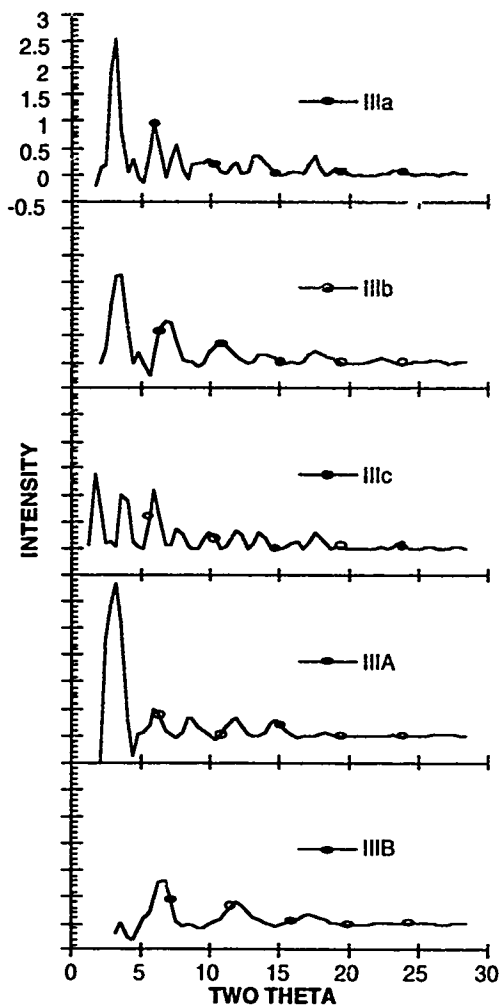
Figure 7.12: Calculated meridional scattering sections for intermolecular arrangements. Intensity values have been scaled by 10⁶

The simulated scattering sections from the three different global configurations **I, II.** and **IIIb,** shown in Figure 7.13, are different showing, once again, the importance of intramolecular relative orientation of the mesogens. Interestingly, the intensity variations of the "disk" general topology **(I)** were similar to the experimentally observed variations although the d-spacings are better reproduced by the "cylinder" general topology **(IIIb).** Large reflections at very small 2θ reflections for the three models have been omitted. Surprisingly, the d-spacings are very similar for these three different packing schemes. Comparisons to the experimental data indicate the disk model partially reproduces the calculated data. These experimental data have a strong contribution to the intensity at larger angles (15 to 20°) due to imperfect uniaxial ordering of the mesogens. The liquid-like lateral interactions of the mesogens manifest themselves as high angle equatorial reflections. Due to the relatively mild drawing conditions, these equatorial reflections have considerable χ sway and are therefore present on the meridian. The calculated meridional scans assume truly uniaxial order in a cylindrical geometry and therefore any contributions from the smeared equatorial reflections are not present. Further work is in progress in examining various intermolecular packing patterns with the "disk" and "cylinder" models **(I and III).**
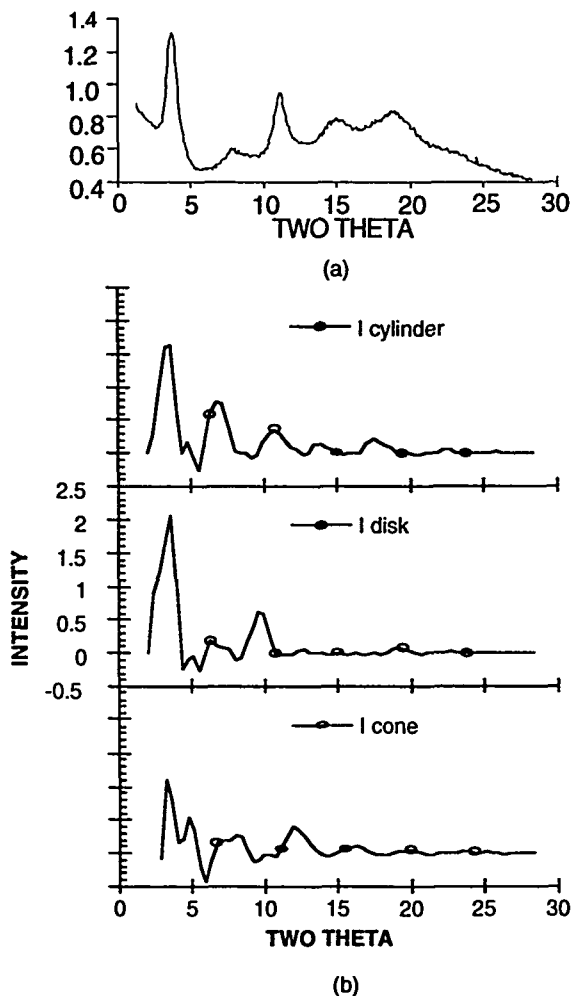
Figure 7.13: Experimental (a) and calculated (b) meridional scattering sections for cone, disk, and cylinder models. Calculated intensities have been scaled by 10^6

7.1.4 Summary

In summary, the molecular simulations of these cyclic siloxane compounds offer an insight into the effects of molecular structure on the intermolecular arrangement of the mesogens pendant on the siloxane ring. Various intermolecular packing models can be evaluated with respect to their calculated X-ray scattering patterns. Although not all variables are fully understood at this time, further work should lead to an understanding of the experimentally derived patterns. The data presented here initially indicate that the cylinder model is the most favored structure energetically. Similarities between the calculated molecular transforms and the experimental data support the hypothesis of string-like packing among the mesogens. Furthermore, interpretation of the calculated X-ray diffraction patterns lend partial support to one of the proposed structural models. Thus, such studies may enable future design of appropriately substituted cyclic siloxane-based liquid crystals.

7.2 Molecular Dynamics

The compound discussed earlier, containing 40% cholesterol and 60% biphenyl, also served as the basis for a series of molecular dynamics calculations. Insight into the conformational flexibility and molecular organization of this compound at room temperature has been presented in detail elsewhere[11,12]. This investigation provided an assessment of the relative stability and indicated the degree of conformational flexibility among the mesogens and its effects on mesogen interdigitation.

254

In general, a molecular dynamics simulation consists of heating, equilibration, and simulation periods[13]. The potential energy of the molecular system was obtained by application of the semi-classical molecular technique, followed by a molecular dynamics (MD) simulation at elevated temperatures. Computational details for these simulations have been presented elsewhere[11,12]. Again, X-ray scattering calculations were performed on the resulting structures.

Changes in the three global disk, cylinder, and cone conformations were examined by comparing various torsional angles during the simulation to those in the initial structure. Figure 7.14 shows an example of the starting and lowest energy structures for a MD run for the disk isomer. Two results can be obtained by examining variations in the torsional angles during the simulation: the mean variation which is a measure of the relative stability and the range which is a measure of the conformational flexibility of that particular dihedral angle.

A set of five different dihedral angles was examined in detail for all three conformations. These indicate the relative stability of a particular model with respect to the proximity of the mesogens (1), conformational flexibility in the position of the mesogens relative to the siloxane ring (2), the ability of the mesogens to rotate with respect to the leader group (3), rotation among phenyl units within the biphenyl mesogens, (4) and the flexibility and conformational variation of the internal siloxane ring dihedral angles (5). These are referred to as torsions 1, 2, 3, 4, and 5 in the following figures.

(a)

(b)
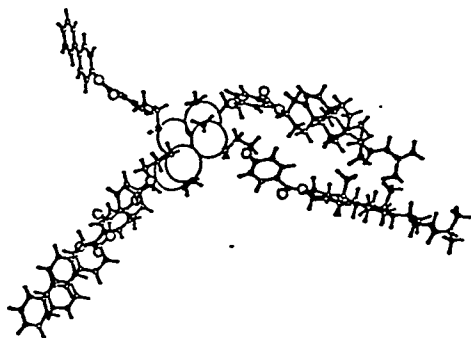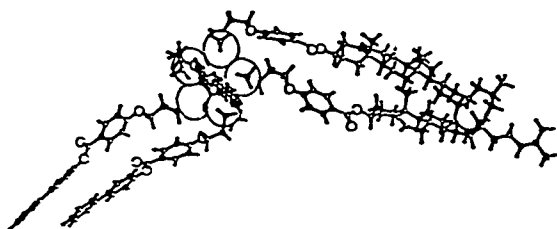
*Figure 7.14: Lowest energy (a) and statistically averaged (b)
conformations for a MD run on the disk isomer*

Examinations of the three global conformations indicate a much larger degree of instability for the cone model. Motion of the pendant mesogens was much more constrained for this model than the other two. The greatest possibility for conformational flexibility in the position of the mesogens relative to the siloxane ring was exhibited by the disk model, which can be partially explained by lower steric interactions between mesogens. This is indicated by the first three torsions in Figures 7.15 and 7.16. Especially indicative are the large range, yet the relatively small difference between the initial and final MD dihedral angles for the disk model. A small amount of change for the first three torsions was observed (shown in Figure 7.15), but these torsions had a great deal of flexibility as evidenced by Figure 7.16. This is contrary to the cone model which in general exhibited very large changes in the dihedral angles (Figure 7.15) indicating instability, but very small range values (Figure 7.16) indicating reduced flexibility.

The advantage in conformational flexibility for the disk may be important with regard to the liquid crystalline phase behavior observed for these materials. In general, the amount of interdigitation is primarily governed by the flexibility of the leader groups and intermolecular interactions of nearby mesogens[14]. Also important is the persistence of the interdigitation, which may also be influenced by the conformational flexibility. Based on these two criteria, the data may support the disk model over the other two as a more favorable choice for a model of a highly interdigitated, splayed mesogenic liquid crystalline phase.
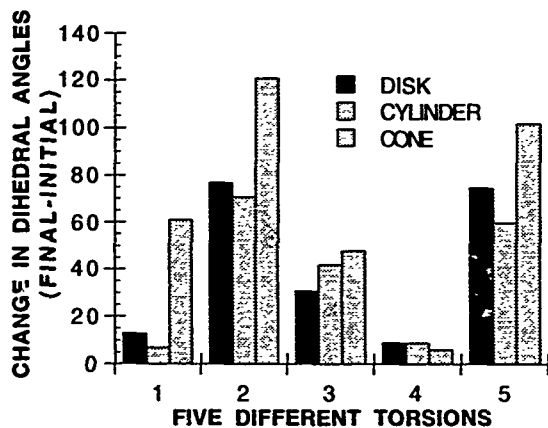
*Figure 7.15:   Changes in the fi.. torsions exhibited by the three
global   topologies*

Figure 7.16: Range values for the five torsions exhibited by the three global topologies

Molecular dynamics simulations were also carried out on molecular pairs, where the intermolecular ordering patterns considered for the global molecular topologies were based on the "interdigitation of mesogens" structural supposition based on experimental data[8].   The starting molecular arrangement for the MD run, shown in Figure 7.17(a), was based on the cylinder model. Two rings with their pendant groups interdigitated had been previously minimized to remove close contacts among atoms.   Since no constraints were applied to the siloxane rings in these molecules (CASE I), they did not remain parallel to one another during the simulation as shown in Figure 7.17(b).   This freedom of movement may not be as energetically favorable in the liquid crystalline phase due to constraints from other nearby molecules in the system, which can be dealt with by constraining the siloxane rings. Nonetheless, it is interesting to note the large degree of interdigitation among the {B} and {C} mesogens after a 10 ps dynamics simulation, which is comparable to that seen in the minimum energy starting structure.   Although a short simulation time of 140 ps (including equilibration) was used, no tendency of the system to dissociate was observed.
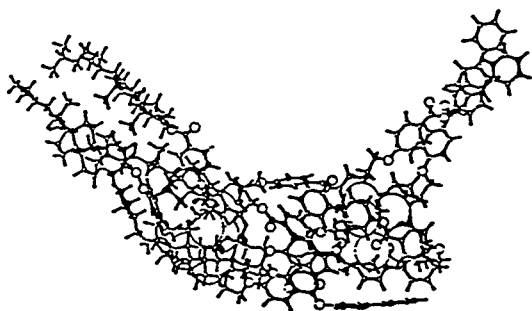
(a)
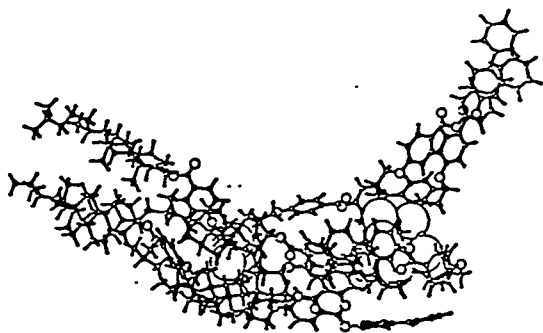
(b)

Figure 7.17: Lowest energy (a) and statistically averaged (b) structures for CASE 1

Changes in four of the torsional angles disclose no difference in the conformational flexibility or stability of the interdigitated mesogens as compared to the results from an isolated cylinder. On the other hand, larger changes were observed in the conformational variation of the internal siloxane rings dihedral angles for this cylinder pair than for the isolated cylinder model. This indicates that the siloxane ring undergoes a large amount of torsional change when the mesogens become interdigitated, inplying an ability of the siloxane rings to absorb internal energy created by motion of the sterically hindered mesogens.

To examine what would happen when the ability of the siloxane rings to change their relative orientation was removed, an additional calculation was carried out in which atom constraints were applied to all the siloxane rings atoms (CASE II). By constraining the rings, the internal energy of the system previously evidenced by large changes in the siloxane dihedral angles would have to be shifted elsewhere. The results of this MD calculation showed less interdigitation than in CASE I, as the pendant mesogens, especially {B}, moved outward from the central region between the siloxane rings as shown in Figure 7.18. Examination of the changes in the torsions during the dynamics calculation revealed differences between these two cases. By constraining the siloxane ring, larger movements of torsions 1 and 2 near the siloxane ring were observed. To further investigate liquid crystalline behavior, the rings should be left unconstrained but a series of molecules should be placed around the interior mesogens. This would constrain the movement of the interior mesogens.
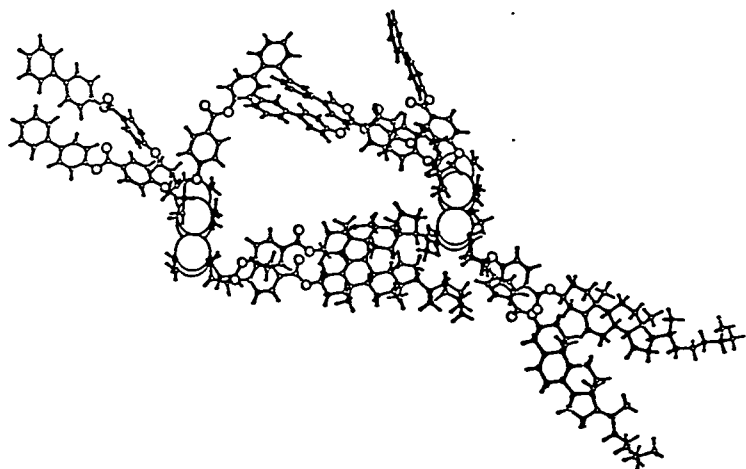
(a)
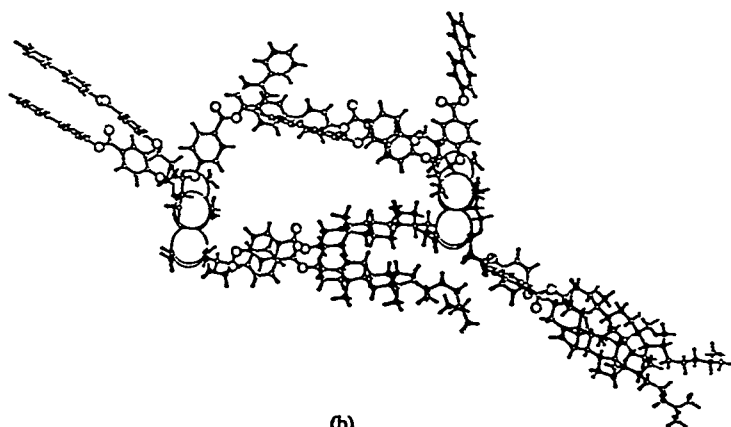
(b)

Figure 7.18: Lowest energy (a) and statistically averaged (b) structures for CASE II

Simulated X-ray diffraction patterns of the two molecular pair systems (CASES I and II) were examined. The simulated meridional scattering patterns from the starting cylinder molecular pair model (START), and the lowest energy structures from the MD runs of the unconstrained and constrained cases are shown in Figure 7.19. Small 2θ values were omitted due to a large peak caused by the relatively small number of units. It has been shown that longer units have an effect on the resulting X-ray pattern[5] due to effects of noninterdigitated end mesogens. As Figure 7.19 shows, there is a disruption of the packing as evidenced by the fewer number and weaker reflections for both cases compared to the starting structure. Table 7.2 shows the tabulated values for all three cases as well as experimental data[8]. The START d-spacings do not correspond to multiple reflections as indicated by their 2θ positions in addition to the intensity variation among peaks. Only the first reflection is strong for CASE I with an additional reflection of 15.9Å appearing. The simulated scattering for CASE II is much different and no 24.8Å reflection is observed. This indicates the mesogens movement out of an interdigitated structure. By constraining the ring, the buffering effect of the flexible siloxane ring has been lost. A systematic investigation is yet to be performed in order to compare experimental versus simulated data quantitatively. The lower order observed is anticipated since no boundary conditions are simulated for the pendant mesogens. The qualitative agreement of the starting structure reflections and those shown by the experimental data is, however, encouraging.
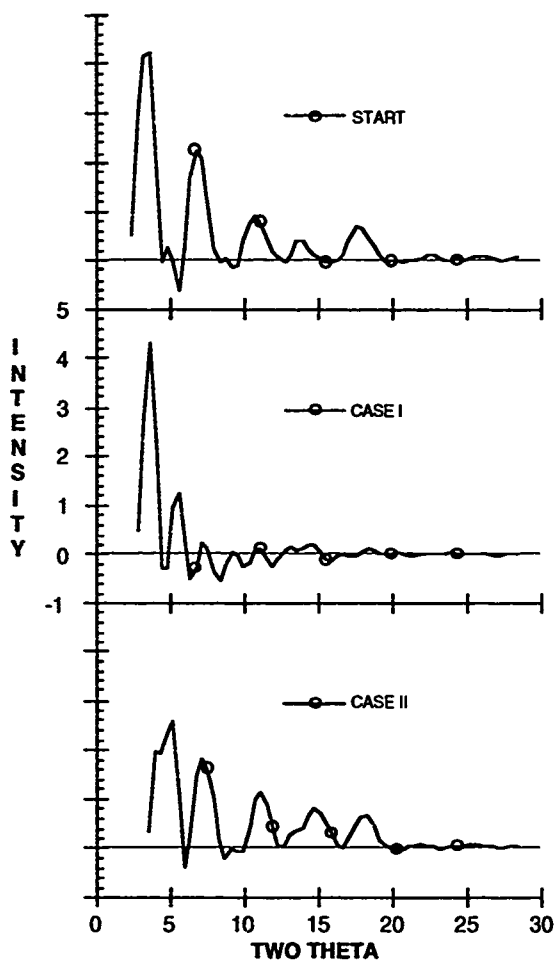
Figure 7.19: Calculated X-ray scattering sections for the starting (START), unconstrained (CASE I), and constrained (CASE II) cylinder structures. Intensity values have been scaled by 10^6.

Table 7.2

X-ray diffraction maxima (Å) from calculated meridional scattering patterns of the experimental, starting, and lowest energy of the unconstrained and constrained MD structures

Experimental	START	CASE I	CASE II
49.0			
24.4	24.8	24.8	17.1
12.0	13.1	15.9	12.4
8.0	8.3	12.4	8.0
6.2	6.4		6.0
	5.1		4.8

7.2.1 Summary

Molecular dynamics simulations offer new insights into the conformational flexibility of cyclic siloxane-based liquid crystals. Interdigitation between the {C} and {B} mesogens pendant on the siloxane ring is definitely present in the simulated structure, but a quantitative measure of the interdigitation is still to be calculated, possibly by the application of boundary conditions. The isolated disk model exhibited the most flexibility and greatest stability as indicated by mean dihedral angles and range for certain principal torsions. In general, all three isolated models displayed large conformational flexibility, which may be important with regard to the liquid crystalline phase behavior. Results from the dynamics simulation of the cylinder molecular pairs indicate the large conformational flexibility of the siloxane rings. Movements of the interdigitated mesogens were much higher for a fixed ring system. This may indicate the siloxane ring ability to absorb internal

energy.   X-ray scattering pattern calculations for the lowest energy structures generated during the dynamics run demonstrate lower order than for the initial models, which is expected due to lack of boundary conditions.

7.3   Force-Feedback ARM Calculation

A series of calculations were performed at the Molecular Graphics Lab at the Department of Computer Science in the University of North Carolina-Chapel Hill.   A collaboration with Dr. William Wright to use the force feedback ARM shown in Figure 7.20 has been started.   The force-feedback ARM uses a parallel MasPar computer (MP-1) operating with 4096 processors in order to calculate the intermolecular energy (using a combination of electrostatic and Lennard-Jones potentials, the parameters used were those of the CHARMm force-field) between a rigid structure and a movable docking model.   The resulting force information is used interactively to feed the ARM, so that the best position for the docked structure can be found by manipulating the movable structure on the screen.   The structural model can be further improved by an energy minimization.   This approach may be used for the modeling of interdigitation in these liquid crystalline materials.   A number of experiments, listed in Table 7.3 were performed.   All cases listed indicate attachment to two rings both in a cylinder topology.   Interdigitation of the mesogens between ring systems was examined.   One set of mesogens was held constant while the second set was moved relative to this structure.   In each case, a few starting positions were attempted.   These experiments

267

were initially conducted to debug the UNC software and to make suitable suggestions regarding the improvement of the system. However, the results indicate qualitatively that the interdigitation of the biphenyl mesogens is more favorable in all cases. Attempts to dock the cholesterol mesogens were more difficult and indicate an inherent difficulty in packing due to steric considerations as has been demonstrated previously[15,16].
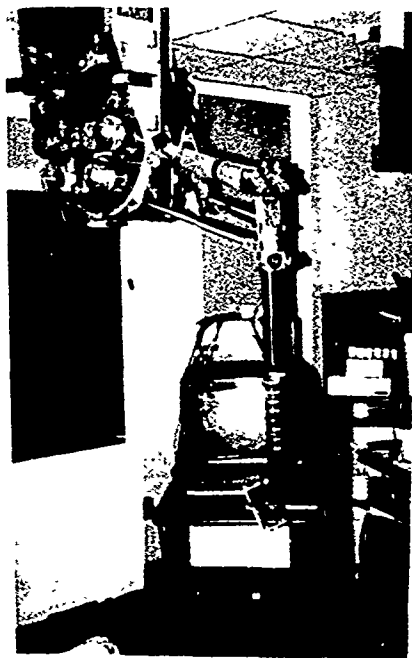
Figure 7.20: Force-feedback ARM

Table 7.3

Experiments performed with force-feedback ARM

Case	Rigid Structure	Movable Structure
1	2C	2C
2	2C	3B
3	3B	2C
4	3B	3B
5	2C + 2C[a]	3B
6	2C + 2C[b]	3B
7	2C + 2C[b]	2C
8	3B + 3B[b]	3B
9	3B + 3B[b]	2C
10	3B + 3B[b]	3B + 3B
11	2C + 2C[b]	3B + 3B

[a] - second set of mesogens translated 17Å in the y direction
[b] - second set of mesogens translated 12Å in the y direction

269

7.4 All-Biphenyl Molecules

To eliminate the number of variables, an all-biphenyl molecule in a cylinder topology has also been examined. Various intermolecular packing models have been built and X-ray diffraction patterns have been examined. These calculations are currently being compared to diffraction results from highly aligned samples (see section 8.3). Surprisingly, there is very good agreement in the molecular transform of a cylinder model with interdigitated biphenyl molecules to the experimental data. Due to the complexity of the experimental data of compound 1, a number of molecular simulations have been and are currently being examined. These include the crystal packing, degree of interdigitation, global topology, and fiber diffraction patterns. The elimination of one of the mesogens should allow for more insight into the different effects of these variables.

7.5 Summary

Molecular mechanics and dynamics calculations are being used to explore the possible global and intermolecular conformations of cyclic-siloxane ring compounds. Simulated X-ray scattering sections from these molecular conformations can be compared to experimental data, thereby allowing for the determination of the structure. Preliminary results indicate that the cone model is the least favored energetically while the cylinder and disk models are similar. Molecular dynamics calculations indicate that the disk is the most flexible and stable of these

270

conformations. This advantage in flexibility may be important with regard to the liquid crystalline phase behavior. The molecular dynamics calculations also indicated the siloxane rings ability to absorb internal energy which also may be a governing factor in the formation of liquid crystalline phases. When the ring flexibility was computationally hindered, the attached molecules had a reduced ability to remain parallel and interdigitated. Interpretation of the simulated scattering sections is in its infancy. These sections reveal the importance of intermolecular and intramolecular arrangements of molecules. Several qualitative agreements between simulated and experimental X-ray diffraction patterns are encouraging. Force-feedback ARM calculations performed at the University of North Carolina support the experimentally observed data that biphenyl-based molecules innterdigitate to a much greater degree than cholesterol-based molecules.

271

7.6 References

(1) Edwards, C.J.C., Rigby, D., Stepto, R.F.T., Dodgson, K., and Semylen, J.A., *Polymer*, **24**, 395(1983).

(2) Edwards, C.J.C., Rigby, D., Stepto, R.F.T., Dodgson, K., and Semylen, J.A., *Polymer*, **24**, 391-394(1983).

(3) Everitt, D.R.R., Care, C.M., and Wood, R.M., *Mol. Cryst. Liq. Cryst.*, **201**, 41-49(1991).

(4) Everitt, D.R.R., Care, C.M., and Wood, R.M., *Mol. Cryst. Liq. Cryst.*, **153**, 55-62(1987).

(5) Pachter, R., Bunning, T.J., and Adams, W.W., *Comp. Polym. Sci.*, **1**(3), 179-187(1991).

(6) Quanta/Charm, *Chemistry at Harvard Macromolecular Mechanics*, **Release 3.0**, Polygen Corporation(1990).

(7) Bunning, T.J., Klei, H.E., Samulski, E.T., Adams, W.W., and Crane, R.L., *Characterization of Cholesteric Cyclic Siloxane Liquid Crystalline Materials*, Wright Laboratory, WL-TR-91-4089, (1991).

(8) Bunning, T.J., Klei, H.E., Samulski, E.T., Crane, R.L., and Linville, R.J., *Liq. Cryst.*, **10**(4), 445-456(1991).

(9) *Diffraction of X-rays by Chain Molecules*, Vainsthein, B.K., Ed., Elsevier; Amsterdam, (1966).

(10) Software, "Cerius" Program, *Cambridge Molecular Design Corporation*, **release 2.1**, (1990).

(11) Socci, E.P., Farmer, B.L., Pachter, R., Adams, W.W., and Bunning, T.J., *Computer Simulation of Cyclic Siloxane-Based Liquid Crystals: Molecular Dynamics and X-ray Scattering*, Wright Laboratory, Laser Hardened Materials Branch, Technical Report WL-TR-91-4137, (1991).

(12) Socci, E.P., Farmer, B.L., Bunning, T.J., Pachter, R., and Adams, W.W., *submitted to Liq. Cryst.*, (1992).

(13) Brooks, B.R., Bruccoleri, R.E., Olafson, B.D., States, D.J., Swamihnathan, S., and Karplus, M., *J. Comp. Chem.*, **4(187)**, (1983).

(14) Leadbetter, A.J. in *Thermotropic Liquid Crystals*, G. W. Gray, Ed., John Wiley & Sons; Chichester, **22,** pp 1-27, (1987).

(15) Freidzon, Ya.S., Kharitonov, A.V., Shibaev, V.P, and Plate, N.A., *Eur. Polym. J.*, **21(3)**, 211-216(1985).

(16) Freidzon, Ya.S., Tropsha, Ye.G., Tsukruk, V.V., Shilov, V.V., Shibayev, V.P., and Lipatov, Yu.S., *Polym. Sci. USSR*, **29(7)**, 1505-1511(1987).

CONCLUSIONS AND RECOMMENDATIONS FOR FUTURE WORK

8.1   Conclusions

The packing behavior of commercially available liquid crystalline cyclic-siloxane compounds containing various percentages of biphenyl- and cholesteryl-4-allyloxybenzoate mesogens was determined. Two molecular packing schemes dependent on the composition, one a S_{Ad}-like bilayer with extensive association of the mesogens and the second a S_{A2} layer of partially interdigitated cholesterol mesogens, were deduced although only materials within a very limited range of composition were commercially available. Electron microscopy and X-ray diffraction data support a structural model where the cyclic siloxane mesogens organize into a twisted (helicoidal) lamellar arrangement having hydrocarbon-rich bilayer-like strata that may be reinforced and delineated by the immiscible siloxane component.

To investigate these materials more thoroughly, three dozen new siloxane compounds were synthesized using an inert atmosphere/vacuum system and standard hydrosilation chemistry. The size and shape of the siloxane core, the leader group length, and the ratio of the two mesogens within a given molecule were varied. Proton NMR indicates a side-reaction present with allyloxy-containing leader groups whose extent varied depending on the structure of the siloxane core used. One siloxane core, a "star" compound, was shown to be unstable in the presence of a complex metal catalyst as this side reaction took place.

A complex phase diagram was obtained for the five-membered ring with increasing amounts of cholesterol attached. The low x_{chol} compounds exhibited nematic or cholesteric phases while those above $x_{chol}=0.5$ exhibited lower temperature smectic phases in addition to a cholesteric phase. The macroscopic packing behavior of the molecules (planar versus homeotropic) was determined as a function of composition. The addition of cholesterol caused a switch from a planar to homeotropic orientation of the director with respect to the surface of thin films. X-ray diffraction examinations as a function of composition support the previously proposed packing models. At low x_{chol}, an interdigitated S_{Ad}-like structure is present. Sharp primary layer reflections indicate a tendency to layer pack. A large number of periodic reflections indicate a tendency for these compounds to form strings of molecules. Magnetically aligned samples (see section 8.3) of the all-biphenyl system supports this supposition as a complex diffraction pattern was obtained. The diffraction pattern is indicative of a smectic structure although this compound was clearly nematic based on its phase diagram. The splitting of the first-order reflection could be caused by a tilting of the molecular layers or a lattice-packing scheme.

As the cholesterol content was increased, a second packing scheme due to partially interdigitated cholesterol molecules became dominant. Cholesterol served both to disrupt the molecular packing homogeneity and to increase the tendency to form layered smectic structures. The measured d-spacings of the primary layer spacings support the presence of an immiscible siloxane interface between

275

pendant mesogens. Replacing the cholesterol compound with a nonsteroidal, chiral molecule increased the packing efficiency. No low angle-reflections were observed and d-spacings similar to the all-biphenyl compound were obtained.

Fibers could only be drawn from the nematic and cholesteric compounds. The orientation of the mesogens was parallel to the fiber axis. The all-biphenyl compound (nematic) exhibited partially crystalline fiber diffraction patterns. Replacing cholesterol with a nonsteroidal chiral molecule allowed for much longer length fibers to be drawn. This indicates that fiber drawing ability may be a function of the chirality of the compounds in addition to their viscosity.

Variations in the leader group length had the same qualitative effect as decreasing the cholesterol content. Longer leader groups allowed sufficient flexibility for the mesogens to become fully interdigitated into a smectic structure. Compounds with vinyl leader groups showed much weaker tendencies to layer pack. The thermal properties were also highly dependent on the leader group length. Longer length leader group compounds could not be drawn into fibers.

Variations in the siloxane ring size had little effect on the molecular packing, but large changes in the selective reflection properties were observed. Linear polysiloxanes exhibited similar diffraction patterns to cyclic analogs containing the same composition. D-spacings were similar indicating comparable packing schemes but large differences in the macroscopic conformations were observed. Fibers drawn from linear

compounds exhibited opposite orientation of the molecules along the fiber axis than their cyclic analogs. Low molecular weight compounds exhibited much different phase behavior than the cyclic counterparts. Very small changes in the chemical structure resulted in large changes in the phase transitions. These were attributed to differences in the flexibility of the siloxane cores. Packing schemes for three low molecular weight siloxane cores with either biphenyl or cholesterol attached have been proposed. A finite interface of siloxane is present in all models.

A major advantage in using cyclic siloxane ring compounds versus linear siloxane compounds is their greater processability under the conditions discussed in this report. Optically clear thin films and fibers were readily obtained from ring compounds and not from corresponding linear materials. The molecular and macromolecular packing structures could be controlled by both chemical synthesis and alignment techniques.

Molecular modeling calculations give insight into the most favored of the three proposed conformations of the siloxane core. The cylinder conformation was the most favored energetically. Molecular dynamics results on the tendency to interdigitate for the biphenyl and cholesterol molecules agree with those observed experimentally. The disk model allowed the greatest conformational flexibility. Calculated diffraction patterns were used to screen different packing structures. Trends with respect to the degree of interdigitation, global conformation, composition, and nature of the siloxane can be evaluated.

The structure/property relationships obtained were used to successfully synthesize optically active siloxane compounds. A novel, photochromic system containing spiropyran-based mesogens exhibits multifunctional properties including thermochromism and photochromism. Optically clear, photochromic thin films and fibers were obtained having potential uses in a number of applications. These compounds have successfully been integrated into holographic thin films. Molecular changes due to laterally attached spiropyran-based mesogen give insight into the structural compatibility among mesogens. A second class of siloxanes, containing second-order NLO chromophores has been successfully prepared. Preliminary investigations indicate they exhibit and retain NLO response after being corona-poled.

8.2   Recommendations for Future Work

The packing structure of a magnetically aligned compound (see section 8.3) has yet to be confirmed. To explore which model proposed is correct and to extrapolate these models to the packing behavior in thin films and fibers, a more systematic examination of other magnetically aligned compounds should be performed. These examinations should be coupled with continuing investigations at CHESS (see sections 8.4) on the real-time alignment of liquid crystalline materials. These examinations should allow a determination of which one of the two packing schemes proposed for this compound is valid. More quantitative results should be obtainable from the X-ray reflections of these highly aligned mesophases. Investigations into distribution functions, order

278

parameters, correlation lengths, and molecular packing schemes will be valuable in the development of optically clear, defect free thin films of liquid crystals for nonlinear optical applications.

Another question that needs to be addressed concerns the flexibility of siloxane moieties. This could be detrimental to the formation of temporally stable nonlinear optical glasses. The second-order nonlinear responses from the spiropyran-based and MAONS-based compounds should be investigated. Investigations into the multifunctional compounds should be continued. Other compositions of the spiropyran-containing compounds should be investigated to fully understand the interactions affecting the photochromic ring-opening reaction. Nematic mesophases containing these NLO chromophores should be aligned into monodomains followed by investigating the temporal stability of the NLO response as a function of time, temperature, and composition.

Examinations into the fiber drawing capabilities should be examined more closely. Results indicate that it may be a function of the chirality and/or the viscosity of the mesophase.

Chemically, several investigations should be continued to examine the structure/property relationships of these materials. The large changes in phase behavior of the low molecular weight compound suggest other analogs will give insight into dominant factors. An understanding of the crystal structures of these materials would yield information regarding the translational and orientational packing behavior. The propene elimination reaction,

examined qualitatively in this work should be examined in more detail.

Molecular modeling should be continued to help identify the packing behavior of the siloxane core with respect to the pendant mesogens. Dynamics calculations and simulated diffraction patterns will facilitate this understanding.

The understanding of the structure/property relationships of this class of compounds will benefit in their applications. The ability to tailor the micro- and macrostructure of molecules will lead to enhanced performance. The understanding and control of the microstructure are essential for uniform optically transparent ordered structures. The ability of the spiropyran compounds to form nonlinear optical and birefringent fibers should be investigated for possible photonic applications. Similarly, holographic thin films of these compounds should be investigated further.

8.3   Magnetically Aligned Diffraction Patterns from Compound 1

As discussed in Section V, the observation of periodic reflections indicates a tendency to form strings of mesogens. This behavior can be probed by examining highly aligned samples[1]. To compare fiber patterns with those from a monodomain, compound 1 was magnetically aligned. This compound, chosen due to the positive magnetic anisotropy of the biphenyl, was aligned with an NMR magnet. The material, held in a thin walled (0.01mm) capillary, was placed in the bottom of a 5mm diameter NMR tube filled with silicone oil. The sample was heated above its clearing

280

point by warming the oil with a heat gun. It was dropped into a NMR magnet (8.4T) and allowed to cool through the liquid crystalline mesophase to room temperature over the course of 10 minutes. By cooling to room temperature with the magnetic field applied, the induced alignment was frozen into a liquid crystalline glass The resulting monodomain was optically clear indicating it had not crystallized. WAXS and SAXS patterns revealed a complex packing as shown in Figures 8.1 and 8.2. No signs of the partial crystallization present for the fiber patterns were observed. The patterns contained much more detail than corresponding thin film or fiber patterns. The orientational order was very good and similar to that exhibited by the low temperature electric field samples at CHESS. The first Bragg reflection was absent and replaced by two diffuse spots lying on the meridian.
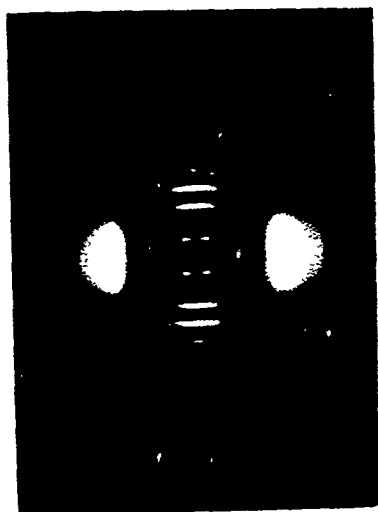
Figure 8.1: WAXS pattern of compound 1 aligned in magnetic field

Figure 8.2:   SAXS pattern of compound 1 aligned in magnetic field

Discussions with Dr. A.M. Levelut suggest a more complex packing model than previously proposed. The four-spot pattern was indexed as 101 reflections and weak spots on the same layer were indexed as 301 reflections. The appearance of two reflections on a layer line can be explained by a lattice packing scheme[1,2]. These Bragg reflections have been attributed to the formation of a centered rectangular lattice of intercalated ribbons of molecules with spacings of a=35Å and c=22.7Å as shown in Figure 8.3. The width of each ribbon would correspond to 17.5Å and would cover about three mesogenic groups. The cause of the undulation of the siloxane rings (checker board pattern) was attributed to a difference in the area per mesogens and the area per siloxane monomer[3]. Because only a weak second order Bragg reflection was observed, a weak smectic character was indicated. The large number of periodic diffuse lines indicates a columnar stacking of the mesogens. Differences between these patterns and those of thin film edges and fibers indicate the importance of aligning the molecules to get a true representative picture of the molecular packing schemes involved.

The large difference between these patterns and those of the thin film edge and fiber patterns indicates the importance of aligning the molecules fully to obtain a representative picture of the molecular packing scheme. Differences in the orienting technique can, however, play a role in the interpretation of the data[2].
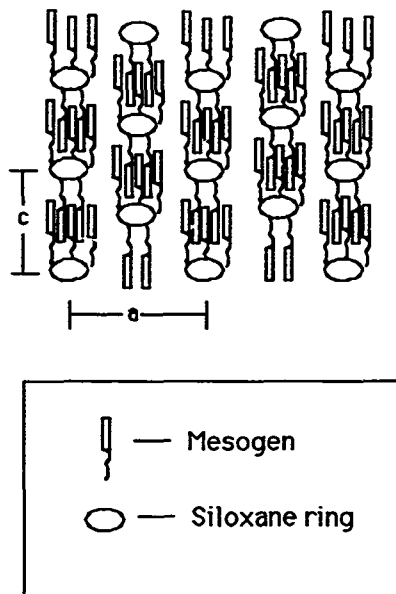
284

Figure 8.3: Rectangular lattice packing proposed for magnetically aligned sample of compound 1

Based on the phase diagram (Figure 5.1), this compound exhibits an apparent nematic mesophase. The 301 reflections, which indicate a lattice packing, were very weak at best in the diffraction patterns. The similarity of these patterns (minus the 301 reflections) to those exhibited by nematic mesophases previously[4,5] may indicate another explanation is possible. This packing structure would also have a stacking of the mesogens as suggested by Levelut above based on the large number of periodic meridional reflections. The strength and number of these reflections indicate an increased tendency to form extended linear

arrays.   Six strong meridional reflections exhibited a complex
intensity variation as shown in Figure 8.4.   The intensity of the
third reflection is strongest followed by the fourth and fifth
reflections.   There was also an odd-even effect as the   diffuse lines
were more extended laterally for the even orders than for the odd
orders.   In addition to the strong wide-angle equatorial crescents,
there was an additional weaker equatorial reflection at 9.1Å.   The
alignment exhibited for this sample was greater than that exhibited
by film edge patterns.   The radial variation in the wide-angle
spacing was much broader for the shear-aligned sample than for
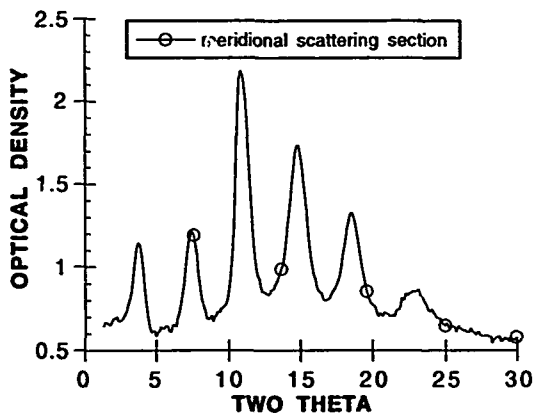the magnetically aligned sample as shown in Figure 8.5.

Figure 8.4 Meridional scattering section for magnetically aligned compound 1
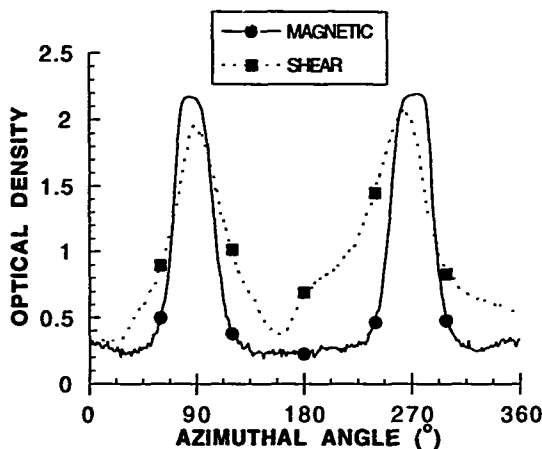
Figure 8.5: Wide-angle azimuthal distributions

However, the splitting of the first-order reflection has been previously attributed to a cybotactic-nematic packing structure[4,6]. In this case, the splitting angle would correspond to 33° as shown in Figure 8.6. The presence of two spots symmetrically placed about the meridian on the first layer line indicates regularly shifted fragments of molecules tilted at 33°[2]. This model would be more consistent with the previously proposed model[7] for low x_{chol} samples which postulated a thin interface of siloxane between pendant mesogens. The layering may be enhanced by the chemical dissimilarities among backbone and pendant mesogens.
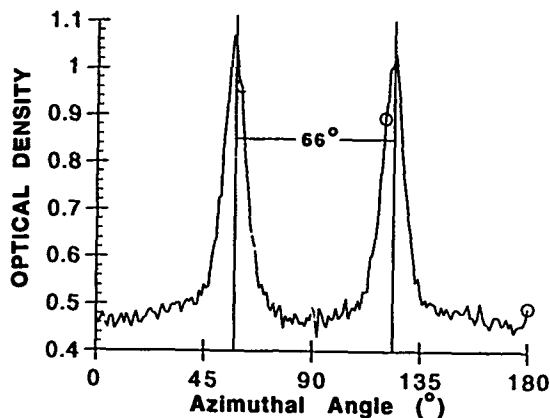
287

Figure 8.6: Splitting of the first-order reflection of compound 1

Until further work is done on other magnetically aligned samples, the packing structure giving rise to these complex patterns can be only speculated.

8.4 Synchrotron Diffraction Studies

Preliminary investigations of the influence of an electric field on liquid crystalline structures have been performed at the Cornell High Energy Synchrotron Source (CHESS). A brief summary of some of the more important observations is discussed here. A number of the aforementioned compounds have been examined and results from only a few will be discussed. The experimental details were discussed in Section II.

A number of materials exhibited strong surface alignment tendencies without the application of an electric field. This alignment has been attributed to microgrooves on the inside surface of each electrode introduced during the polishing. Compound 23 exhibited strong alignment as shown in Figure 8.7 as sharp reflections on the equator indicate the molecules were aligned parallel to the electrode surfaces. This is contrary to the typical homeotropic packing previously observed for thin films of this compound. The large number of reflections in the mesophase is indicative of columns of molecules as discussed in Section V. The large number of strong diffuse lines for a low molecular material indicates the packing structure contains the rigidity of a quasi-ordered system[3]. Similar behavior was observed by Azaroff[8] with nitroimine dimers. Strong association of terminal dipoles caused a linear succession of molecules which gave rise to periodic molecular arrays exhibiting a number of meridional reflections when magnetically aligned. A similar behavior caused by chemical dissimilarities of the siloxane and pendant mesogens is proposed for these compounds. While in the mesophase, the compound spontaneously aligned in a planar orientation yielding diffraction patterns exhibiting six reflections on the equator. The intensity distribution of the first-order reflection indicates very large and well ordered domains in addition to reflections from a small amount of poorly aligned domains. The effect of an applied electric field will be discussed later. Compound 21 did not exhibit this behavior as powder diffraction patterns were obtained. Only one reflection was observed in the mesophase region. This indicates that the

dimer symmetry may be important with regard to its ability to layer pack. The three biphenyl materials did not surface align to this extent although a slight sharpening of the primary layer reflection on the equator was observed for all compounds.

Figure 8.7:   Strong surface alignment for compound 23 induced by the   electrodes

The electric field had various effects on the molecular packing depending on the structure and phase type. Cholesteric compounds 4, 31, and 33 showed little change in their diffraction patterns upon application of the electric field. Only two of the compounds containing 100% cholesterol were examined. Compound 8 showed equatorial reflections similar to compound 23 caused by surface alignment. These corresponded to the low-angle and primary layer reflections discussed earlier. Application of the electric field had little effect on the spacings and intensities of these reflections. Upon cooling from the isotropic region, an even intensity azimuthal ring appears slowly forming into two equatorial arcs as the temperature was lowered. However, when allowed to sit at 211°C for 30 minutes, there were faint reflections on the meridian. This behavior is consistent with that observed for the other all-cholesterol sample, compound 23. The surface alignment discussed earlier showed a strong dependence on temperature and frequency of the applied field. Upon heating or cooling near the clearing temperature, the equatorial spots of the primary layer reflection would split into four spots, two being on the meridian. The appearance of biaxiality indicates the electric field was trying to align the material in an orientation opposite to its preferred equatorial alignment. Multiple heating and cooling scans without the electric field applied did not exhibit this behavior. The clearing temperature also showed a strong dependence on the frequency of the electric field for both heating and cooling runs as shown in Table 8.1.

Table 8.1

Clearing temperatures on heating and cooling for compound 23 with an applied electric field at different frequencies

heating transitions	
Frequency (Hz)	Clearing Temp. (^{o}C)
W/O	220-225 (DSC=225)
100	210-220
10	200
1	205

cooling transitions	
Frequency (Hz)	Clearing Temp. (^{o}C)
W/O	DSC=210
100	180
10	170
1	173

DSC data indicate a clearing temperature of 225°C on heating and 210°C on cooling. Application of the electric field lowers the clearing temperature on both heating and cooling with the lowest values being observed at frequencies of 10 and 1 Hz. Much larger changes were observed for the cooling runs. This has been attributed to the formation of an induced pseudo-isotropic phase on application of the electric field. This was caused by competition between surface effects which aligns the molecules on the equator and the electric field which aligns the molecules on the meridian.

292

The appearance of a faint meridional first-order reflection upon annealing for compound 8 is consistent. Difference in the ability align with the field is caused by the higher viscosity of the ring system. Other all-cholesterol systems, compounds 13, 21, 25, and 18 should be examined to investigate differences due to the siloxane molecular architectures.

The all-biphenyl compounds showed little tendency to surface align. They did show different degrees of alignment with the electric field although all materials contained a siloxane "core" with attached biphenyl derivatives. Compound 1 showed the most dramatic change in orientation upon application of the electric field. Application of an electric field while in the isotropic phase followed by cooling into the nematic phase aligned the molecules parallel to the direction of the field. Alignment of the molecules was better at 120°C (Figure 8.8) than at 170°C (Figure 8.9) due to decreases in the local thermal fluctuation although the response at the higher temperature was faster (seconds versus minutes). The aligned diffraction patterns closely resembled those from the magnetically aligned sample of this compound. At both temperatures, six meridional reflections were observed corresponding to a primary layer spacing of 23.0Å, and strong equatorial crescents corresponding to 4.6Å. Splitting of the first-order meridional reflection, seen in Figure 8.8, indicates a cybotatic-like packing behavior. No 301 reflections were observed at either temperature. Orientational data as a function of temperature, frequency, applied field, and time are currently being analyzed.
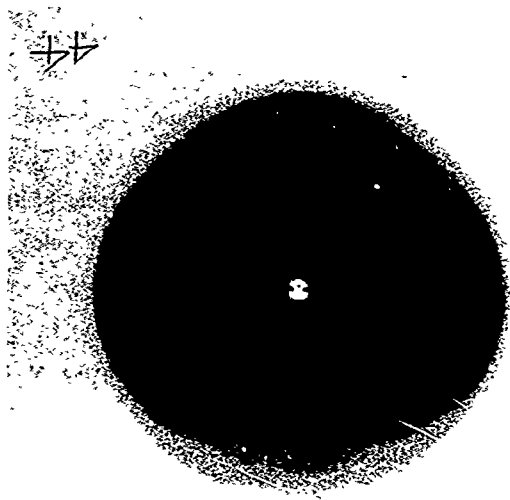
Figure 8.8: Diffraction pattern from aligned nematic phase of compound 1 at 120°C after applying electric field
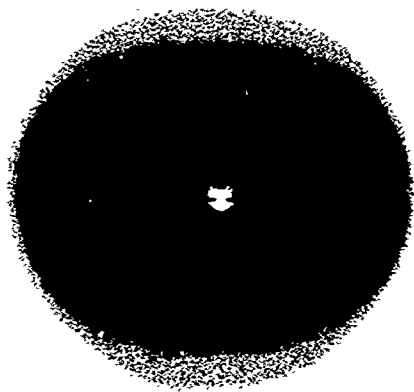
Figure 8.9: Diffraction pattern from aligned nematic phase of compound 1 at 170ºC after applying electric field

Qualitative differences in the behavior of the other all-biphenyl compounds can be discussed. Compound 17, identical to compound 1 except that it possessed shorter vinyl leader groups, did not respond to the applied field based on its wide-angle reflection. This lack of ability to sufficiently respond may indicate the side-chains do not possess enough flexibility to cooperatively reorient. The lack of a well-defined small-angle reflection in either the aligned or unaligned state indicates much poorer trans ational order than compound 1. The side-chain linear polysiloxane, compound 9, although exhibiting a small-angle reflection of 23Å, did not respond to the electric field either. Diffraction patterns of the nematic phase after cooling from the isotropic upon application of the field were identical to those obtained without the field.

The three low molecular weight analogs were all affected by the electric field although not nearly to the same degree as compound 1. Compound 22 showed little response at all frequencies even close to the clearing point. This is probably a direct consequence of its smectic phase which is inherently more difficult to align due to its layered structure[9]. Compounds 24 and 26 also responded as evidenced by a strengthening of the meridional reflections. Compound 26 exhibited better orientation at temperatures below the clearing point region. Orientation obtained within the nematic mesophase for compound 24 was transferrable to the smectic phase. Application of the electric field while in the smectic phase had no visible effect on the alignment. Compound 24 tended to align quicker and to a greater degree than compound 26

indicating a strong influence on the interior flexibility of the "core" molecules.

The ability of compound 1 to align in a manner much different from the other five compounds indicates the complex structural interactions present for these systems although they are remarkably similar in structure. The absence of alignment in compounds 9 and 17 was peculiar and may indicate a strong dynamic coupling of the side-chain and siloxane "cores" motion. The reduced orientational behavior of the small molecular weight compounds 24 and 26 compared to that of compound 1 may support this hypothesis as slight changes in the siloxane core changed the response characteristics dramatically. The ability to examine the time/temperature/electric/structural properties in real-time allows for a better understanding of these fundamental quantities. The system of compounds presented here demonstrates both the complexity of the interactions and the promise of dynamic X-ray diffraction techniques. An improved understanding of both the changes in structural organization associated with field alignment and the impact of molecular architecture on liquid crystalline behavior are fundamentally important. A more systematic examination is needed to fully understand the complex physical interactions.